

AN ABSTRACT OF THE THESIS OF

Theodore Alekel III for the degree of Doctor of Philosophy in
Chemistry presented on 08 April 1993.

Title: Synthesis and Study of New Borate Optical Hosts

Redacted for Privacy

Abstract approved: _____
/Douglas A. Keszler

The central focus of the work presented here was directed toward the discovery and fundamental characterization of new solid-state crystalline materials for potential use as lasers, phosphors, and imaging media. The investigations have included the development of synthetic routes to new compounds, structural determination of microscopic environments, and preliminary measurement of selected physical properties of these novel substances.

The scope of this study has been primarily confined to the class of oxide, alkaline-earth borates, that includes a sizeable expansion of known borate halide structures. A large family of borates described by the general formula $A_6MM'(BO_3)_6$ has been discovered with over 150 derivatives known to exist. The structure type, termed as *STACK*, can assume a myriad of compositions, but

particular attention was given to selected derivatives with the intent of characterizing potential new optical materials for laser and phosphor applications.

Other new borate compounds, incorporating halides in their integral formulae, also demonstrate potential as new optical materials. The compound $\text{Ba}_5(\text{B}_2\text{O}_5)_2\text{F}_2$ is formed around highly contorted pyroborate units and has incorporated several optically significant lanthanide dopant ions into its framework. From the same phase system, $\text{Ba}_7(\text{BO}_3)_3\text{F}$ is a noncentrosymmetric structure that exhibits a capability for second harmonic optical frequency conversion and self-doubling laser applications. Both of these new compounds assume three-dimensional frameworks that contain three types of Ba sites, feature thermal evidence of melting congruently, and constitute the only structurally known members in the $\text{BaF}_2 - \text{B}_2\text{O}_3 - \text{BaO}$ phase system.

Mimicking the stoichiometry of the widely used apatite phosphors, $\text{Sr}_5(\text{BO}_3)_3\text{X}$ ($\text{X} = \text{F}, \text{Cl}, \text{Br}$) is a new group of borate halides that may also prove to be good phosphor hosts. These compounds form three-dimensional lattices that contain three cationic sites that are chemically dissimilar from each other. The Eu^{2+} -doped samples of $\text{Sr}_5(\text{BO}_3)_3\text{Cl}$ exhibit efficient blue luminescence upon excitation by UV light.

Two new alkaline-earth borate bromides, $\text{A}_2\text{BO}_3\text{Br}$ ($\text{A} = \text{Sr}, \text{Ba}$), possess a uniquely symmetrical layered structure. When doped with a divalent lanthanide species, such as Eu^{2+} , these borate bromides demonstrate efficient emission and potential energy storage behavior that may be useful for learning more about the X-ray / UV imaging process.

SYNTHESIS AND STUDY OF NEW BORATE OPTICAL HOSTS

by

Theodore Alekel III

A THESIS

submitted to

OREGON STATE UNIVERSITY

in partial fulfillment of
the requirements for the
degree of

Doctor of Philosophy

Completed 08 April 1993

Commencement June 1993

APPROVED:

Redacted for Privacy

Professor of Chemistry in charge of major

Redacted for Privacy

Head of Department of Chemistry

Redacted for Privacy

Dean of Graduate School

Date thesis is presented 08 April 1993

Prepared and presented by Theodore Alekel III

ACKNOWLEDGMENTS

Dr. Doug Keszler deserves my utmost gratitude and respect. Beyond his patient instruction and resourceful intellect, his enthusiasm for his research and confidence in his group members create a rare combination of both a pleasant and productive work environment. I am proud to have been associated with a professor of his caliber.

My colleagues deserve a multitude of thanks for their enlivening dialogue and scholarly counsel. Jim Cox is a good friend and conscientious chemist that has tremendously supported the advancement of my research. For several years Dr. Kathy Schaffers led the progress of the Keszler Power Group, and I thank her for her friendship, time, baked goods, and willingness to expedite my crystallographic knowledge. Sure, Dr. Tom Reynolds is a great tennis partner, but his specialized instruction in spectroscopic physics will be a great help to me for years to come. The diversity of talents of the current members of the Keszler Power Group has aided my work and enriched my life. One cannot ignore the inspirational vitality of Annapoorna Akella, the outlandish wit of Chris Orf, the persistent drive of George Pon, the productive output of Jun-Ming Tu, and Yaobo Yin's American Dream. The synthetic efforts of Mike Nashner and Lee Willis are appreciated; I wish them the best in their science careers. It has been a pleasure to work with these comrades.

The inspiration and guidance of Dr. Frasier Nyasulu and Dr. Steven Lee largely directed me into a career of chemistry.

I owe my success to my parents, Ted and Theresa, for their continual guidance and encouragement. My father seeded my interest in science and gave me the hands-on opportunity to develop my aspiration; my mother provided an active education and intellectual example that I have attempted to emulate.

My dear wife Roxanne has truly been my most positive influence: I could never have come this far without her love, confidence, and support. Her attributes

of skillful organization, attention to detail, and attainment of excellence have constantly motivated me to attempt the greatest challenges.

At every crossroad in the course of my career, Jesus Christ has directed my life with celestial speed, unusual poise, and abundant blessings. If ever I had a glimmer of enlightenment, it certainly has been a gift of heaven.

CONTRIBUTION OF AUTHORS

The data presented in Chapter 6 resulted from a collaboration of Dr. Kathleen I. Schaffers, Dr. Paul D. Thompson, myself, James R. Cox, and Dr. Douglas A. Keszler. Specifically, Dr. Kathleen I. Schaffers performed the structure analysis on $\text{Sr}_6\text{Ho}_{0.964}\text{Sc}_{1.036}(\text{BO}_3)_6$ and $\text{Sr}_6\text{La}_{0.84}\text{Sc}_{1.16}(\text{BO}_3)_6$, examined the solid solution series $\text{Sr}_6\text{Ho}_x\text{Sc}_{2-x}(\text{BO}_3)_6$, and worked with James R. Cox on the $\text{Sr}_6\text{La}_x\text{Sc}_{2-x}(\text{BO}_3)_6$ solid solution series. Dr. Paul D. Thompson examined the solid solution series $\text{Sr}_6\text{Sc}_{2-x}\text{Al}_x(\text{BO}_3)_6$ and $\text{Sr}_6\text{Y}_{2-x}\text{Al}_x(\text{BO}_3)_6$ for $0 \leq x \leq 2$. I performed the crystal studies on $\text{Sr}_6\text{Y}_{1.07}\text{Al}_{0.93}(\text{BO}_3)_6$, initiated the exploratory powder studies on the mixed valency derivatives with the general formulae $\text{Ln}^{3+}\text{A}^{2+}_5\text{M}^{3+}\text{M}^{2+}(\text{BO}_3)_6$ and $\text{A}_6\text{M}^{2+}\text{M}^{4+}(\text{BO}_3)_6$ derivatives, and investigated the optical properties of various dopant ions primarily in the $\text{Sr}_6\text{YAl}(\text{BO}_3)_6$ compound. James R. Cox solved the structure of $\text{Ba}_6\text{Gd}_{1.28}\text{Sc}_{0.72}(\text{BO}_3)_6$, aided in the study of the solid solution series $\text{Sr}_6\text{La}_x\text{Sc}_{2-x}(\text{BO}_3)_6$, and provided all of the data on the $\text{A}_6\text{MM}'(\text{BO}_3)_6$ derivatives where $\text{A} = \text{Ba}$. Dr. Douglas A. Keszler solved the crystal structure of $\text{Sr}_6\text{Er}_{1.40}\text{Sc}_{0.60}(\text{BO}_3)_6$. All other data (specifically the powder studies summarized in Table 10.3) were accumulated from a combined effort of the aforementioned contributors.

TABLE OF CONTENTS

CHAPTER 1: INTRODUCTION	1
Laser Hosts	3
Phosphors	5
Storage Materials	8
References	13
 CHAPTER 2: STRUCTURE OF $\text{Sr}_5(\text{BO}_3)_3\text{Cl}$	 15
Abstract	16
Introduction	17
Experimental	18
Discussion	24
Acknowledgments	30
References	31
 CHAPTER 3: NEW STRONTIUM BORATE HALIDES $\text{Sr}_5(\text{BO}_3)_3\text{X}$ (X = F or Br)	 33
Abstract	34
Introduction	35
Experimental	36
Synthesis	36
Crystallographic Study	36
Results	41
$\text{Sr}_5(\text{BO}_3)_3\text{F}$	41
$\text{Sr}_5(\text{BO}_3)_3\text{Br}$	46
Discussion	50
Symmetry Relationships	50
Bond Valence Calculations	51
Structure Comparisons	52
Acknowledgments	55
References	56
 CHAPTER 4: THE PYROBORATE $\text{Ba}_5(\text{B}_2\text{O}_5)_2\text{F}_2$	 58
Abstract	59
Introduction	60
Experimental	61
Synthesis	61
Thermal Measurements	61

X-ray Work	61
Results	65
Structure Description	65
Thermal Properties	71
Acknowledgments	75
References	76

CHAPTER 5: STRUCTURE AND Eu ²⁺ LUMINESCENCE OF THE NEW BORATES AE ₂ BO ₃ Br (AE = Sr and Ba)	78
Abstract	79
Introduction	80
Experimental	82
Synthesis	82
Thermal Analysis	82
Optical Apparatus	83
Crystallographic Study	83
Results	89
Structure Description	89
Thermal Properties	94
Optical Properties	94
Discussion	101
Acknowledgments	106
References	107

CHAPTER 6: CRYSTAL CHEMISTRY OF STACK [A ₆ MM'(BO ₃) ₆] ..	110
Abstract	111
Introduction	112
Experimental	113
Synthesis	113
Crystal Growth	114
Single-crystal Work	115
Sr ₆ Y _{1.07} Al _{0.93} (BO ₃) ₆	115
Sr ₆ Ho _{0.964} Sc _{1.036} (BO ₃) ₆	117
Sr ₆ Er _{1.40} Sc _{0.60} (BO ₃) ₆	117
Sr ₆ La _{0.84} Sc _{1.16} (BO ₃) ₆	118
Ba ₆ Gd _{1.28} Sc _{0.72} (BO ₃) ₆	118
Results and Discussion	122
STACK Structure	122
Summary	144
Acknowledgments	145
References	146

CHAPTER 7: STRUCTURE OF $\text{Ba}_7(\text{BO}_3)_3\text{F}_5$: A NEW NON-CENTROSYMMETRIC ORTHOBORATE FLUORIDE .	147
Abstract	148
Introduction	149
Experimental	150
Synthesis	150
X-ray work	150
Results	155
Discussion	163
Acknowledgments	168
References	169
 BIBLIOGRAPHY	 170
 CURRICULUM VITAE	 177

LIST OF FIGURES

<u>Figures</u>	<u>Page</u>
1.1	A sketch of a single octahedral chain in the structure of STACK. 7
1.2	A model of the PSL mechanism in a X-ray storage phosphor. 11
2.1	Schematic unit cell drawing of $\text{Sr}_5(\text{BO}_3)_3\text{Cl}$. The small shaded circles represent Sr atoms, the large dark circles represent Cl atoms, the large pale circles represent O atoms, and the small black circles represent B atoms, here, and in ensuing figures. The four crystallographically distinct Sr atoms are numerically labeled. 25
2.2	Sr3- and Sr4-centered distorted square antiprisms in $\text{Sr}_5(\text{BO}_3)_3\text{Cl}$. 26
2.3	Chain of Cl-centered distorted octahedra extending along the 2_1 screw axis in $\text{Sr}_5(\text{BO}_3)_3\text{Cl}$. 28
3.1	Schematic unit-cell drawing of $\text{Sr}_5(\text{BO}_3)_3\text{F}$. The small open circles represent Sr atoms, the large shaded circles represent O atoms, the small black circles represent B atoms, and the large open circles represent F atoms. (Atomic legend used in subsequent figures, unless noted.) The Sr and O atoms are numerically labeled. 42
3.2	Sr3-centered distorted monocapped square antiprisms in $\text{Sr}_5(\text{BO}_3)_3\text{F}$, illustrating the three- and four-point face-sharing of the polyhedra. The monocapping interaction is 3.04 Å. 45
3.3	Schematic unit-cell drawing of $\text{Sr}_5(\text{BO}_3)_3\text{Br}$. The large open circles represent Br atoms; the Sr and O atoms are numerically labeled. 47
3.4	Stereo views illustrating the connectivity of alkaline-earth-centered polyhedra that coordinate to the columns of halides within the following labeled structures: (a) $\text{Sr}_5(\text{PO}_4)_3\text{Cl}$, (b) $\text{Sr}_5(\text{BO}_3)_3\text{Br}$, (c) $\text{Ca}_5(\text{PO}_4)_3\text{F}$, and (d) $\text{Sr}_5(\text{BO}_3)_3\text{F}$. The small open circles portray the alkaline-earth metal, and the large open circles represent the halide. The c axis is vertical in the page except for (d), where the a axis is vertical. 54
4.1	A schematic unit cell drawing of $\text{Ba}_5(\text{B}_2\text{O}_5)_2\text{F}_2$ along the b -axis. The small open circles represent Ba atoms, the large shaded circles represent O atoms, the small black circles represent B atoms, and

	the large open circles represent F atoms. (Atomic legend continued for subsequent figures.) The Ba layers and the O atoms are numerically labeled.	66
4.2	A b-axis projected stereo view of the unit cell along the <i>b</i> -axis.	67
4.3	Illustrations of the interconnectivity between selected polyhedra: (a) The shared edges between the coplanar Ba1 centers are highlighted as shaded bonds; the other layer is labeled <i>Ba1'</i> . (b) The pyroborate connectivity to the Ba polyhedra; the Ba atoms and the pyroborate O atoms are numerically labeled.	68
4.4	The pyroborate geometry of Ba ₅ (B ₂ O ₅) ₂ F ₂ : (a) the B–O–B angle and (b) the interplanar angle.	72
4.5	DTA data for Ba ₅ (B ₂ O ₅) ₂ F ₂ .	73
5.1	Block diagram of the optical instrumentation used for excitation and luminescence spectra.	84
5.2	A packing diagram for the compounds AE ₂ BO ₃ Br (AE = Sr, Ba), viewed as a (110) projection with the <i>c</i> axis vertical in the page. The small empty circles represent Sr atoms, the large pale circles represent O atoms, the large shaded circles represent Br atoms, and the small black circles represent B atoms.	90
5.3	A schematic of the unit cell of AE ₂ BO ₃ Br (AE = Sr, Ba). The Sr atoms are numerically labeled. The shadings are duplicated from Figure 5.2.	91
5.4	A DTA profile for Sr ₂ BO ₃ Br. The heating curve is below the cooling curve.	95
5.5	A DTA profile for Ba ₂ BO ₃ Br. The heating curve is below the cooling curve.	96
5.6	Photoexcitation and luminescence data for Sr ₂ BO ₃ Br.	97
5.7	Photoexcitation and luminescence data for Ba ₂ BO ₃ Br at 300 K.	98
5.8	A sketch of the energy levels for Eu ²⁺ (4f ⁷ configuration). The position of the 5d band is host dependent.	102
6.1	Chain of alternately stacked metal-centered octahedra linked by	

	BO ₃ groups.	128
6.2	Sketch of the 3-dimensional structure of STACK viewed along the trigonal axis; the one-dimensional chains (Figure 6.1) are linked by Sr atoms.	129
6.3	Cell volumes for the series Sr ₆ Sc _{2-x} Al _x (BO ₃) ₆ (top) and Sr ₆ Y _{2-x} Al _x (BO ₃) ₆ (bottom) for 0 ≤ x ≤ 1.2.	131
6.4	Cell parameters for the series Sr ₆ Sc _{2-x} Ho _x (BO ₃) ₆ for 0 ≤ x ≤ 2.0.	133
6.5	Unit cell volumes (Å ³) for the solid solution series Sr ₆ Sc _{2-x} La _x (BO ₃) ₆ .	135
6.6	Cell parameters for the series Ba ₆ Dy _{2-x} Sc _x (BO ₃) ₆ .	141
6.7	Unit cell volumes for the solid solution series Ba _{3-x} Sr _x Sc(BO ₃) ₃ and Sr _{3-x} Ca _x Sc(BO ₃) ₃ .	142
7.1.	A schematic view of the unit cell for Ba ₇ (BO ₃) ₃ F ₅ . The small open circles represent Ba atoms, the small black circles represent B atoms, the pale large circles represent O atoms, and the shaded large circles represent F atoms. Shading legend continued in subsequent figures. The Ba atoms are numerically labeled.	156
7.2	The Ba3 coordination centers in Ba ₇ (BO ₃) ₃ F ₅ .	159
7.3.	Coordination environments for the F atoms in Ba ₇ (BO ₃) ₃ F ₅ . The F atoms are numerically labeled.	162
7.4.	A proposed arrangement of BO ₃ groups for obtaining high nonlinearity and low birefringence.	165
7.5.	The arrangement of BO ₃ groups in Ba ₇ (BO ₃) ₃ F ₅ .	166

LIST OF TABLES

<u>Tables</u>	<u>Page</u>
1.1 Desirable PSL properties and their effects.	10
2.1 Positional parameters for $\text{Sr}_5(\text{BO}_3)_3\text{Cl}$.	20
2.2 Selected interatomic distances (\AA) and angles ($^\circ$) for $\text{Sr}_5(\text{BO}_3)_3\text{Cl}$.	21
2.3 Anisotropic displacement coefficients for $\text{Sr}_5(\text{BO}_3)_3\text{Cl}$.	23
3.1 Crystallographic Data for $\text{Sr}_5(\text{BO}_3)_3\text{F}$ and $\text{Sr}_5(\text{BO}_3)_3\text{Br}$.	38
3.2 Positional parameters for $\text{Sr}_5(\text{BO}_3)_3\text{F}$ and $\text{Sr}_5(\text{BO}_3)_3\text{Br}$.	40
3.3 Selected bond distances and angles for $\text{Sr}_5(\text{BO}_3)_3\text{F}$.	43
3.4 Selected bond distances and angles for $\text{Sr}_5(\text{BO}_3)_3\text{Br}$.	48
4.1 Crystallographic data.	63
4.2 Atomic coordination and thermal displacement coefficients.	64
4.3 Selected bond distances and angles.	70
5.1 Crystallographic Data for $\text{A}_2\text{BO}_3\text{Br}$ ($\text{A} = \text{Sr}, \text{Ba}$).	86
5.2 Positional parameters and B_{eq} for $\text{A}_2\text{BO}_3\text{Br}$ ($\text{A} = \text{Sr}, \text{Ba}$).	87
5.3 Bond Lengths of $\text{AE}_2\text{BO}_3\text{Br}$ ($\text{AE} = \text{Sr}, \text{Ba}$).	92
5.4 Selected Bond Angles for $\text{AE}_2\text{BO}_3\text{Br}$ ($\text{AE} = \text{Sr}, \text{Ba}$).	93
5.5 The Maxima of the $4f^6(^7F_0)5d$ Excitation / Emission Bands and the FWHM bandwidths (Γ) for $\text{A}_2\text{BO}_3\text{Br}$ ($\text{A} = \text{Sr}, \text{Ba}$). All spectral values are expressed in nm.	100
5.6 The wavelengths (nm) at peak luminescence intensity for selected Eu^{2+} -doped barium bromide materials ($T = 300 \text{ K}$).	104
6.1 Crystal data for $\text{Sr}_6\text{YAl}(\text{BO}_3)_6$, $\text{Sr}_6\text{ErSc}(\text{BO}_3)_6$, $\text{Sr}_6\text{HoSc}(\text{BO}_3)_6$,	

	LaSr ₆ Sc(BO ₃) ₆ , and Ba ₆ GdSc(BO ₃) ₆ .	116
6.2a	Positional parameters for Sr ₆ YAl(BO ₃) ₆ , Sr ₆ ErSc(BO ₃) ₆ , and Sr ₆ HoSc(BO ₃) ₆ .	120
6.2b	Positional parameters for LaSr ₆ Sc(BO ₃) ₆ and Ba ₆ GdSc(BO ₃) ₆ .	121
6.3	Cell parameters for the family A ₆ MM'(BO ₃) ₆ (STACK).	123
6.4	Interatomic distances (Å) for Sr ₆ YAl(BO ₃) ₆ , Sr ₆ ErSc(BO ₃) ₆ , Sr ₆ HoSc(BO ₃) ₆ , LaSr ₆ Sc(BO ₃) ₆ , and Ba ₆ GdSc(BO ₃) ₆ .	138
6.5	Interatomic angles (°) for Sr ₆ YAl(BO ₃) ₆ , Sr ₆ ErSc(BO ₃) ₆ , Sr ₆ HoSc(BO ₃) ₆ , LaSr ₆ Sc(BO ₃) ₆ , and Ba ₆ GdSc(BO ₃) ₆ .	139
7.1.	Crystallographic Data for Ba ₇ (BO ₃) ₃ F ₅ .	151
7.2.	Positional parameters and B _{cq} for Ba ₇ (BO ₃) ₃ F ₅ .	153
7.3.	U values for Ba ₇ (BO ₃) ₃ F ₅ .	154
7.4.	Selected bond distances (Å) for Ba ₇ (BO ₃) ₃ F ₅ .	157
7.5.	Selected bond angles (°) for Ba ₇ (BO ₃) ₃ F ₅ .	158
7.6.	Bond Valence Calculation for Ba ₇ (BO ₃) ₃ F ₅ .	161

SYNTHESIS AND STUDY OF NEW BORATE OPTICAL HOSTS

CHAPTER 1

INTRODUCTION

With the advent of semiconductor devices in the late 1950's came a wave of technological development that has snowballed over the decades into a leading industrial market and having an overwhelming influence on the lifestyle of modern societies. From the p-n junction of two solid-state compositions, a myriad of electronic devices have been designed that may use billions of these microscopic building blocks to assemble the most sophisticated devices ever developed. The maturation of this technology has progressed in less than a century, and now we are at the point where a seed of a new technological building block has sprouted: *photonics*: a combination of electrical signals and optical processes. The wheels are already in motion — fiber optics, miniature laser diode light sources, optical data storage, molecular computing, optical imaging and holography, solid-state photomultipliers, to name a few (1–3) — and photonics is poised for an expanding future. The next wave of technological advancement will be the ubiquitous use of optical "building block" devices, and an intensified level of frontier research will drive this budding innovation and development.

At this point, most optical devices utilize materials that have been long known and fundamentally characterized; this information is stored away in the archives of scientific knowledge. (Some would say much of the groundwork was provided by those with an academic curiosity, otherwise known as *basic research*.) For example, compositions of glass have not changed very much over the years, yet the production of glass fibers and optical amplifiers for communication lines (4) and

the growth of large glass boules as laser hosts for fusion research (5) currently depend upon known formulations for forefront application in optical science.

In the crystalline realm, most of the host materials used for lasers and other optical devices derive their origins from minerals: garnet, fluorite, sapphire, apatite, emerald, alexandrite, scheelite, colquiriite, matlockite, hilgardite, etc. Clearly, research within the domain of known materials has not even begun to exhaust the potential for the development of innovative optical devices. On the other hand, a preparative solid-state chemist may draw on his chemical intuition and attempt to synthetically create a material with desirable properties. Rather than investigate every possible combination of ingredients in a brute-force approach to finding compounds with the optimal physical characteristics, an imaginative chemist might direct his efforts to design a new composition with superior properties. One may even predict the existence of an unknown phase that could suit design goals. This has been the approach of my research contribution at OSU.

On the basis of the points discussed above, it is evident that new optical materials are strongly needed to continue and support the advancement of technology. Thus, I have approached my research horizontally — after synthesizing new compounds to meet research goals, I characterized their structural nature, studied their physical attributes, and then attempted to relate their observed behavior with their known microscopic arrangement. Thus, the beginning phase of evaluating their performance was initiated in the investigation of their potential as new optical materials.

If a new phase had indeed been created, a method of characterization was needed to identify it. Solid-state experimentalists extensively use X-ray diffraction methods to probe the atomic positions and bonding in a compound; powder diffraction aids in new phase identification of microcrystalline powders, while crystals grown in the laboratory are analyzed on a single crystal diffractometer to pinpoint the locations of atoms in the structure. After the atomic environment had been established, the host material was formed with optically active ion(s) substitutions at impurity levels, and its basic spectral properties were investigated.

If the compound appeared promising for a suitable application, then plans were made for more sophisticated spectroscopic analyses (e.g., lifetimes, quantum efficiencies, energy storage behavior, etc.).

Although the field of optical materials is quite diverse, the motivation of my work has been directed toward three fields of interest: new laser hosts, efficient phosphors, and energy storage media. Henceforth, each of these applications will be separately explained in more detail.

Laser Hosts. Solid-state lasers offer the qualities of efficiency, stability, reliability, flexibility, and compact dimensions that are attractive for future innovations. A recent resurgence of interest in the development of solid-state laser systems has been fueled by the rapid advances of the diode laser as a convenient pump source, U.S. government pressure to eliminate liquids in laser systems (3), and a widespread need for the efficient production of blue laser light. Traditional solid-state lasers operate *via* the population inversion of electronic transitions of lanthanide or transition-metal chromophores within the host (6). To extract higher frequency light from this process, the active ion must possess widely separated energy levels with no electronic states between them so as to eliminate unwanted pathways that can bleed away the excited state energy from laser output into lower-energy intermediate states.

Unfortunately, laser materials with such energetic prerequisites are not plentiful or commercially available. Extraordinarily, the cations Ce^{3+} and Tm^{3+} have been made to lase UV and blue light, respectively, in the host material LiYF_4 (7,8). Nevertheless, even if an ideal solid-state system were accessible, the problem of efficiently pumping the laser crystal without unnecessarily dumping excess energies into the material that are outside the absorption band of the active ion still remains — simple narrowband UV/violet sources for photoexcitation are not conveniently available. Therefore, the current pursuit of upconversion lasers (9) and efficient frequency converters (10) continues to dominate the forefront of new laser technology. In fact, hand-held blue lasers are now available that are pumped with near-IR laser diodes. Through clever engineering, the third-order harmonic

of Nd:YAG is able to produce 335 nm light in a compact housing (11). Also, 428 nm light is currently under production for medical instrumentation and optical data storage applications by doubling 856 nm laser diodes through a KNbO_3 frequency doubling crystal (12). In fact, the high energy limit for frequency conversion is defined by the material $\text{KBe}_2\text{BO}_3\text{F}_2$ (KBBF), capable of generating the 5th harmonic of Nd:YAG (213 nm) and phase-matching to 185 nm (13).

Another method of generating blue laser light is to combine the functions of a laser host and second harmonic generator (SHG) into one material — a self-doubling solid-state laser. An example of producing doubled laser energy in a single media is the borate $\text{Nd:Y}_3(\text{Al,Cr})(\text{BO}_3)_4$ (14). The 1064 nm light is converted to 532 nm as it resonates within the noncentrosymmetric host lattice. This system is analogous to placing a conventional SHG crystal within the laser cavity, which has been shown to be advantageous (15): the fundamental laser intensity is much higher within the resonator than the escaping external beam, so the conversion efficiency is much higher. Therefore, using a self-doubling laser host can potentially maximize the production of the second harmonic, providing that the crystal is an efficient frequency converter and its nonlinear properties effectively match those of the lasing ion in the host.

Other members of this group have examined the theoretical aspects of nonlinear optical (NLO) materials containing D_{3h} chromophores. By considering symmetry aspects observed NLO properties have been modeled solely on the basis of a crystal structure. This analysis can be applied to any non-centrosymmetric compound that relies on planar trigonal anions for frequency conversion — anions such as nitrates, carbonates, and most importantly, orthoborates. The reader is referred to the Ph.D dissertation of Kathleen I. Schaffers for the pertinent background information on this subject (16).

It makes sense that, if the triangular anions in a structure are all oriented in the same direction, their individual contributions to the nonlinearity of the bulk material will constructively sum and provide a maximized susceptibility. This type of ideal arrangement is almost exemplified by the structure of LiCdBO_3 where the

sum of the microscopic contributions is achieved from a series of layers. These layers, however, produce two unwanted traits — a high angular sensitivity to phase matching and increased threshold power.

One viable arrangement of the chromophores that would maximize the nonlinearity of a material while avoiding the high associated birefringence was conceived by D. A. Keszler (17). He proposed that if a structure existed where the triangles were arranged around a rotation axis, e.g., possessing C_3 symmetry, and they were all pointed in one direction, then one would observe the properties as predicted above. Since then, in my study of the $BaO-BaF_2-B_2O_3$ phase system, a new noncentrosymmetric material $Ba_7(BO_3)_3F_5$ was discovered with an orthoborate alignment very similar to this ideal case: triangular units rotated about three-fold symmetrical axes that are generally aimed in one direction. The structure and thermal properties are presented in Chapter 7.

Phosphors. Phosphors are materials that efficiently generate steady-state photoluminescence through some form of excitation energy conversion. When a particular wavelength region is required, much of the radiated energy from black-body sources is thrown away, primarily as heat. The minimization of these energy losses, along with the achievement of optimal frequency output and color rendition are the present-day research concerns in the development of new phosphor materials. Although many materials are known and employed, the need for better light sources continues to exist. A practical example for improved luminescent compounds is the "compact" fluorescent lamp (18). An efficient alternative to the 130 year old Edison light bulb could be realized with a very small, but radiant, fluorescent source. Such a device would require a much higher UV flux than fluorescent light tubes. The phosphor candidate for this lamp must have robust UV and thermal stabilities, much higher than traditional phosphors.

$Sr_6YAl(BO_3)_6$ is one member of a recently discovered oxide family having the generic formula $A_6MM'(BO_3)_6$. Over 150 derivatives of the STACK structure have been synthesized (Chapter 6), and my contribution has emphasized those compositions of interest as a potential phosphor. The derivative $Sr_6YAl(BO_3)_6$

warranted further study for several reasons:

1. Facile synthetic formation
2. Ordered material of high stability
3. Distinctive octahedral environments
4. Accommodates important lanthanide phosphor agents

The most successful method of making this host employs flash heating of the stoichiometric mixture of the metal oxides at 1000°C for 3-4 h (19). These synthetic conditions are much less severe (i.e., costly) than those used to create today's prominent aluminate phosphors, which typically require temperatures of 1200-1600°C (20). The ease of synthesis of $\text{Sr}_6\text{YAl}(\text{BO}_3)_6$ makes it competitive to phosphors currently in use.

Phosphor efficiency is grounded in the quantum yield of a material, which is ultimately determined by the persistence of other nonradiative pathways that compete with luminescence. Concentration quenching usually extracts potential emission by radiatively transferring its energy to adjacent chromophores (via absorption). This can be minimized in two ways: 1) by crystallographically isolating the active ions in structural features of the host structure or 2) by reducing the number of ions in the host framework to an impurity level (e.g., ~ 2%); the low-level random ion distribution decreases the probability of having adjacent ions quenching the luminescence through absorption but at the expense of total number of luminescent site contributors. The balance between both effects determines the maximum efficiency of the phosphor.

The STACK compounds possess chains of octahedra connected together by BO_3 anion triangles (along the c-axis, Figure 1.1). The unique structural feature of interest in this structure is the two distinct octahedral environments for the M atoms; they are dissimilar in size, allowing preferred occupation between two different sized M atoms. This implies that optically active ions may preferentially occupy only one M octahedral site (depending on the size of the ion), extending the distance between adjacent photoactive ions. Even if the ion resides in both M and M' octahedra, they are still separated from each other by intervening BO_3 triangles,

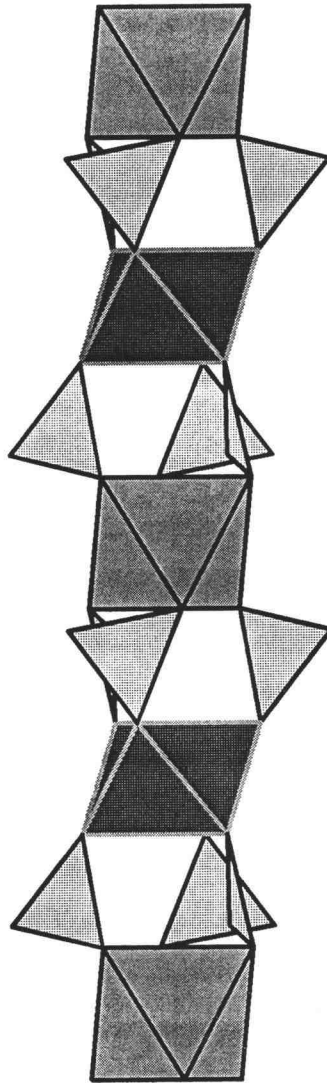


Figure 1.1 A sketch of a single octahedral chain in the structure of STACK.

and the quantum efficiency should be enhanced because of the expected diminished crosstalk. Of course, if the active species preferentially occupy the alternating sites in the stacks of octahedra, the effects of radiative quenching will be further minimized.

On the other hand, if the chromophore occupies the A site, then this aforementioned advantage fades away because adjacent A sites are linked together through common edges and faces. Careful regulation of the photoactive ion doping levels will be the only effective means of reducing concentration quenching. Evidence suggests that the larger lanthanide chromophores prefer the larger A site by interchanging with the smaller Sr atom ($A \leftrightarrow M$, in Chapter 6). $\text{Sr}_6\text{YAl}(\text{BO}_3)_6:\text{Eu}^{3+}$ (2 mole %) exhibits luminescent peaks that should be very weak in a centrosymmetric site ($\bar{3}$) (21), but are in fact prominent in the emission spectrum. Therefore, it seems that the Eu^{3+} ion inhabits both A and M sites. This may limit the efficiency of rare earth photoluminescence in the STACK structure because of the ease of energy transfer from A-to-A sites.

Many borates work well as phosphor hosts. They inherently possess a high optical damage threshold and a very wide transparency window (180-1500 nm) (22), enabling them to withstand a high UV flux. High quantum efficiencies have also been observed in borates (up to 93%) (23) so the STACK structure with its structural features is expected to be a good phosphor host candidate. It has the advantage of accommodating many types of active ions (Pb^{2+} , Sb^{3+} , Sn^{2+} , Bi^{3+} , Ce^{3+} , Tb^{3+} , Gd^{3+} , Eu^{3+} , Eu^{2+} , Mn^{2+} , Ti^{3+}), especially with additional ions serving as sensitizers within the same host (e.g., $\text{LaSr}_5\text{YMg}(\text{BO}_3)_6:\text{Ce,Tb,Eu}$). Many combinations can be assembled to tailor the spectral output of the phosphor and may possibly provide brilliant simultaneous colors from a single compound.

Storage Materials. This is the most recently developed field in optics that is addressed in this dissertation. In the early 1980's the X-ray storage phosphor $\text{BaClF}:\text{Eu}^{2+}$ was the first commercial medium that optically imaged X-ray doses (24). The process works in the following way: First, a thin screen is made by suspending the powder in a binder and coating it onto a substrate. Then, the

screen, in a light-tight housing, is exposed to an X-ray image at room temperature for a given length of time. Finally, a small red laser is focused onto the surface and rasters over the surface simultaneously with a detector to capture the concurrent emission. The intensity of the luminescence is linearly proportional to the X-ray dose, and the image is recorded digitally into a computer. The sensitivity and contrast of this method are greater than those achieved with film. The data are already encoded for ease of communication, and the medium is reusable after being erased by a bath of UV light. Presently, this process is in use as an area detector for single crystal X-ray diffractometers (25), but one readily imagines that this system will also find its way into radiology (26). Features that would make the "perfect" PSL material for this type of application are listed in Table 1.1 (27).

The technique exploits the process of photostimulated luminescence (PSL) in hosts that are doped with an optically active ion. Although the exact mechanism of this process is currently under investigation (28), basically the effect relies on two conditions: 1) The guest ion needs to be stable in two oxidation states, and 2) the host must transport and localize charges within its framework. A schematic representation of the PSL process is given in Figure 1.2. Upon exposure to the high energy radiation (be it X-rays or even UV light), the ion undergoes oxidation and the mobile electron finds a position in the host with a minimum energy. Depending on the depth of this trap, the electron will remain in this position until energetically prompted to "pop out", either by thermal agitation or photostimulation. Then the electron re-associates with an oxidized impurity ion, and then gives up its energy through a radiative transition to the ground state. This two-dimensional storage system has been shown to be effective for X-ray imaging with a greater sensitivity than film (29).

Binary alkaline-earth halides have been extensively studied and used for this storage phenomenon. Their discovery evolved out of research of color centers (30); these point defects naturally occur in the crystalline lattice and can even be populated in greater numbers by exposing the materials to X-rays (31). Thus, when the halide host is combined with a dopant ion that is content in two oxidation

Table 1.1. Desirable PSL properties and their effects.

<u>Feature</u>	<u>Effect</u>
High density	Encourage X-ray absorption
Short luminescence lifetime	Minimize scanning time
High brightness / Low afterglow	Minimize image noise
Optimum stimulation spectrum	Use convenient laser wavelengths Avoid thermal trap depopulation
Large stimulation cross-section	Lower laser power demands
Low scattering	Attain high image resolution
Optimum fluorescence spectrum	Maximize phosphor detection signal Avoid stimulating laser detection

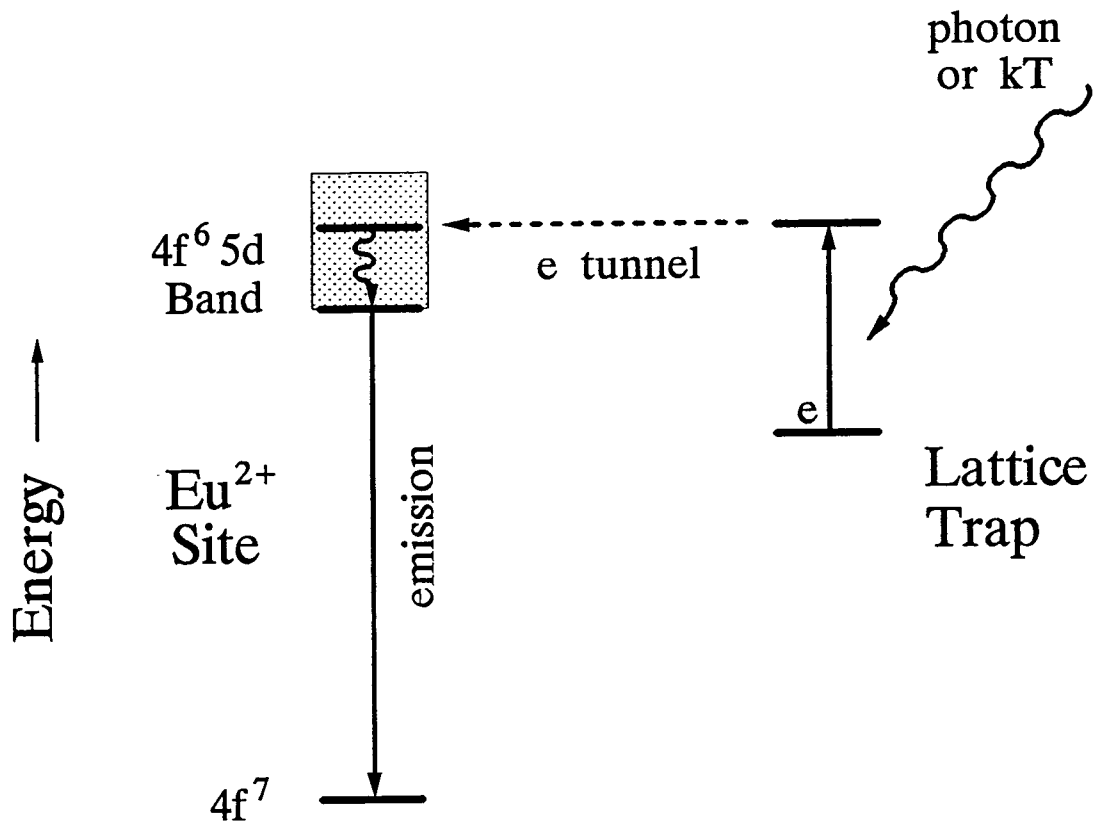


Figure 1.2. A model of the PSL mechanism in a X-ray storage phosphor.

states, a PSL storage material is established. The most successful candidates, other than the matlockite structural derivatives, also contain a high percentage of halides in their stoichiometries. Surely, the investigation of other PSL host hopefuls will reveal properties that have not been witnessed in the simple halide structures. In any case, a variety of structure types are necessary to probe the nature of the environmental conditions that will best serve the desired requirements listed in Table 1.1.

One problem with the alkaline-earth binary halides is their tendency to attract water. The long-term stability of the material, along with the unknown effects on the PSL process, may be compromised by the hygroscopic nature of these hosts. A few other compounds have been investigated for use as storage phosphors that minimize this problem. $\text{Ba}_5\text{SiO}_4\text{Br}_6:\text{Eu}^{2+}$ (32) has been studied, and from initial findings, its performance is comparable to $\text{BaClF}:\text{Eu}$, without the troublesome hygroscopicity. Another notable group of compounds are the Eu-doped derivatives of the mineral hilgardite $\text{A}_2\text{B}_5\text{O}_9\text{X}$ ($\text{A} = \text{Ca}, \text{Sr}, \text{Ba}$; $\text{X} = \text{Cl}, \text{Br}, \text{I}$) (33). In all of these polyanionic compounds, the inclusion of other structural units (i.e., SiO_4^{2-} , BO_4^{5-} , and BO_3^{3-}) serves to diminish their proclivity for H_2O .

In the effort to devise other hosts in which to study the PSL process, the clairvoyant chemist would design a material *a priori* that incorporates the successful features of the alkaline-earth halides with the structural advantages of polyatomic anionic units. In the phase system $\text{SrO}-\text{SrBr}_2-\text{B}_2\text{O}_3$, two new structure types were discovered: $\text{Sr}_2\text{BO}_3\text{Br}$ and $\text{Sr}_5(\text{BO}_3)_3\text{Br}$. From these new compounds, parallel analogues have been made and characterized, and they are described in detail in Chapters 2, 3, and 5. Of these, $\text{Sr}_2\text{BO}_3\text{Br}$ and $\text{Ba}_2\text{BO}_3\text{Br}$ exhibit encouraging properties that may further their study as PSL phosphors.

References

1. M. Shimazu *Photonics Spectra*, **26(11)**, (1992) 66.
2. D.S. Chemela *Phys. Today*, May (1985) 57.
3. "Special Report: Laser Update", *Photonics Spectra*, **25(11)**, (1991) 96.
4. G.M. Kaye *Photonics Spectra*, **25(10)**, (1991) 62.
5. *Nova Laser System*, Lawrence Livermore National Laboratory, CA.
6. A.A. Kaminskii *Laser Crystals*, Springer-Verlag: New York (1981) 12.
7. D.J. Ehrlich, P.F. Moulton, R.M. Osgood *Optics Let.*, **4**, (1979) 184.
8. J.W. Baer, M.G. Knights, E.P. Chiklis, H.P. Jenssen *Proc. Internat. Conf. Laser '78*, December 11-15, Orlando, STS Press: McLean, VA (1979) 770.
9. H-D. Hattendorff, G. Huber, H.G. Danielmeyer *J. Phys. C: Solid-State Phys.*, **11**, (1978) 2399.
10. C.A. Ebber, L.D. DeLoach, M. Webb, D. Eimerl, S.P. Velsko, D.A. Keszler *IEEE J. Quantum Elec.*, **29(2)**, (1993) 497.
11. Coherent Laser Products Division, 3210 Porter Drive, P.O. Box 10042, Palo Alto, CA 94303.
12. G.T. Forrest *Laser Focus World*, April (1990).
13. "Newsbreaks" *Laser Focus World*, **28(9)**, (1992) 9.
14. B-S. Lu, J. Wang, H-F. Pan, M-H. Jiang *J. Appl. Phys.*, (1989) 6052.
Z.D. Luo, J.T. Lin, A.D. Jiang, Y.C. Huang, M.W. Qui *Proc. SPIE Int. Soc. Opt.*, (1989) 1104.
15. R. Wu *Applied Optics*, **32(6)**, (1993) 971.
16. K.I. Schaffers, Ph.D. dissertation, Oregon State University, (1992) Ch. 2.
17. D.A. Keszler, (1992), private communication.

18. F.M. Ryan *J. Luminescence*, **24&25**, (1981) 827.
19. K.I. Schaffers, D.A. Keszler *Inorganic Synthesis*, submitted.
20. A.L.N. Stevels, A.D.M. Schrama-de Pauw *J. Electrochem. Soc.*, **123(5)** (1976) 691.
21. *Philips Technical Review*, **31(10)**, (1970) 309.
22. S. Velsko, Lawrence Livermore National Laboratory, CA (1998) private communication.
23. T. Welker *J. Luminescence*, **48 & 49**, (1989) 49.
24. Fuji Corp., U.S. Pat. 4,239,968; U.S. Pat.4,236,078.
K. Takahashi, K. Kohda, J. Miyahara, Y. Kanemitsu, K. Amitani, S. Shionoya *J. Luminescence*, **31 & 32**, (1984) 266.
25. Molecular Structure Corporation, 3200A Research Forest Drive, The Woodlands, TX 77381, USA.
26. M. Sonoda, M. Takano, J. Miyahara, H. Kato *Radiology*, **148**, 833.
27. M.K. Crawford, L.H. Brixner *J. Luminescence*, **48 & 49**, (1991) 37.
28. F.K. Koschnick, Th. Hangleiter, J-M. Spaeth, R.S. Eachus *J. Phys.: Condens. Matter*, **4**, (1992) 3001.
29. K. Takahashi, Y. Shibahara, J. Miyahara, *Electrochem. Soc. 163rd Meeting*, 921RNP (1983).
30. W.B. Fowler *The Physics of Color Centers*, (ed. W.B. Fowler), Academic Press: New York (1968) Ch. 2.
31. H. von Seggern, T. Voigt, W. Knüpfner, G. Lange *J. Appl. Phys.*, **64(3)**, (1988) 1405.
32. A. Meijerink, G. Blasse, L. Struye *Mater. Chem. Phys.*, **21**, (1989) 261.
33. A. Meijerink, G. Blasse *J. Luminescence*, **43(5)**, (1989) 283.

CHAPTER 2

Structure of $\text{Sr}_5(\text{BO}_3)_3\text{Cl}$

Theodore Alekel III and Douglas A. Keszler*

Department of Chemistry and

Center for Advanced Materials Research

Oregon State University

Gilbert Hall 153

Corvallis, OR 97331-4003

Acta Crystallogr., C48, (1992) 1382.

Abstract

Pentastrontium chloride trisorthoborate, $\text{Sr}_5(\text{BO}_3)_3\text{Cl}$, $M_r = 649.98$, orthorhombic, $C222_1$, $a = 10.000(2)$, $b = 14.202(2)$, $c = 7.421(1) \text{ \AA}$, $V = 1053.9(3) \text{ \AA}^3$, $Z = 4$, $D_x = 4.096 \text{ Mg m}^{-3}$, $\text{Mo K}\alpha$, $\lambda = 0.71069 \text{ \AA}$, $\mu = 24.7 \text{ mm}^{-1}$, $F(000) = 1176$, $T = 295 \text{ K}$, $R = 0.045$ for 911 independent reflections with $I > 3\sigma(I)$. The intricate three-dimensional framework consists of several strontium coordination types — SrO_5Cl_2 , SrO_7Cl_2 , and SrO_8 — interconnected by sharing either faces, corners, or BO_3 triangles. Each Cl atom is surrounded by 6 Sr nearest neighbors, forming zigzag chains that propagate along the c -axis. The plane of the BO_3 group centered by atom B2 is orthogonal to the two-fold rotation, b -axis, and the vector normal of the BO_3 plane centered by atom B1 is only slightly canted from the 2_1 screw axis, portending a small propensity for optical second harmonic generation.

Introduction

The utility of photostimulatable luminescence (PSL) for X-ray imaging has generally been confined to binary alkaline-earth halide hosts i.e. BaFCl:Eu^{2+} (1), yet several oxide-halide materials have succeeded as effective X-ray storage hosts. For instance, the barium silicate halide $\text{Ba}_3\text{SiO}_4\text{Br}_6$ exhibits comparable optical properties to the now standard halide BaFCl:Eu^{2+} , yet the incorporated silicate subdues the hygroscopic tendency of alkaline-earth halides (2). Borates have been shown to be good optical materials for lasers (3) and second harmonic generators (4) because of their wide transparency range and high damage thresholds (5). Therefore, with the introduction of electron-trapping sites, a borate halide should exhibit favorable optical qualities for X-ray storage. A patented prototype already under investigation is Eu^{2+} -doped $\text{A}_2\text{B}_3\text{O}_9\text{X}$ ($\text{A} = \text{Ca, Sr, Ba}$; $\text{X} = \text{Cl, Br, I}$) (6). Considering the recent success of these oxide-halide compounds, the title borate halide was synthesized for optical studies. In addition, initial studies are in progress to investigate its suitability as a second harmonic generator. Here, we describe the structure of this new material.

Experimental

Powder of $\text{Sr}_5(\text{BO}_3)_3\text{Cl}$ was synthesized from a stoichiometric mixture of $\text{Sr}_3(\text{BO}_3)_2$ [laboratory synthesized by reacting $\text{Sr}(\text{NO}_3)_2$ (ÆSAR, ACS grade) and B_2O_3 (ÆSAR, 99.98%), heating at 1273 K] and SrCl_2 (ÆSAR, 99.9%) heated to 1073 K in a Pt crucible for 8 hours. Powder X-ray data collected on an automated Philips diffractometer mimicked the calculated pattern generated with the computer program LAZY-PULVERIX (7) by using the atomic positions determined from the single crystal refinement presented in this paper. Crystals were grown by slowly cooling a 57.4 SrO: 12.9 B_2O_3 : 29.7 SrCl_2 mol% melt from 1123 K to 1023 K in a Pt crucible. A colorless crystalline prism (0.20 x 0.20 x 0.15 mm) was selected for study.

The unit cell parameters were derived by a least-squares analysis of 20 setting angles in the range $30 < 2\theta < 36^\circ$ that were automatically centered on a Rigaku AFC6R diffractometer. Intensity data were collected by using ω - 2θ scans with a scan speed of $16^\circ(\omega)/\text{min}$ over the angular range $2 \leq 2\theta \leq 70^\circ$ containing the corresponding indices $0 \leq h \leq 16$, $0 \leq k \leq 22$, $0 \leq l \leq 11$. Three standards measured every 300 reflections showed no systematic variation (maximum relative deviation: 1.0%), indicating crystalline stability during data collection. The data were corrected for the geometric Lorentz / polarization effects and for secondary extinction with a coefficient of 0.65903×10^{-6} . Of the 1330 measured intensities, 911 unique reflections with $F_o^2 \geq 3\sigma(F_o^2)$ were used in refinement. On the basis of the systematic absences $h + k = 2n + 1$ for hkl , $l = 2n + 1$ for $00l$ and the successful solution and refinement of the structure, the space group was uniquely determined to be $C22_1$.

Calculations were performed on a $\mu\text{VAX II}$ computer by using programs from the TEXSAN crystallographic software package (8). The Sr atoms were located from the results of the direct methods program SHELXS (9); the remaining atomic positions were determined from subsequent electron density maps. F_{calc} was derived from predetermined neutral scattering factors and corrected for anomalous

scattering by using calculated f' and f'' values from *International Tables for X-ray Crystallography* (10). After applying an empirical absorption correction (transmission factors: 0.85 - 1.23) with the program DIFABS (11) and refining each atom (except B2) with anisotropic thermal parameters, minimization of the function $\Sigma w(F_o - F_c)^2$ with 83 variables and 911 observations converged to the final residuals $R = 0.045$ and $R_w = 0.047$ with $S = 1.38$. The weighting scheme was based on counting statistics [$w = 1/\sigma^2(F_o)$] with $p = 0.05$. The maximum shift/e.s.d. in the last cycle was 0.01. The final difference electron density map exhibited a maximum peak of $1.48 \text{ e } \text{\AA}^{-3}$, corresponding to 0.62% of the Sr3 atom peak intensity, and a minimum peak of $-1.99 \text{ e } \text{\AA}^{-3}$. The atomic positions, anisotropic displacement coefficients, and interatomic distances and angles are listed in Tables 2.1, 2.2, and 2.3, respectively.

Table 2.1. Positional parameters for Sr₅(BO₃)₃Cl.

	x	y	z	B _{eq} (Å ²) ^a
Sr1	0.7605(2)	0	0	0.59(5)
Sr2	0.1327(1)	0.87145(9)	0.9371(1)	0.62(3)
Sr3	1/2	0.8651(1)	3/4	0.56(5)
Sr4	1/2	0.1385(1)	3/4	0.63(6)
Cl	0	0.0532(3)	3/4	0.9(1)
O1	0.508(1)	0	0	0.7(4)
O2	0.6712(8)	0.8089(7)	0.009(1)	0.8(3)
O3	0.3553(8)	0.8007(7)	0.986(1)	1.0(3)
O4	0.6969(8)	0.0005(9)	0.337(1)	1.3(3)
O5	0.8817(9)	0.8528(6)	0.883(2)	0.9(3)
B1	0.802(1)	0.789(1)	0.969(2)	0.9(5)
B2	0.374(2)	0	0	0.2(2)

$$^a B_{eq} = (8\pi^2/3) \sum_i \sum_j U_{ij} a_j^* a_i^* a_i \cdot a_j$$

Table 2.2. Selected interatomic distances (Å) and angles (°) for Sr₅(BO₃)₃Cl.

Sr1-Cl	x 2	3.123(2)	Sr4-O1	x 2	2.705(2)
Sr1-O1		2.53(1)	Sr4-O2	x 2	2.586(9)
Sr1-O2	x 2	2.858(9)	Sr4-O3	x 2	2.58(1)
Sr1-O4	x 2	2.578(8)	Sr4-O4	x 2	2.86(1)
Sr1-O5	x 2	2.567(9)			
Sr2-Cl		3.218(4)	B1-O2		1.37(2)
Sr2-Cl		2.881(2)	B1-O3		1.42(2)
Sr2-O2		2.62(1)	B1-O5		1.36(2)
Sr2-O3		2.469(9)			
Sr2-O4		2.60(1)	B2-O1		1.34(2)
Sr2-O5		2.556(9)	B2-O4	x 2	1.40(2)
Sr2-O5		2.397(9)			
Sr3-O1	x 2	2.669(1)			
Sr3-O2	x 2	2.70(1)			
Sr3-O3	x 2	2.451(9)			
Sr3-O4	x 2	2.82(1)			

Cl-Sr1-Cl	79.82(6)	O3-Sr2-O4	69.8(3)	O1-Sr4-O3	74.9(3)
Cl-Sr1-O2	89.7(2)	O3-Sr2-O4	74.7(3)	O2-Sr4-O3	93.2(3)
Cl-Sr1-O4	67.3(2)	O3-Sr2-O5	99.0(3)	O2-Sr4-O3	75.6(3)
Cl-Sr1-O5	69.0(2)	O4-Sr2-O4	50.5(3)	O2-Sr4-O4	84.2(3)
O1-Sr1-O2	71.8(2)	O4-Sr2-O5	80.4(3)	O3-Sr4-O4	71.0(3)
O1-Sr1-O4	75.7(2)	O5-Sr2-O5	77.0(3)	O4-Sr4-O4	92.7(4)
O2-Sr1-O4	84.4(3)				
O2-Sr1-O4	86.7(4)	O1-Sr3-O1	88.20(6)	O2-B1-O3	119(1)
O2-Sr1-O5	51.8(2)	O1-Sr3-O2	72.4(3)	O2-B1-O5	122(1)
O2-Sr1-O4	86.7(4)	O1-Sr3-O3	77.7(3)	O3-B1-O5	119(1)
O4-Sr1-O5	77.7(3)	O1-Sr3-O4	69.6(3)		
		O1-Sr3-O4	51.3(3)	O4-B2-O4	120(1)
Cl-Sr2-Cl	81.94(6)	O2-Sr3-O4	85.4(3)	O1-B2-O4	120.1(7)
Cl-Sr2-O4	89.2(2)	O2-Sr3-O3	75.8(3)		
Cl-Sr2-O4	65.5(2)	O2-Sr3-O3	91.4(3)		
Cl-Sr2-O2	107.9(2)	O3-Sr3-O4	71.1(3)		
Cl-Sr2-O4	65.5(2)	O4-Sr3-O4	94.7(4)		
Cl-Sr2-O4	105.9(2)				
Cl-Sr2-O5	73.2(2)	O1-Sr4-O1	86.70(6)		
Cl-Sr2-O5	68.6(2)	O1-Sr4-O2	73.5(3)		
O2-Sr2-O3	56.5(3)	O1-Sr4-O4	68.4(3)		
O2-Sr2-O5	93.8(3)	O1-Sr4-O4	50.5(3)		

Table 2.3. Anisotropic displacement coefficients for $\text{Sr}_5(\text{BO}_3)_3\text{Cl}$.

	U_{11}	U_{22}	U_{33}	U_{12}	U_{13}	U_{23}
Sr1	0.0061(7)	0.0086(7)	0.0078(6)	0	0	0.0005(8)
Sr2	0.0070(5)	0.0074(5)	0.0093(4)	0.0003(5)	0.0007(4)	0.0004(5)
Sr3	0.0090(7)	0.0067(7)	0.0058(7)	0	0.0009(6)	0
Sr4	0.0083(7)	0.0090(8)	0.0067(7)	0	0.0000(6)	0
Cl	0.012(2)	0.012(2)	0.008(2)	0	0.000(2)	0
O1	0.007(5)	0.008(5)	0.011(4)	0	0	0.003(6)
O2	0.007(4)	0.013(4)	0.009(4)	0.002(3)	0.004(4)	0.005(4)
O3	0.006(4)	0.011(4)	0.020(4)	0.004(3)	0.000(4)	0.003(4)
O4	0.014(4)	0.020(5)	0.015(4)	0.000(5)	0.004(3)	0.002(5)
O5	0.007(4)	0.008(5)	0.017(4)	0.004(4)	0.004(4)	0.002(3)
B1	0.010(6)	0.006(6)	0.017(9)	0.004(5)	0.003(5)	0.005(5)
B2	0.002(2)					

Discussion

The structure is a complex three-dimensional framework of 7-, 8-, and 9-coordinate Sr-centered polyhedra that share O and Cl vertices and BO_3 triangular planes (See Figure 2.1). The distorted $\text{Sr}(1)\text{O}_7\text{Cl}_2$ tricapped trigonal prisms zigzag along the **c**-axis via corner-sharing Cl atoms. Nonacoordinate Sr centers are common in borates as evidenced by their presence in the compound $\text{Sr}_3\text{B}_2\text{O}_6$ (12) and the large oxide family of general formula $\text{A}_6\text{MM}'(\text{BO}_3)_6$, $\text{A} = \text{Sr}$ (13). These prisms also share faces with the distorted $\text{Sr}(2)\text{O}_5\text{Cl}_2$ tetragonal base-trigonal base polyhedra and with the two crystallographically distinct $\text{Sr}(3)\text{O}_8$ and $\text{Sr}(4)\text{O}_8$ square antiprisms. In addition, the SrO_7Cl_2 prisms share two O1-O2-O4 faces with face-condensed $\text{Sr}(3)\text{O}_8$ and $\text{Sr}(4)\text{O}_8$ antiprisms.

The $\text{Sr}(2)\text{O}_5\text{Cl}_2$ sites approximate tetragonal base-trigonal base heptacoordination analogous to the SrO_7 polyhedra found in $\alpha\text{-Sr}_2\text{Cu}(\text{BO}_3)_2$ (14). Their similarity persists with the presence of an additional long Sr-O interaction of 3.014 Å in $\text{Sr}_5(\text{BO}_3)_3\text{Cl}$ that is comparable to a similar weak interaction of 3.11 Å in the strontium copper borate. If this O4 atom is regarded as interacting with atom Sr2, then the local atomic geometry would be an irregular undecahedron. Assuming seven-fold coordination, however, these sites share faces with one another, comprising two Cl atoms and one O atom, and bridge via BO_3 triangles to $\text{Sr}(1)\text{O}_7\text{Cl}_2$ polyhedra.

The antiprisms share mutual O1-O4 rectangular bases in the **ac**-plane and adjoin O1-O2-O3 triangular faces in the **ab**-plane to form double chains extending in the **c**-direction. B2 atoms occupy triangular sites along edges of the rectangular bases, rendering additional coupling of the chains along the **c**-axis as illustrated in Figure 2.2. The chains are linked to one another, in part, by the bridge atom B1. Each Sr atom is displaced from the mean position between the rectangle of atoms O1 and O4 and the rectangle of atoms O2 and O3. Atoms Sr3 and Sr4 are displaced by 1.87 and 1.84 Å, respectively, from the former rectangle and 0.86 and 0.81 Å, respectively, from the latter. These distortions compare to the square

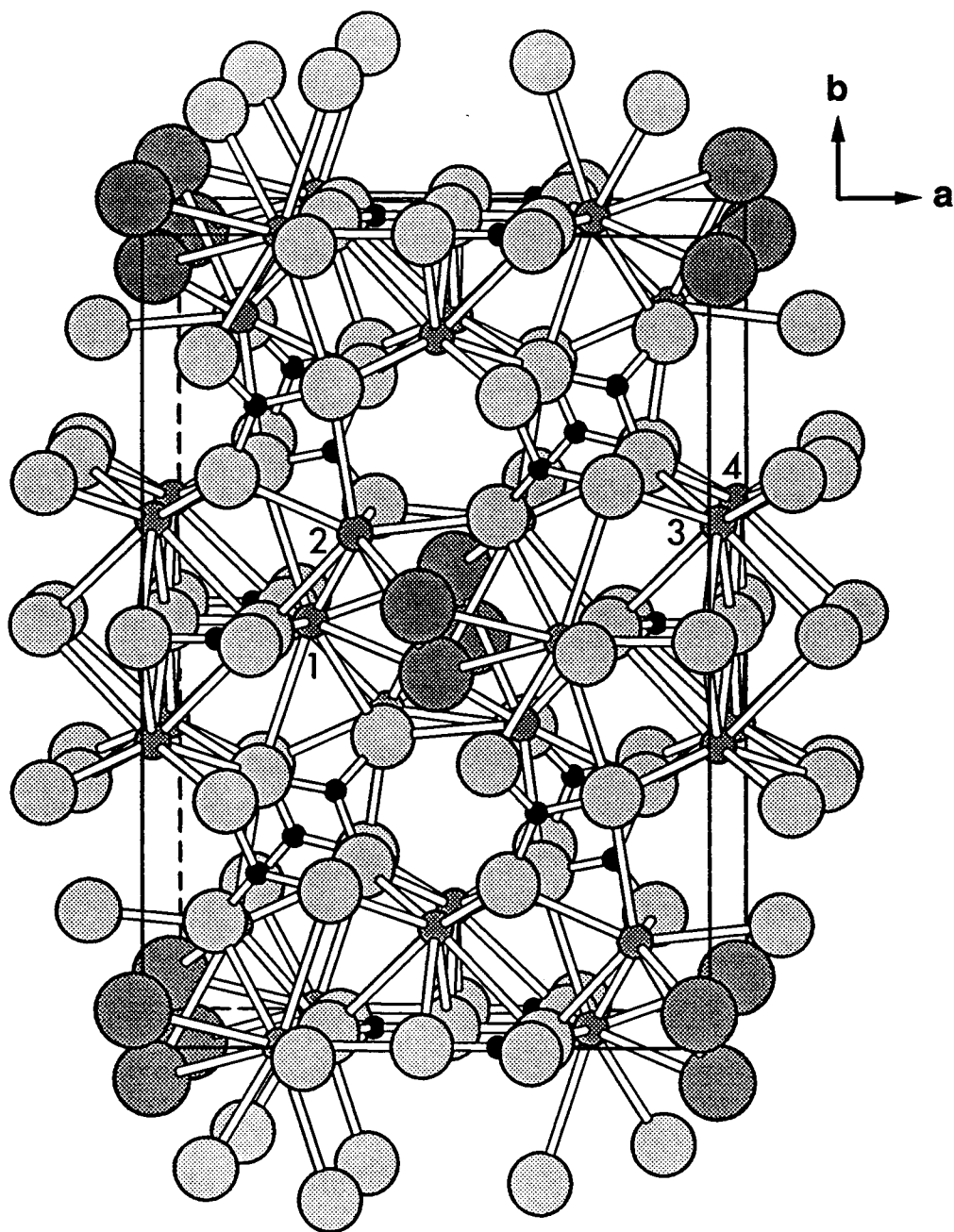


Figure 2.1.

Schematic unit cell drawing of $\text{Sr}_5(\text{BO}_3)_3\text{Cl}$. The small shaded circles represent Sr atoms, the large dark circles represent Cl atoms, the large pale circles represent O atoms, and the small black circles represent B atoms, here, and in ensuing figures. The four crystallographically distinct Sr atoms are numerically labeled.

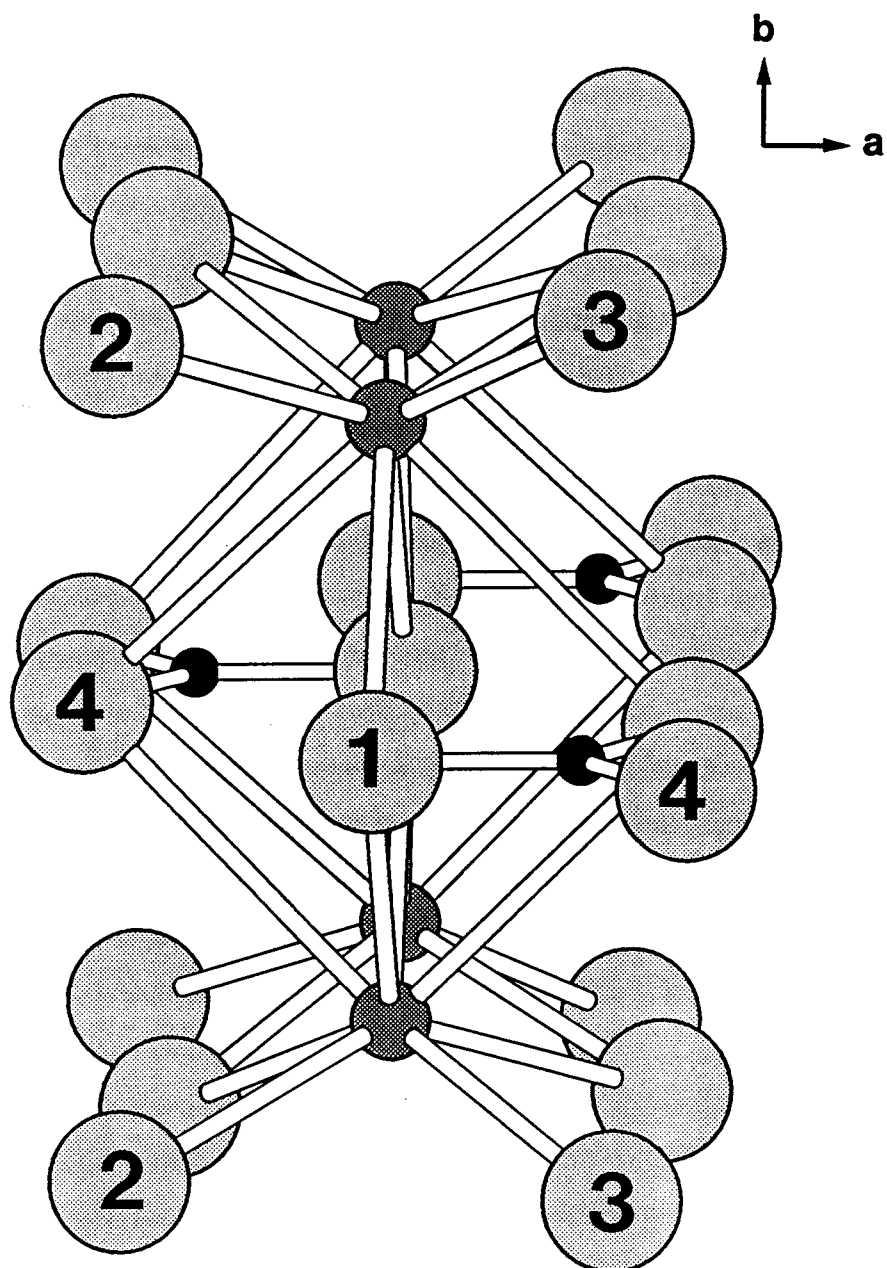


Figure 2.2. Sr3- and Sr4-centered distorted square antiprisms in $\text{Sr}_5(\text{BO}_3)_3\text{Cl}$.

antiprismatic site in β - $\text{Sr}_2\text{Cu}(\text{BO}_3)_2$, where the span between one plane of O atoms and the central Sr atom is 1.95 Å while the other average distance is 0.90 Å (14).

The chloride anions are surrounded by six Sr atoms, forming face-sharing distorted octahedral chains along the *c*-axis (Figure 2.3). The distortion of the chain can be described as triangular Sr faces alternately canted with respect to the zigzag line of Cl atoms, the deviation observed approximately in the *b*-direction. In contrast, the F atom in $\text{Ca}_5(\text{BO}_3)_3\text{F}$ (15) is positioned in a distorted tetrahedral environment of Ca atoms, and Mg atoms triangularly surround the central F atom in $\text{Mg}_5(\text{BO}_3)_3\text{F}$ (16).

The B1- and B2- centered borate groups are regular with O-B-O bond angles near 120° and average B-O distances of 1.38(3) Å for B1-O and 1.36(3) Å for B2-O. The bond angles and distances observed for both BO_3 groups are typical of orthoborates (17). Because $\text{Sr}_5(\text{BO}_3)_3\text{Cl}$ is not centrosymmetric, it should function as an optical second harmonic generator. By applying the free anionic group model to the orientations of the orthoborate groups, we have computed the *d* coefficient for the material. The microscopic hyperpolarizability coefficient for the orthoborate group was determined from the coefficient $d_{11}^{20} = 2.4$ pm/V assumed for the compound $\text{YAl}_3(\text{BO}_3)_4$ (18). The coefficient $d_{14}^{20} = 0.67$ pm/V was then calculated from the structural results of the title compound by assuming each BO_3^- group exhibits D_{3h} symmetry.

$\text{Sr}_5(\text{BO}_3)_3\text{Cl}$ is a thermodynamically stable phase in the $\text{SrO-B}_2\text{O}_3\text{-SrCl}_2$ system with a melting point of 1140 K as determined from differential thermal analysis data from a computer-interfaced Harrop DT 726 thermal analyzer. Two other borate halides represented by the general formula $\text{A}_5(\text{BO}_3)_3\text{X}$ (A = alkaline earth, X = halide) have been reported — $\text{Ca}_5(\text{BO}_3)_3\text{F}$ and $\text{Mg}_5(\text{BO}_3)_3\text{F}$ — but neither compound coincides with the structure of the title compound. The former assumes a monoclinic framework, space group Cm, where the smaller Ca cations prefer distorted octahedral environments. The Mg atoms also adopt a six-fold coordination in $\text{Mg}_5(\text{BO}_3)_3\text{F}$, but this compound orders in the noncentrosymmetric orthorhombic space group, Pna2₁. In comparison, the larger Sr atoms in the title

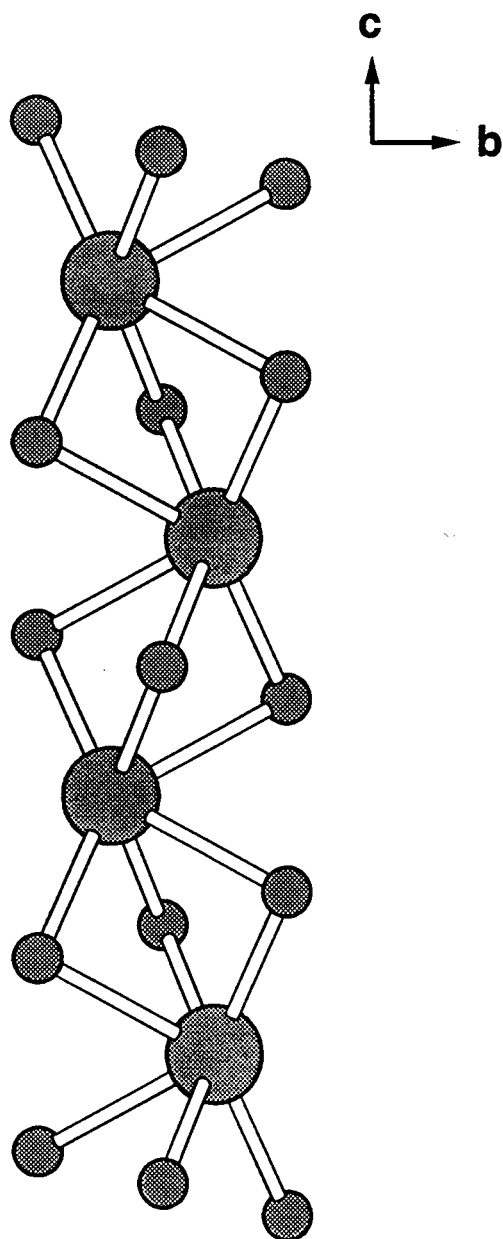


Figure 2.3. Chain of Cl-centered distorted octahedra extending along the 2_1 screw axis in $\text{Sr}_5(\text{BO}_3)_3\text{Cl}$.

structure require 7-, 8-, and 9-coordinate environments. Despite the increase in cationic coordination number and the associated density decrease in $\text{Sr}_5(\text{BO}_3)_3\text{Cl}$, its extensive face-sharing polyhedra maintain a number density of BO_3 groups per unit cell volume comparable with the lighter cation edge- and corner-sharing $\text{Ca}_5(\text{BO}_3)_3\text{F}$ and $\text{Mg}_5(\text{BO}_3)_3\text{F}$ structures.

Acknowledgements

This research was supported by the US National Science Foundation, Solid-State Chemistry Program (DMR-88144332). Acknowledgement is made to the Donors of The Petroleum Research Fund, administered by the American Chemical Society, for partial support of this research. D.A.K. thanks the Alfred P. Sloan Research Foundation for a fellowship, 1989-91.

References

1. K. Takahashi, K. Kohda, J. Miyahara, Y. Kanemitsu, K. Amitani, S. Shionoya *J. Luminescence*, **31 & 32**, (1984) 266.
2. A. Meijerink, G. Blasse, L. Struye *Mater. Chem. Phys.*, **21**, (1989) 261.
3. I. Schütz, I. Freitag, R. Wallenstein *Optics Comm.*, **77(2,3)**, (1990) 221.
4. D. Eimerl, L. Davis, S. Velsko, E. Graham, A. Zalkin *J. Appl. Phys.*, **62**, (1987) 1968.
5. S. Velsko, Lawrence Livermore National Laboratory, (1988) private communication.
6. G. Blasse, A. Meijerink, D. Terrell, L. Neyens (1988) **Eur. Pat. Appl. EP 353,805** (Cl. C09K11/86), 07 Feb 1990, EP Appl. 88/201,693, 05 Aug 1990; 20 pp.
7. K. Yvon, W. Jeitschko, E. Parthe *J. Appl. Cryst.*, **10**, (1977) 73.
8. Molecular Structure Corporation, 3200A Research Forest Drive, The Woodlands, TX 77381, USA.
9. G.M. Sheldrick *Crystallographic Computing 3*, Oxford: Oxford University Press, (1985) 175-189.
10. *International Tables for X-ray Crystallography*, Vol. IV, Birmingham: Kynoch Press (1974). (Present distributor: Kluwer Academic Publishers, Dordrecht.)
11. N. Walker, D. Stuart *Acta Crystallogr., Sect. A*, **39**, (1983) 158.
12. L. Richter, F. Müller *Z. Anorg. Allg. Chem.*, **467**, (1980) 123.
13. K.I. Schaffers, P.D. Thompson, T. Alekel III, J.R. Cox, D.A. Keszler *Chem. of Mat.*, to be published.
14. R.W. Smith, D.A. Keszler *J. Solid State Chem.*, **81**, (1989) 305.
15. L. Shirong, H. Qingzhen, Z. Yifan, J. Aidong, C. Chuangtain *Acta Crystallogr., Sect. C* **45**, (1989) 1861.

16. A. Brovkin, L. Nikishova *Kristallographia*, **20**, (1975) 415.
17. R. Shannon, C. Prewitt *Acta Crystallogr., Sect. B*, **25**, (1968) 925.
18. A. Filimonov, N. Leonyuk, L. Meissner, T. Timchenko, I. Rez *Kristall und Technik*, **9(1)**, (1974) 63-66.

CHAPTER 3

New Strontium Borate Halides
 $\text{Sr}_5(\text{BO}_3)_3\text{X}$, X = F or Br

Theodore Alekel III and Douglas A. Keszler*

Department of Chemistry and
Center for Advanced Materials Research
Oregon State University
Gilbert Hall 153
Corvallis, OR 97331-4003

Inorganic Chemistry, **32**(1), (1993) 101.

Abstract

Two new strontium borate halides, $\text{Sr}_3(\text{BO}_3)_3\text{F}$ and $\text{Sr}_5(\text{BO}_3)_3\text{Br}$, have been synthesized and structurally characterized by single crystal X-ray diffraction techniques. The two compounds are structurally similar, 3-dimensional frameworks of interconnecting Sr polyhedra and orthoborate groups, but do not crystallize with the same symmetry. The fluoride forms in the centrosymmetric orthorhombic space group, Pnma , with cell parameters $a = 7.220$ (2), $b = 14.092$ (2), $c = 9.810$ (1) Å, and $Z = 4$. Three distinct Sr-centered O environments exist in this structure: distorted SrO_7F undecahedra, irregular SrO_6F coordination sites, and distorted SrO_8 square antiprisms, monocapped by a very weak Sr—O interaction of 3.04 Å. A trio of Sr atoms caps each F atom to form a shallow pyramid. $\text{Sr}_5(\text{BO}_3)_3\text{Br}$ crystals are also orthorhombic in the noncentrosymmetric space group $\text{C}222_1$ with $a = 10.002$ (2), $b = 14.197$ (1), $c = 7.458$ (2) Å, and $Z = 4$. Four Sr-centered polyhedra join to each other: distorted SrO_7Br_2 tricapped trigonal prisms, irregular octacoordinate SrO_6Br_2 undecahedra, and two dissimilar SrO_8 distorted square antiprisms. Six Sr nearest neighbors bond to each Br atom and define Sr octahedra that share triangular faces along the c direction to form zigzag chains.

Introduction

For many years haloapatites $[(\text{Ca},\text{Sr})_5(\text{PO}_4)_3(\text{Cl},\text{F})]$ have been employed as host materials in commercial phosphors for fluorescent lighting (1). Their robust physical properties coupled with high quantum efficiencies have made them standard phosphor hosts for optically active dopants such as Sb^{3+} , Mn^{2+} , and Eu^{2+} (2).

Borates also intrinsically possess characteristics that are advantageous for optical materials, which include high photon flux damage thresholds and wide optical transparency windows (3). The commercial material $(\text{Ce},\text{Gd})\text{MgB}_5\text{O}_{10}:\text{Tb}^{3+}$, which converts 254 nm Hg discharge energy into green light with 93% quantum efficiency (2,4) illustrates the effectiveness of borate phosphor hosts. In this report we describe two new borates that stoichiometrically mimic the apatite compounds. The new materials $\text{Sr}_5(\text{BO}_3)_3\text{F}$ and $\text{Sr}_5(\text{BO}_3)_3\text{Br}$ have emerged from our study of the $\text{SrO}-\text{B}_2\text{O}_3-\text{SrX}_2$ ($\text{X} = \text{F}, \text{Cl}, \text{Br}$) phase systems (5).

Here, we describe the structures of these compounds, each of which orders in separate space groups, and note their similarities. The previously reported material $\text{Ca}_5(\text{BO}_3)_3\text{F}$ (6), which differs structurally from the title compounds, has been compared to fluorapatite, $\text{Ca}_5(\text{PO}_4)_3\text{F}$, illustrating the positional substitution of BO_3 triangles for PO_4 tetrahedra (7). These comparisons will be extended here with a consideration of the new Sr compounds.

Experimental Section

Synthesis. A microcrystalline powder of $\text{Sr}_5(\text{BO}_3)_3\text{Br}$ was synthesized by using standard high-temperature solid-state techniques and high purity reactants. $\text{Sr}_3(\text{BO}_3)_2$ was a laboratory-synthesized precursor formulated by heating a stoichiometric mixture of $\text{Sr}(\text{NO}_3)_2$ (ÆSAR, ACS grade) and anhydrous B_2O_3 (ÆSAR, 99.98%) at 900 K for 1 h, followed by additional heating at 1273 K for 24 h. A stoichiometric mixture of this reactant and anhydrous SrBr_2 (ALFA, 99%) was heated in a Pt crucible at 1073 K for 20 h. $\text{Sr}_5(\text{BO}_3)_3\text{Br}$ crystals were grown in a Pt crucible in air by cooling a melt of composition 57.0 SrO: 12.8 B_2O_3 : 30.2 SrBr_2 mol% at a rate of 8 K/h from 1200 to 1077 K, then rapidly cooling to room temperature. A clear prism of approximate dimensions 0.1 x 0.1 x 0.1 mm was physically separated from the matrix for single-crystal measurements described henceforward.

Because of the integrity of commercial SrF_2 at temperatures below 1200 K, we could not produce single phase $\text{Sr}_5(\text{BO}_3)_3\text{F}$ by using the preceding synthesis temperature. However, reacting freshly prepared SrF_2 [$\text{Sr}(\text{NO}_3)_2$ heated under $\text{HF}(\text{g})$ at 800 K for 2-3 h] with $\text{Sr}_3(\text{BO}_3)_2$ at 1450 K in a Pt crucible afforded the title borate fluoride. Crystals were grown by melting the reactants at 1500 K and then cooling to 1000 K at the rate of 10 K/h. An alternate precipitation method was also found to be successful: $\text{Sr}(\text{NO}_3)_2$ and H_3BO_3 (ÆSAR, ACS grade) were dissolved in water with 10 mL of a 8% (w/v) $\text{HF}(\text{aq})$, followed by gentle evaporation at ~350 K to dryness. Crystals were prepared by melting the resulting precipitate in a Pt crucible in air and cooling at 8 K/h from 1373 to 1223 K. An irregularly-shaped prism of approximate dimensions 0.15 x 0.10 x 0.20 mm from this crystal growth method was culled for X-ray study.

Crystallographic Study. The selected crystals were mounted on glass fibers and analyzed on a Rigaku AFC6R single crystal X-ray diffractometer. The $\text{Sr}_5(\text{BO}_3)_3\text{F}$ unit cell parameters were accurately derived by a least-squares refinement of 19 automatically-centered reflections in the angular range $2\theta < 2\theta$

$< 48^\circ$. For the compound, $\text{Sr}_5(\text{BO}_3)_3\text{Br}$ unit cell parameters were determined from 20 reflections within the limits $30 < 2\theta < 36^\circ$. Intensity data for each borate halide were collected at room temperature by using the ω - 2θ scan technique with a rate of $16^\circ(\omega)/\text{min}$ and peak widths within $1.50 + 0.30 \tan \theta$. Three standard reflections demonstrated crystalline stability of $\text{Sr}_5(\text{BO}_3)_3\text{F}$ during the data collection, amounting to 1.6% maximum relative intensity deviation. 1812 unique reflections ($F_o^2 > 3\sigma(F^2)$) were collected with $\sin \theta_{\text{max}}/\lambda = 0.807 \text{ \AA}^{-1}$ and the associated indices, $0 \leq h \leq 14$; $0 \leq k \leq 19$; $0 \leq l \leq 10$. Three standard peak orientations, measured every 200 reflections, indicated no intensity deterioration of $\text{Sr}_5(\text{BO}_3)_3\text{Br}$ throughout the collection, waiving the need for decay corrections. Of the 4764 measured reflections in the range $2 \leq 2\theta \leq 70^\circ$ with corresponding indices $0 \leq h \leq 15$, $0 \leq k \leq 22$, $-11 \leq l \leq 11$, a total of 2532 were observed [$F_o^2 > 3\sigma(F^2)$]. General crystallographic parameters are listed in Table 3.1.

The atomic arrangements in the title compounds were determined by using programs contained in TEXSAN crystallographic software (8) with all calculations performed on a Digital μ VAX II computer. The $\text{Sr}_5(\text{BO}_3)_3\text{F}$ data exhibit systematic absences $0kl$: $k+1 = 2n + 1$; $hk0$: $h = 2n + 1$ that are consistent with the two space groups, $\text{Pn}2_1\text{a}$ and Pnma . Intensity statistics and the succeeding refinement support the assignment of the centric group. The Sr atoms were located by using the direct methods program SHELXS (9) and the anions and B atoms were positioned from successive analysis of difference electron density maps. Following refinement with isotropic displacement coefficients, the data were corrected for absorption with the program DIFABS (10) and averaged ($R_{\text{int}} = 0.10$). The final refinement cycle with 825 observed F_o values, where $I > 3\sigma(I)$, included anisotropic displacement coefficients for the three heavy Sr atoms. The weighting scheme was based on counting statistics [$w = 1/\sigma^2(F_o)$] with $p = 0.05$. F_{calc} was derived from predetermined neutral scattering factors and corrected for anomalous scattering with calculated f' and f'' values from *International Tables for X-ray Crystallography* (1974, Vol. IV). The height of the largest peak in the final difference electron density map was 1.28% of the Sr2 atom. For $\text{Sr}_5(\text{BO}_3)_3\text{Br}$, the noncentrosymmetric

Table 3.1. Crystallographic Data for Sr₅(BO₃)₃F and Sr₅(BO₃)₃Br

empirical formula	Sr ₅ (BO ₃) ₃ F	Sr ₅ (BO ₃) ₃ Br
formula weight, amu	633.52	694.43
space group	Pnma (#62)	C222 ₁ (#20)
a, Å	7.220(2)	10.002(2)
b, Å	14.092(2)	14.197(1)
c, Å	9.810(1)	7.458(2)
V, Å ³	998.1(5)	1059.0(3)
Z	4	4
d _{calc} g/cm ³	4.215	4.355
F ₀₀₀	1144	1248
radiation	Mo Kα (λ = 0.71069 Å)	
temperature, K	298	298
scan type	ω-2θ	ω-2θ
scan rate	16	16
scan range	2 - 70	2 - 60
linear abs coeff μ, cm ⁻¹	258.0	280.2
transmission factors	0.76 - 1.23	0.73 - 1.49
total no. measured data	4764	1812
p factor	0.03	0.05
no. Observations F _o ² ≥ 3σ(F _o ²)	825	692
no. of variables	56	83
R, wR ^a	0.053, 0.057	0.057, 0.063

$$^a R = \frac{\sum ||F_o| - |F_c||}{\sum |F_o|} \quad wR = \sqrt{\frac{\sum w(|F_o|^2 - |F_c|^2)^2}{\sum w|F_o|^4}}$$

space group $C222_1$ is assigned unambiguously on the basis of the absences **hkl**: $h+k = 2n + 1$ and **00l**: $l = 2n + 1$. Direct methods were employed to pinpoint the Sr atoms, while the remaining atoms were located from analysis of difference electron density maps. After the isotropic refinement of the best-fit $Sr_3(BO_3)_3Br$ enantiomer, the DIFABS empirical absorption correction was performed and ensued with a final least-squares refinement of $|F|$ with anisotropic displacement coefficients for every atom, barring B2. The final difference electron density map revealed a minimum peak of $-4.22 e \text{ \AA}^{-3}$ and a maximum peak of $6.51 e \text{ \AA}^{-3}$, corresponding to 3.93% of the Sr3 atom peak intensity. The positional and thermal parameters for both structure solutions are outlined in Table 3.2.

Table 3.2. Positional parameters for Sr₅(BO₃)₃F and Sr₅(BO₃)₃Br

	Sr ₅ (BO ₃) ₃ F				Sr ₅ (BO ₃) ₃ Br ^a			
	x	y	z	B _{eq} ^b	x	y	z	B _{eq}
Sr1	0.2887(3)	1/4	0.4814(2)	0.33 (6)	0.2404(3)	0	0	1.5 (1)
Sr2	0.2490(2)	0.3801(1)	0.1260(1)	0.54 (4)	0.8665(2)	0.1289(1)	0.0645(3)	1.3 (1)
Sr3	0.0286(2)	0.3880(1)	0.7470(2)	0.36 (4)	1/2	0.1355(2)	1/4	1.2 (1)
Sr4	—	—	—	—	1/2	0.8620(2)	1/4	1.4 (1)
F/Br	0.135(2)	1/4	0.265(1)	0.8 (2)	0	0.9429(4)	1/4	2.4 (2)
O1	0.283(2)	1/4	0.748(1)	0.3 (2)	0.492(2)	0	0	1.3 (7)
O2	0.774(2)	0.4301(7)	0.930(1)	0.8 (2)	0.330(1)	0.192(1)	0.988(2)	1.4 (6)
O3	0.281(1)	0.4543(7)	0.8956(8)	0.6 (1)	0.644(1)	0.199(1)	0.020(2)	1.5 (6)
O4	0.119(2)	1/4	0.955(2)	0.7 (2)	0.305(1)	0.997(1)	0.659(2)	1.9 (6)
O5	0.910(2)	0.0902(9)	0.153(1)	1.0 (2)	0.166(1)	0.146(1)	0.112(2)	1.5 (6)
O6	0.445(2)	1/4	0.963(2)	0.9 (3)	—	—	—	—
B1	0.799(2)	0.040(1)	0.061(1)	0.4 (2)	0.199(2)	0.212(2)	0.028(3)	1.0 (1)
B2	0.286(3)	1/4	0.891(2)	0.1 (3)	0.629(3)	0	0	0.8 (5)

^a To convert the C22₁ cell to the Sr₅(BO₃)₃F Pnma cell, use the following translational transformation:

$${}^b B_{eq} = (8\pi^2/3) \sum_i \sum_j U_{ij} a_i^* a_j^* a_i \cdot a_j$$

$$\begin{bmatrix} 0 & 0 & 1 \\ 0 & -1 & 0 \\ 1 & 0 & 0 \end{bmatrix} + \begin{bmatrix} 0.2886 \\ 0.2500 \\ 0.4710 \end{bmatrix}$$

Results

$Sr_5(BO_3)_3F$. Figure 3.1 represents the unit cell of the compound. The structure is an intricate 3-dimensional framework of interconnecting Sr-centered polyhedra and BO_3 triangles. The framework can be simply described as two adjoined moieties that proliferate along the b axis: a double chain of Sr3-centered monocapped square antiprisms with B2 atoms situated amongst the special-position O atoms and secondly, rows of F atoms encircled by Sr1 / Sr2 polyhedra. The B1-centered borates assist in coupling the two moieties together.

The three Sr atom types possess distinctive coordination environments. The Sr1 atom assumes a distorted undecahedron coordinated by seven O atoms and one F atom. It shares O5 ··· O6 ··· F faces with two Sr2 atoms and two O1 ··· O2 ··· O6 faces with two Sr3 atoms. In addition, Sr(1)O₇F shares edges with two B1 borates and corners to three B2 borates. The irregular 7-coordinated Sr2 site also contains an F atom in its periphery, along with six O atoms. Unlike the Sr1 site, Sr(2)O₆F couples to itself by sharing O4 ··· O6 ··· F faces to two other Sr2 atoms. It also has an O3 ··· O4 edge in common with an Sr3 atom and a common edge with the B2 borate, resting on a mirror plane. Additional borate connectivity is realized by three B1 groups that share corners with Sr(2)O₇F. The third Sr type is a distorted square antiprism that is monocapped by a weak O5 interaction. The Sr(3)O₈+O polyhedra share mutual O1 ··· O4 ··· O6 ··· O1 square bases in the ac plane and triangular O1 ··· O2 ··· O3 faces in the bc plane, as viewed in Figure 3.2. A B1-centered borate shares the edge of O3 and the weakly-bound O5, while B2 atoms occupy triangular sites along edges of the aforementioned condensed square bases.

Selected bond distances and angles for $Sr_5(BO_3)_3F$ are presented in Table 3.3. For the Sr1 site, the Sr—O bond lengths range from 2.47 to 2.75 Å, bearing an average distance of 2.64 (3) Å that closely matches the calculated crystal radius of 2.63 Å (11). The average Sr2—O distance of 2.62 (2) Å, encompassing a spread of 2.49 to 2.81 Å, also correlates to the expected value. Possessing only O nearest

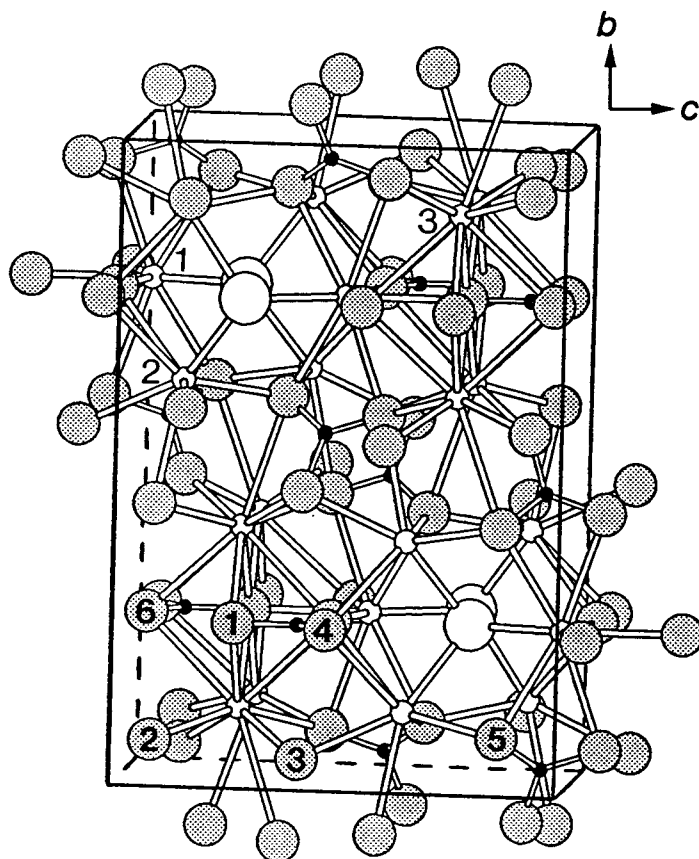


Figure 3.1. Schematic unit-cell drawing of $\text{Sr}_5(\text{BO}_3)_3\text{F}$. The small open circles represent Sr atoms, the large shaded circles represent O atoms, the small black circles represent B atoms, and the large open circles represent F atoms. (Atomic legend used in subsequent figures, unless noted.) The Sr and O atoms are numerically labeled.

Table 3.3. Selected Bond Distances and Angles for $\text{Sr}_5(\text{BO}_3)_3\text{F}$.

bond distances, Å		bond angles, deg	
Sr1—F	2.40 (1)	F—Sr1—O2	105.6 (2)
Sr1—O1	2.61 (1)	O1—Sr1—O2	71.1 (2)
Sr1—O2	2.69 (1)	O1—Sr1—O4	76.1 (5)
Sr1—O2	2.69 (1)	O2—Sr1—O4	87.8 (3)
Sr1—O4	2.47 (1)	O4—Sr1—O5	79.3 (3)
Sr1—O5	2.75 (1)	F—Sr1—O5	73.9 (3)
Sr1—O5	2.75 (1)	O2—Sr1—O5	52.8 (3)
Sr1—O6	2.54 (2)	O2—Sr1—O6	83.9 (3)
Sr2—F	2.43 (1)	F—Sr2—O4	73.4 (4)
Sr2—O2	2.74 (1)	O2—Sr2—O3	54.2 (3)
Sr2—O3	2.50 (1)	O2—Sr2—O5	92.2 (3)
Sr2—O4	2.49 (1)	O3—Sr2—O4	75.5 (3)
Sr2—O5	2.49 (1)	O3—Sr2—O6	83.4 (3)
Sr2—O5	2.50 (1)	O4—Sr2—O5	80.7 (4)
Sr2—O6	2.81 (1)	O4—Sr2—O6	50.9 (4)
Sr3—O1	2.68 (1)	O1—Sr3—O1	85.7 (1)
Sr3—O1	2.63 (1)	O1—Sr3—O4	49.7 (4)
Sr3—O2	2.63 (1)	O2—Sr3—O3	91.5 (3)
Sr3—O2	2.55 (1)	O2—Sr3—O5	70.8 (3)
Sr3—O3	2.51 (1)	O3—Sr3—O5	86.1 (3)
Sr3—O3	2.46 (1)	O3—Sr3—O6	72.4 (3)
Sr3—O4	2.89 (1)	O4—Sr3—O6	95.6 (2)
Sr3—O5	3.04 (1)	O4—Sr3—O5	111.7 (3)
Sr3—O6	2.90 (1)	O2—Sr3—O6	79.4 (4)
B1—O2	1.36 (2)	O2—B1—O3	120 (1)
B1—O3	1.40 (2)	O2—B1—O5	122 (1)
B1—O5	1.41 (2)	O3—B1—O5	118 (1)
B2—O1	1.41 (2)	O1—B2—O4	117 (2)
B2—O4	1.35 (2)	O1—B2—O6	122 (2)
B2—O6	1.35 (3)	O4—B2—O6	121 (2)

neighbors, Sr3 atoms feature the widest variation of Sr—O distances (2.46 - 3.04 Å) and a greater average bond distance of 2.70 (3) Å.

The Sr(3)O₆ monocapped square antiprisms are moderately distorted with the Sr cation displaced from the center of the polyhedron along the *b* axis toward the capping O atom (See Figure 3.2). The O2 / O3 base is not planar, with respective *b* axis distances of 0.98 Å and 0.64 Å from the medial cation. The capping O5 atom interacts with the Sr3 atom (3.04 Å) through this base, so all of these are general position O atoms, accounting for the positional variability. However, the O1 · · O4 · · O6 · · O1 base is constrained to planarity by symmetry and situated 1.95 Å away from the Sr atom. The bases are not square, and their distortion can be described by an aspect ratio of the rectangular O—O side lengths projected onto the *ac* plane. For the O2 / O3 base, the ratio characterizing its deviation from a square is 1.12. Additionally, both bases are not rectangular; the O2 / O3 base exhibits an angle of 83.5° as a projected parallelogram. Because the other base contains three distinct O atoms, the O1 / O4 / O6 planar base assumes a quadrilateral shape with an average aspect ratio of 1.34.

The Sr—F bond lengths of 2.40 and 2.42 Å for Sr1 and Sr2 fall short of the calculated distances 2.56 and 2.51 Å, respectively, from Shannon's fluoride radii (12), indicating intimate bonding between the F atoms and both Sr types. Each F atom is surrounded by three bonding Sr atoms, but it does not reside in a triangular planar environment. Instead, the F atom is displaced from the center of the Sr1 · · Sr2 · · Sr2 triangle by 0.92 Å, forming two Sr1—F—Sr2 bond angles of 109.9 (4)° and one Sr2—F—Sr2 angle of 98.0 (4)°; the site symmetry is C_s.

The two borate types in Sr₅(BO₃)₃F assume regular orthoborate geometry but deviate from the ideal trigonal planar configuration. The B(1)O₃ group exhibits a slightly compressed B1—O2 bond length of 1.36 Å with an average distance of 1.39 (3) Å. The B2-centered triangle features C_{2v} point symmetry with an elongated B2—O1 bond length of 1.41 Å and an average distance of 1.37 (4) Å. Both borate types maintain O—B—O bond angles within 3° of the three-fold symmetrical 120° angle.

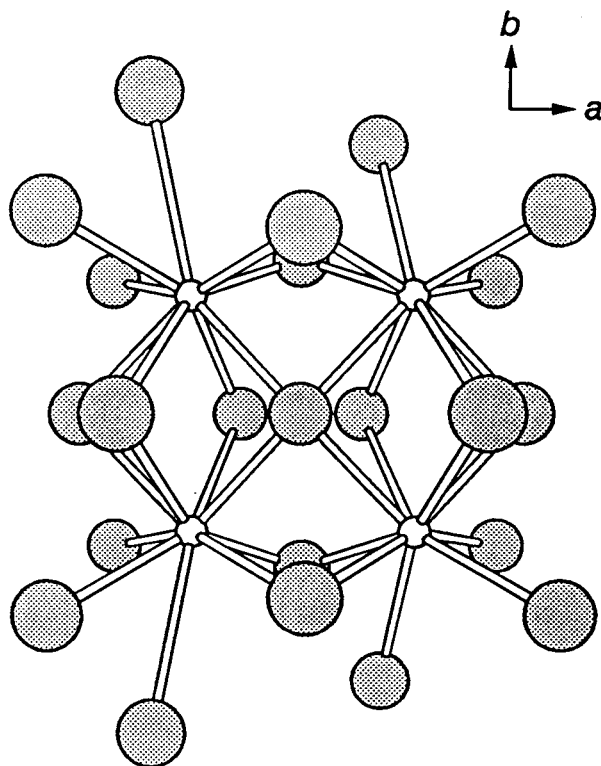


Figure 3.2. Sr3-centered distorted monocapped square antiprisms in $\text{Sr}_5(\text{BO}_3)_3\text{F}$, illustrating the three- and four-point face-sharing of the polyhedra. The monocapping interaction is 3.04 Å

$Sr_5(BO_3)_3Br$. The unit cell for the compound is depicted in Figure 3.3. It is isostructural to the $Sr_5(BO_3)_3Cl$ analogue, which we have previously described (5). At a casual glance it appears to be identical to the fluoride title compound, but upon continued examination, one recognizes a sizable shift in the halide position between the two. Six Sr atoms coordinate to each Br atom, constituting a distorted octahedron with opposite triangular Sr faces canted toward one another in the **b** direction; linked together by common faces, the octahedra form chains that extend along the *c* axis.

One of the Sr types that coordinates to the Br atom occupies a distorted tricapped trigonal prism [Sr(1)O₇Br₂]; it shares Br corners with adjacent Sr1 polyhedra along the 2₁ screw axis to form a zigzag chain. The nonacoordinate Sr1 centers share faces with Sr2-centered polyhedra and with the Sr(3)O₈ / Sr(4)O₈ distorted square antiprisms. Four irregular Sr(2)O₆Br₂ undecahedra also surround each Br atom, connecting to one another along the *c* axis via common Br · · Br · · O4 · · O4 and Br · · O5 · · O5 faces. The Sr2 polyhedra are linked together by B(1)O₃ borate groups in the **a** and **b** directions, as well.

The association between the Sr3 and Sr4 square antiprisms is similar to those arranged in $Sr_5(BO_3)_3F$, minus the additional monocapping O atom. Besides sharing triangular faces in the **ab** direction, the antiprisms incorporate B2 atoms that are confined in the *ac* plane square bases. Both Sr(3)O₈ and Sr(4)O₈ polyhedra share O2/O3 corners with B(1)O₃ triangles that bridge to Sr(2) undecahedra. The square antiprisms also adjoin with Sr(2)O₆Br₂ polyhedra via O3 · · O4 · · O4 faces.

Selected bond distances and angles are listed for $Sr_5(BO_3)_3Br$ in Table 3.4. Two Br atoms bond to Sr1 at a distance of 3.149 (2) Å, which exceeds the calculated length of 3.08 Å from crystal radii. The average Sr1—O bond length of 2.66 (3) Å compares to the 2.68 Å average span of the nonacoordinate SrO₉ site in $Sr_6YAl(BO_3)_6$ (13) and approximates the calculated distance of 2.63 Å. The broad range of Sr2—O bond lengths (2.43 - 3.04 Å) and the dissimilar Sr2—Br distances (3.266 and 2.884 Å) define the irregular shape of the Sr(2)O₆Br₂

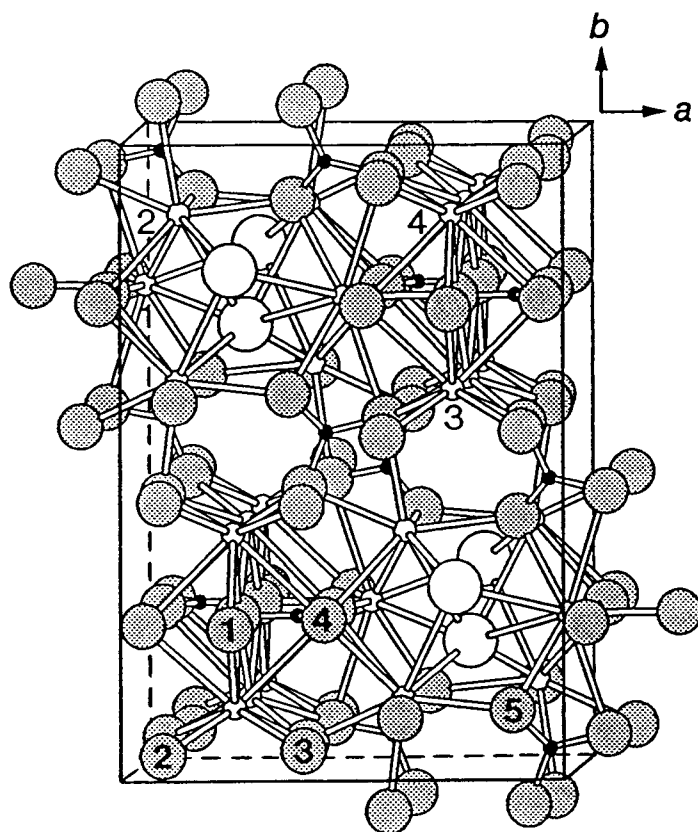


Figure 3.3. Schematic unit-cell drawing of $\text{Sr}_5(\text{BO}_3)_3\text{Br}$. The large open circles represent Br atoms; the Sr and O atoms are numerically labeled.

Table 3.4. Selected bond distances and angles for $\text{Sr}_5(\text{BO}_3)_3\text{Br}$

bond distances, Å		bond angles, deg	
Sr1—Br	3.149 (2)	Br—Sr1—O4	67.6 (3)
Sr1—Br	3.149 (2)	Br—Sr1—O5	68.8 (3)
Sr1—O1	2.51 (2)	O1—Sr1—O2	71.8 (2)
Sr1—O2	2.87 (1)	O2—Sr1—O4	84.8 (5)
Sr1—O2	2.87 (1)	O2—Sr1—O5	52.8 (4)
Sr1—O4	2.63 (1)	O4—Sr1—O4	151.3 (6)
Sr1—O4	2.63 (1)	O1—Sr1—O4	75.6 (3)
Sr1—O5	2.56 (1)	O4—Sr1—O5	78.0 (5)
Sr1—O5	2.56 (1)	O5—Sr1—O5	121.3 (6)
Sr2—Br	3.266 (5)	F—Sr2—O4	73.4 (4)
Sr2—Br	2.884 (3)	Br—Sr2—Br	82.5 (1)
Sr2—O2	2.60 (1)	O2—Sr2—O3	56.9 (3)
Sr2—O3	2.46 (1)	O3—Sr2—O4	70.5 (4)
Sr2—O4	3.04 (2)	Br—Sr2—O4	88.1 (3)
Sr2—O4	2.58 (2)	O4—Sr2—O4	49.1 (6)
Sr2—O5	2.53 (1)	Br—Sr2—O4	67.0 (3)
Sr2—O5	2.43 (1)	O4—Sr2—O5	80.9 (5)
Sr3—O1	2.680 (2)	O1—Sr3—O1	88.3 (1)
Sr3—O1	2.680 (2)	O1—Sr3—O4	70.3 (4)
Sr3—O2	2.71 (1)	O1—Sr3—O2	72.0 (4)
Sr3—O2	2.71 (1)	O2—Sr3—O4	86.3 (4)
Sr3—O3	2.42 (2)	O1—Sr3—O3	78.3 (4)
Sr3—O3	2.42 (2)	O2—Sr3—O3	91.2 (4)
Sr3—O4	2.79 (2)	O3—Sr3—O4	70.5 (4)
Sr3—O4	2.79 (2)	O4—Sr3—O4	95.0 (6)
Sr4—O1	2.706 (2)	O1—Sr4—O1	87.1 (1)
Sr4—O1	2.706 (2)	O1—Sr4—O4	68.7 (5)
Sr4—O2	2.57 (2)	O1—Sr4—O2	73.5 (4)
Sr4—O2	2.57 (2)	O2—Sr4—O4	85.5 (4)
Sr4—O3	2.63 (1)	O1—Sr4—O3	74.3 (4)
Sr4—O3	2.63 (1)	O2—Sr4—O3	94.1 (4)
Sr4—O4	2.87 (2)	O3—Sr4—O4	71.1 (5)
Sr4—O4	2.87 (2)	O4—Sr4—O4	91.8 (6)
B1—O2	1.38 (3)	O2—B1—O3	121 (2)
B1—O3	1.42 (3)	O2—B1—O5	120 (2)
B1—O5	1.41 (3)	O3—B1—O5	119 (2)
B2—O1	1.38 (4)	O1—B2—O4	119 (1)
B2—O4	1.35 (2)	O1—B2—O4	119 (1)
B2—O4	1.35 (2)	O4—B2—O4	122 (3)

undecahedron.

In its square antiprism the Sr3 atom is displaced from the O1 / O4 plane by 1.92 Å and from the O2 / O3 plane by 0.85 Å. The respective distances for the Sr4 atomic position are 1.96 and 0.82 Å. For the rectangular O1 / O4 base defining the Sr3 site (and the analogous Sr4 site parameters following parenthetically), the ratio characterizing its deviation from equal side lengths (projected onto the *ac* plane) is 1.32 (1.32), while the O2 / O3 base aspect ratio is 1.17 (1.19). Both projected bases are parallelograms with internal angles of 83.5° (83.5°) and 82.8° (89.0°) for the respective O1 / O4 and O2 / O3 bases. A regular square antiprism maintains a twist angle between the bases of 45°, but in the title bromide, the twist angle between the bases, as approximated by the *b* axis projected O3—Sr3—O4 (O1—Sr4—O2) angle, is 32° (41°).

The two B atoms constitute slightly distorted orthoborates [B(1)O₃ and B(2)O₃ exhibits C_s and C_{2v} symmetry, respectively] with collective O—B—O angles that range between 119 - 122° and bearing an average angle of 120 (4)°. The B1-centered triangle is larger than the symmetrical B2 borate; the average B1—O distance is 1.41 (3) Å, while the average B2—O length is 1.37 (3) Å.

Discussion

Symmetry Relationships. The atomic positions in the $\text{Sr}_5(\text{BO}_3)_3\text{Br}$ unit cell can be converted to closely match those of the centric title fluoride for direct comparison. By assigning the Sr1 atoms in each structure to be spatially equivalent, the cell transformation matrix and translational vector presented in Table 3.2 generate a cell analogous to $\text{Sr}_5(\text{BO}_3)_3\text{Br}$. The following discussion refers to the transformation of the title bromide atomic locations to the centric reference framework $\text{Sr}_5(\text{BO}_3)_3\text{F}$ ($\text{C}222_1 \Rightarrow \text{Pnma}$).

The distinction between the two structures is best illustrated by the position of the halides in each matrix. The Br atom is displaced from the corresponding F atom in $\text{Sr}_5(\text{BO}_3)_3\text{F}$ by roughly 10, 5, and 0.5 % of a unit cell dimension in the respective *a*, *b*, and *c* directions. The resulting changes in symmetry of this shift are twofold. First, the face-centering element of the $\text{C}222_1$ lattice disappears in the title fluoride Pnma arrangement; the zigzag chains of Br sites observed along the *c* screw axis, a consequence of the centering origin ($\frac{1}{2}, \frac{1}{2}, 0$), contrasts with the inline F atoms similarly viewed in $\text{Sr}_5(\text{BO}_3)_3\text{F}$. Second, a center of inversion in the title fluoride is not present in $\text{Sr}_5(\text{BO}_3)_3\text{Br}$. This is also visualized by the different halide positions between both structures. Because the F atom resides on a *b* axis mirror plane in Pnma , the four collective F atoms in the unit cell are centrosymmetrically related, unlike the zigzag Br atom arrangement in $\text{C}222_1$.

The other types of atomic shifts within the unit cells are henceforth described. The Sr3 cations exhibit a nominal difference in position between the two structures, but the Sr2 atoms exhibit a large spatial dissimilarity in the *ac* plane. Every O type notably differs in location between the two compounds, repositioned by 1 to 100 σ . The B2 atoms that fit within the shared faces of the square antiprisms show little deviation, but the bridging B1-centered borates show a small displacement in the *a* direction, nearly orthogonal to the triangular plane, causing a tilt of the BO_3 groups in the fluoride relative to the bromide that conforms to inversion symmetry of the Pnma cell.

Although many of the corresponding atomic positions between the two title structures are very similar, the aforementioned deviations modify several site geometries. As stated previously, the most dramatic observed difference involves the Sr sites that interact with F/Br atoms. Rather than possessing two halide atoms in its coordination sphere, as Sr1 and Sr2 in $\text{Sr}_5(\text{BO}_3)_3\text{Br}$, the Sr1 and Sr2 atoms in $\text{Sr}_5(\text{BO}_3)_3\text{F}$ bond with only one F atom per site. The next-nearest F atom to the Sr1 and Sr2 atoms is positioned 3.48 and 3.50 Å away, respectively — far too long to form a second Sr—F interaction per site.

Bond Valence Calculations. We were curious about the Sr coordination environments, especially the degree of bonding at the Sr3 site in the $\text{Sr}_5(\text{BO}_3)_3\text{F}$ structure. Brown's empirical bond valence method (14) was implemented to determine the extent of interaction between Sr and O or F atoms. Because no parameters are available for bonds between Sr and Br, we were limited to strictly Sr—O calculations for $\text{Sr}_5(\text{BO}_3)_3\text{Br}$; nevertheless, we were able to analyze each Sr type in the fluoride structure.

Each of the Sr atom sites in $\text{Sr}_5(\text{BO}_3)_3\text{F}$ experiences distinctive bonding geometries. The eight anions of the Sr(1) O_7F site decisively bond to the Sr atom, yielding a total valence sum of 1.97, which closely matches formal alkaline-earth divalency. In contrast, even though every nearest neighbor anion significantly interacts with the Sr2 atom, the lower number of surrounding anions at the Sr(2) O_6F site reduces the Sr atom, as evidenced by the calculated total bond valence of 1.85. The distorted square antiprismatic Sr3 site achieves a completed calculated valency of 2.02. However, a 3.04 Å Sr—O distance was initially questioned as an actual bond, but upon evaluation of the calculated Sr3 bond valency, we considered the 4.3 % contribution to be significant.

Of the two distorted square antiprismatic sites in the $\text{Sr}_5(\text{BO}_3)_3\text{Br}$ structure, the Sr3 atom valence determination suggests a completed bonding environment, possessing a calculated valency of 1.99. However, the structural dissimilarity of the Sr(4) O_8 antiprism from the Sr3 site affects the calculated valency of 1.67. No other anions reside nearby to make up the covalent deficiency, unlike the mirror plane

symmetric square antiprisms in the $\text{Sr}_5(\text{BO}_3)_3\text{F}$ structure that have a long bond to a ninth O atom.

Structure Comparisons. $\text{Sr}_5(\text{BO}_3)_3\text{Cl}$ (5) and $\text{Sr}_5(\text{BO}_3)_3\text{Br}$ have no alkaline earth stoichiometric homologues for comparison, but $\text{Sr}_5(\text{BO}_3)_3\text{F}$ can be compared to two other fluorides that have been previously described: $\text{Ca}_5(\text{BO}_3)_3\text{F}$ and $\text{Mg}_5(\text{BO}_3)_3\text{F}$ (6,15). They arrange in separate space groups, Cm and Pna2₁, respectively. Even though the noncentrosymmetric orthorhombic space group Pna2₁ of the magnesium borate fluoride is simply a subgroup of the title fluoride (Pnma), the atomic arrangement notably differs between the two: chains of Mg-centered, edge-sharing octahedra, interconnected by BO_3 triangles, define the framework. The Ca atoms in $\text{Ca}_5(\text{BO}_3)_3\text{F}$ also occupy distorted octahedral sites that are linked by corner-sharing BO_3 groups. The title fluoride requires larger sites of higher coordination to accommodate the Sr atom. The various Sr polyhedra not only extensively share faces and edges with each other, but the two edge- and corner-sharing borate groups also contribute to the high degree of connectivity in $\text{Sr}_5(\text{BO}_3)_3\text{F}$.

The F atom environment of this series also demonstrates the variation of the three compounds. The cationic grouping about the F atom in the $\text{Mg}_5(\text{BO}_3)_3\text{F}$ structure is triangular with each Mg atom residing in a unique octahedral site. Thus, three of the five Mg octahedra types include one F atom. Similarly, the F atom in $\text{Sr}_5(\text{BO}_3)_3\text{F}$ is threefold coordinated, but it is bonded to only two Sr atom types, both with one F atom per polyhedron. In contrast, the F atom in $\text{Ca}_5(\text{BO}_3)_3\text{F}$ is situated in a slightly distorted tetrahedral site created by two Ca types. The F atom is shared among two octahedral sites, $\text{Ca}(2)\text{O}_4\text{F}_2$ and $\text{Ca}(3)\text{O}_5\text{F}$. From this homologous series [$\text{A}_5(\text{BO}_3)_3\text{F}$; A = Mg, Ca, Sr], it is evident that the cation requirements of size and bonding coordination ultimately determine the atomic arrangement of these compounds.

The polyatomic anion substitution of BO_3 in $\text{Ca}_5(\text{BO}_3)_3\text{F}$ for the phosphate in fluorapatite $\text{Ca}_5(\text{PO}_4)_3\text{F}$ has previously been described (7), but the parallel strontium haloapatite stoichiometric analogues [$\text{Sr}_5(\text{PO}_4)_3\text{F}$ or $\text{Sr}_5(\text{PO}_4)_3\text{Br}$] of

$\text{Sr}_5(\text{BO}_3)_3\text{F}$ and $\text{Sr}_5(\text{BO}_3)_3\text{Br}$ have not been structurally reported. Even so, because of the importance of the phosphate as laser hosts (16) and phosphors, we compare here the alkaline-earth environments of $\text{Sr}_5(\text{PO}_4)_3\text{Cl}$ (17) and $\text{Ca}_5(\text{PO}_4)_3\text{F}$ (18) to the title structures (see Figure 3.4). The two phosphate structures primarily differ in the positions of the halide anions. Each apatite has two cations on special positions with C_3 and C_4 site symmetries; the former site consists of nine O atoms around the metal center, but the latter is either $\text{Sr}(2)\text{O}_6\text{Cl}_2$ or $\text{Ca}(2)\text{O}_6\text{F}$, depending on the position of the halide in the structure. Subsequently, the Cl^- anion is octahedrally coordinated by Sr atoms, while the F^- anion is trigonally surrounded by three Ca nearest neighbors. Like the Sr(2)-centered polyhedra in $\text{Sr}_5(\text{PO}_4)_3\text{Cl}$ that interconnect by sharing mutual Cl edges, one $\text{Sr}(1)\text{O}_7\text{Br}_2$ and two $\text{Sr}(2)\text{O}_6\text{Br}_2$ polyhedra in $\text{Sr}_5(\text{BO}_3)_3\text{Br}$ trilaterally share a $\text{Br} \cdots \text{Br}$ edge. As a result, the Br anion is also bonded to six cations. The distorted pentagonal bipyramid Ca(2) sites in $\text{Ca}_5(\text{PO}_4)_3\text{F}$ are joined through a common F corner. Likewise in $\text{Sr}_5(\text{BO}_3)_3\text{F}$, one $\text{Sr}(1)\text{O}_7\text{F}$ and two $\text{Sr}(2)\text{O}_6\text{F}$ polyhedra triangularly coordinate a single F atom.

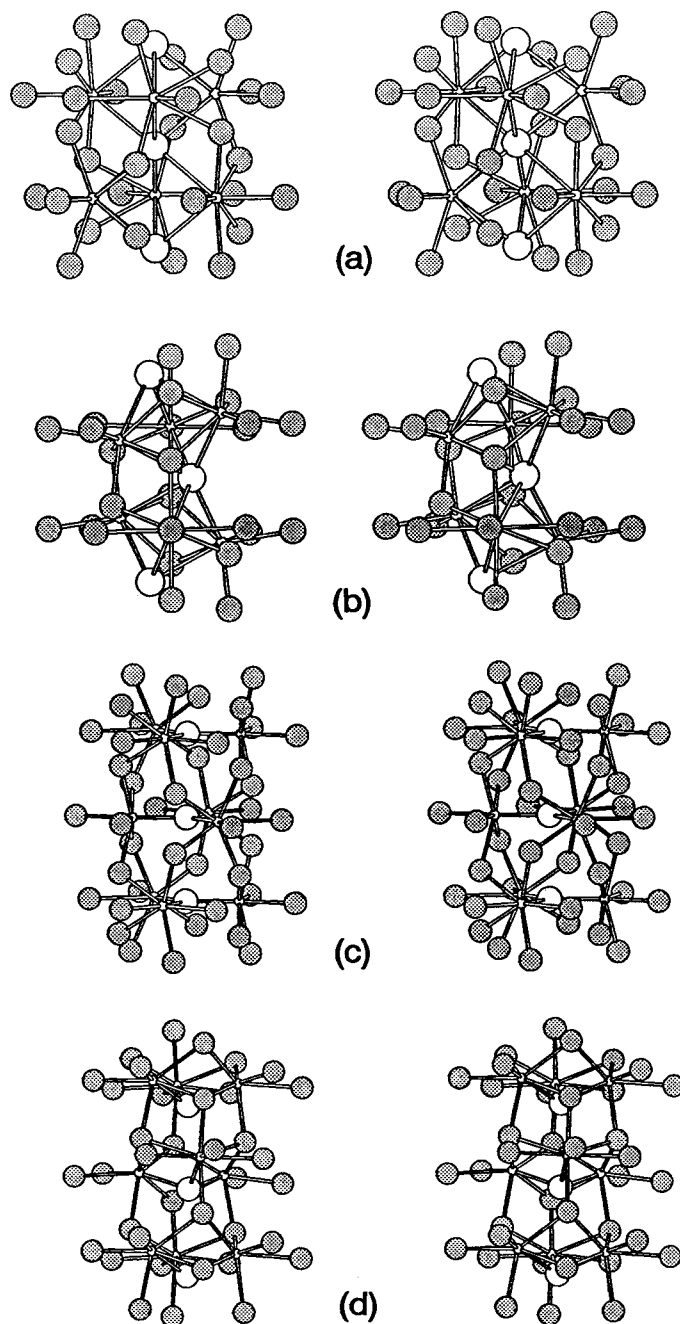


Figure 3.4. Stereo views illustrating the connectivity of the alkaline-earth-centered polyhedra that coordinate to the columns of halides within the following labeled structures: (a) $\text{Sr}_5(\text{PO}_4)_3\text{Cl}$, (b) $\text{Sr}_5(\text{BO}_3)_3\text{Br}$, (c) $\text{Ca}_5(\text{PO}_4)_3\text{F}$, and (d) $\text{Sr}_5(\text{BO}_3)_3\text{F}$. The small open circles portray the alkaline-earth metal, and the large open circles represent the halide. The c axis is vertical in the page except for (d), where the a axis is vertical.

Acknowledgment

This research was supported by the US National Science Foundation, Solid-State Chemistry Program (DMR-8814432). Acknowledgment is made to the Donors of The Petroleum Research Fund, administered by the American Chemical Society, for partial support of this research. D.A.K. thanks the Alfred P. Sloan Research Foundation for a fellowship.

References

1. T. Soules, M. Hoffman *Kirk-Othmer: Encyclopedia of Chemical Technology*, 3rd Ed.; Vol. 14, John Wiley & Sons: New York, (1981) 527.
2. T. Welker *J. Luminescence*, **48 & 49**, (1989) 49.
3. C. Chen, Y. Wu, L. Ru *J. Cryst. Growth*, **99**, (1990) 790.
4. B. Saubat, C. Fouassier, P. Hagemuller *Mat. Res. Bull.*, **16**, (1991) 193.
5. T. Alekel, D.A. Keszler *Acta Crystallogr., Sect. C*, **48**, (1992) 1382.
6. L. Shirong, H. Qingzhen, Z. Yifan, J. Aidong, C. Chuangtain *Acta Crystallogr., Sect. C*, **45**, (1989) 1861.
7. J.G. Fletcher, F.P. Glasser, R.A. Howie *Acta Crystallogr., Sect. C*, **47**, (1991) 12.
8. Molecular Structure Corporation, 3200A Research Forest Drive, The Woodlands, TX 77381, USA.
9. G. Sheldrick *Crystallographic Computing 3*, Eds: G. Sheldrick, C. Krüger, R. Goddard. Oxford University Press: New York, 1985, 175.
10. N. Walker, D. Stuart *Acta Crystallogr., Sect. A*, **89**, (1983), 158.
11. R. Shannon, C. Prewitt *Acta Crystallogr., Sect. B*, **25**, (1968) 925.
12. R. Shannon *Acta Crystallogr., Sect. A*, **32**, (1976) 751.
13. K.I. Schaffers, P.D. Thompson, T. Alekel III, J.R. Cox, D.A. Keszler *Chem. Mat.*, to be published.
14. I.D. Brown *Structure and Bonding in Crystals, Vol. II*, Academic Press: New York, (1981) Ch. 14.
15. A. Filimonov, N. Leonyuk, L. Meissner, T. Timchenko, I. Rez *Krist. Tech.*, **9**, 63.
16. G. Huber, F. Lutz *J. Cryst. Growth*, **52**, (1981) 646.

17. K. Sudarsanan, R.A. Young *Acta Crystallogr., Sect. B.*, **30**,(1974) 1381.
18. K. Sudarsanan, P.E. Mackie, R.A. Young *Mat. Res. Bull.*, **7**, (1972) 1331.

CHAPTER 4

The Pyroborate Fluoride $\text{Ba}_5(\text{B}_2\text{O}_5)_2\text{F}_2$

Theodore Alekel III and Douglas A. Keszler*

*Department of Chemistry and
Center for Advanced Materials Research
Oregon State University
Gilbert Hall 153
Corvallis, OR 97331-4003*

J. Solid State Chem., in press.

Abstract

The new material $\text{Ba}_5(\text{B}_2\text{O}_5)_2\text{F}_2$ represents the first confirmed structure of a pyroborate-halide anionic mixture in a crystalline phase. The structure contains four formula units in the monoclinic space group $C2/c$ (No. 15) with cell parameters $a = 20.726(3) \text{ \AA}$, $b = 7.115(2)$, $c = 8.589(2)$, $\beta = 95.05(5)^\circ$, and $V = 1261.7(5) \text{ \AA}^3$. Its characterization reveals a three-dimensional structure of three face- and edge-sharing Ba-centered polyhedra that are also united through nonplanar pyroborate anions. These irregular polyhedra are eight- and nine-coordinate, and contain one or two F atoms(s) at their peripheries. The geometry of the pyroborate is unusual in that the principal planes of the double triangles are rotated from one another by $86.6(1)^\circ$, the closest angular approach to the theoretical 90° limit of any known pyroborate; its B–O–B angle of $121.6(5)^\circ$, however, is typical. Differential thermal analysis reveals single events on heating and cooling that are indicative of a congruently melting compound.

Introduction

With a dozen structures reported (1-12), pyroborates represent a very small, but growing, percentage of all the known borate compounds. The pyroborate group can be viewed as two orthoborate units that link together *via* a common O atom. Typically, as the boron concentration of a borate increases in composition with respect to the other cations present, the borate groups condense to form more complex polyatomic anions. $\text{Sr}_3(\text{BO}_3)_2$ (13) *versus* $\text{Sr}_2\text{B}_2\text{O}_5$ (2) exemplifies this trend: when the compositional B:Sr ratio (mol%) increases, the condensed borate arrangement is favored. Intermediately, between the exclusive formation of either orthoborate or pyroborate, the compounds $\text{Sr}_2\text{Sc}_2\text{B}_4\text{O}_{11}$ [$\equiv \text{Sr}_2\text{Sc}_2\text{B}_2\text{O}_5(\text{BO}_3)_2$] and $\text{Ba}_2\text{Sc}_2\text{B}_4\text{O}_{11}$ (1) incorporate **both** borate configurations within the same structure.

The compound $\text{Ba}_5(\text{B}_2\text{O}_5)_2\text{F}_2$ represents an additional example of a pyroborate containing a mixture of anions and, in fact, the first pyroborate halide structurally confirmed to exist. Two other pyroborate fluorides, $\text{Al}_2(\text{B}_2\text{O}_5)\text{F}_2$ (14) and $\text{Sc}_2(\text{B}_2\text{O}_5)\text{F}_2$ (15), have been proposed, but their structural identity has not been verified. The title compound is also distinctive in that it is one of the first barium borate fluorides to be described (16). Even though a phase diagram for the binary system $\text{BaF}_2\text{-B}_2\text{O}_3$ has been proposed (17) and a barium fluoroborate, BaBOF_3 , is purported to exist (18), our investigations indicate this phase system to be more complex than previously reported. In this paper we describe the structural and thermal properties of $\text{Ba}_5(\text{B}_2\text{O}_5)_2\text{F}_2$.

Experimental

Synthesis. The synthesis of $\text{Ba}_5(\text{B}_2\text{O}_5)_2\text{F}_2$ was achieved by a high temperature solid-state reaction of high purity reagents. Samples were obtained by melting a stoichiometric mixture of BaCO_3 (ÆSAR, 99.9%), BaF_2 (Alfa, optical grade), and B_2O_3 (Alfa, 99.98%) at 1175 K for 1 h and allowing the material to cool to room temperature by turning off the furnace. Crystals were originally grown from a melt with the mol% ratio of 65.25 BaO: 24.87 BaF_2 : 9.88 B_2O_3 ; the title compound and the new material $\text{Ba}_7(\text{BO}_3)_3\text{F}_5$ (18) coprecipitated from this melt. Their coexistence was confirmed by powder X-ray diffraction analysis. Experimental patterns were compared with calculated patterns that were generated with the program LAZY-PULVERIX (19). Upon discovering the true components in the mixture, a pure batch of clear pyroborate crystals were made by slowly cooling a stoichiometric ratio of the reagents.

Thermal Measurements. To determine melting characteristics of the compound, differential thermal analysis (DTA) was performed. Measurements were made on a Harrop 726 Differential Thermal Analyzer that had been interfaced to a personal computer through a Metrabyte M1531 resistance-to-voltage converter and a Real Time Devices AD100A analogue-to-digital converter. The system was calibrated with a pure gold reference, the samples (~5 mg) were held in Pt containers. The heating and cooling rates were ± 20 K/min.

X-Ray Work. A clear prismatic block of dimensions 0.09(1) x 0.12(1) x 0.22(1) mm was mounted on a glass fiber and analyzed on a Rigaku AFC6R single crystal X-ray diffractometer. Unit cell parameters were derived from a least-squares fit of 20 automatically-centered setting angles within the angular range $30 < 2\theta < 36^\circ$. Peaks were measured to a width of $1.50 + 0.30 \tan\theta$ by using ω scans at a rate of $16^\circ(\omega)/\text{min}$. The stability of the crystal was confirmed by the constancy of three standards measured every 300 reflections, so no decay correction was implemented. From 2032 reflections measured to $2\theta = 60^\circ$ with Miller index limits $0 \leq h \leq 30$; $0 \leq k \leq 10$; $-12 \leq l \leq 12$, 1661 data were found to have $F_o^2 > 3\sigma(F_o^2)$.

General crystallographic information is summarized in Table 4.1.

Data analysis was performed on a Digital μ VAX II computer, and the crystal structure was determined by using the TEXSAN crystallographic software package (20). The systematic absences $h0l: l = 2n + 1$ and $00l: l = 2n + 1$ are consistent with the monoclinic space groups $C2/c$ and Cc . On the basis the statistical distribution of intensities (21) and the successful solution, we favor the centrosymmetric group $C2/c$. The Ba atoms were located with the direct methods program SHELXS-86 (22), and the remaining atoms were found by subsequent analysis of an electron density map. The values of F_{calc} were derived from predetermined neutral scattering factors and adjusted for anomalous dispersion by using f' and f'' factors from *International Tables of X-ray Crystallography (Vol. IV, 1974)*. Following refinement with isotropic displacement coefficients on each atom, the data were corrected for absorption with the program DIFABS (23) and subsequently averaged ($R_{\text{int}} = 0.064$). All atoms were then refined with anisotropic displacement parameters. Least-squares convergence ($\Delta/\sigma < 0.01$) with a secondary extinction coefficient = $0.9(3) \times 10^{-6}$ affords the residuals $R = 0.043$ and $R_w = 0.058$, where $\sigma(F^2) = [C + \frac{1}{4}(t_o/t_b)^2(b_1+b_2) + (pI)^2]^{1/2}$ and $p = 0.03$. The maximum peak in the final difference electron density map of $1.905 \text{ e } \text{\AA}^{-3}$ amounts to 0.80% of the Ba1 atom, and the minimum peak is $-2.237 \text{ e } \text{\AA}^{-3}$. Atomic positions and equivalent isotropic displacement coefficients are listed in Table 4.2.

Table 4.1. Crystallographic Data

Chemical formula	Ba ₅ (B ₂ O ₅) ₂ F ₂
Formula weight (amu)	965.88
Space group	C2/c (No. 15)
a (Å)	20.726(3)
b (Å)	7.115(2)
c (Å)	8.589(2)
β (°)	95.05(5)
V (Å ³)	1261.7(5)
Z	4
ρ _{calc} (g cm ⁻³)	5.084
μ (cm ⁻¹)	154.82
Transmission factors	0.83 - 1.23
Diffractometer	Rigaku AFC6R
Radiation	Mo Kα ^a
T (K)	300
Data Collection	h, k, ±l
No. Observations	4144
R, R _w ^b	0.043, 0.058

^a Graphite monochromated, λ = 0.71069 Å

$${}^b R = \frac{\sum ||F_o| - |F_c||}{\sum |F_o|} \quad R_w = \sqrt{\frac{\sum w(|F_o| - |F_c|)^2}{\sum w|F_o|^2}}$$

Table 4.2. Atomic Coordinates and Thermal Displacement Coefficients

	x	y	z	$B_{\text{eq}} (\text{\AA}^2)^a$
Ba1	0.30022(2)	0.11327(5)	0.69253(4)	0.95(1)
Ba2	0.08508(2)	0.11605(5)	0.60801(4)	1.00(1)
Ba3	0	0.44454(8)	¼	1.03(2)
F	0.4204(3)	0.3262(7)	0.6960(5)	1.6(2)
O1	0.4036(3)	-0.0002(8)	0.9599(7)	1.6(2)
O2	0.3494(2)	0.2968(8)	0.9632(5)	1.2(1)
O3	0.2196(3)	-0.0318(7)	0.9419(6)	1.5(2)
O4	0.3127(3)	-0.2628(8)	0.7152(5)	1.2(1)
O5	0.0413(3)	0.2350(9)	0.9216(7)	1.6(2)
B1	0.4057(3)	0.180(1)	0.0051(8)	0.9(2)
B2	0.1890(3)	0.131(1)	0.9180(8)	0.9(2)

$$^a B_{\text{eq}} = (8\pi^2/3) \sum_i \sum_j U_{ij} \mathbf{a}_i^* \mathbf{a}_j^* \mathbf{a}_i \cdot \mathbf{a}_j$$

Results

Structure Description. A labeled drawing of the unit-cell contents is given in Figure 4.1 for atomic identification purposes. To discern the connectivity within the cell, the stereo drawing of Figure 4.2 provides a more suitable view. $\text{Ba}_5(\text{B}_2\text{O}_5)_2\text{F}_2$ forms a three-dimensional framework of face- and edge-sharing Ba-centered polyhedra that are interconnected through nonplanar pyroborate units. Although the overall arrangement is not layered, each of the three Ba types exclusively resides on a bc plane, repeating along the a axis as Ba3-Ba2-Ba1-Ba1-Ba2 strata. The F^- and $(\text{B}_2\text{O}_5)^{4-}$ anions contribute to linking these Ba^{2+} cations in all directions and establishing the full three-dimensional structure.

In considering the nature of each Ba site, we see that the Ba1 atom has a unique coordination environment in comparison with the other two types. It is surrounded by eight O atoms and one F atom at the vertices of an irregular s-tricapped trigonal prism. On the other hand, the Ba2 and Ba3 atoms are octacoordinate (distorted undecahedra and bicapped trigonal prisms — capping on one square face — respectively), each bonding to eight O atoms and two F atoms. Since the Ba3 atom is the only one that rests on a special position in the cell, it alone possesses any symmetry (C_2) other than simple identity.

The connectivity within the structure is illustrated in Figure 4.3 and is hereby described: The $\text{Ba}(1)\text{O}_8\text{F}$ polyhedra share common O · · O edges with other Ba1 atoms in the same bc plane and additional O · · O edges with Ba1 atoms (1') that are located in an adjacent plane displaced along the a direction (Figure 4.3a). Furthermore, they share O · · O and O · · F edges with $\text{Ba}(2)\text{O}_6\text{F}_2$ distorted undecahedra (cf. Figures 4.2 and 4.3a) and adjoin to $\text{Ba}(3)\text{O}_6\text{F}_2$ bicapped trigonal prisms through common O · · F · · O faces (Figure 4.3b). With respect to the pyroborate groups, each Ba1 environment shares two edges with $(\text{B}_2\text{O}_5)^{4-}$ anions, consisting of a bridging O atom (O_b) and a terminal O atom (O_t) of the pyroborate group. An additional edge of the Ba1-centered polyhedron spans two O_t atoms, one from each BO_2 end-member, to establish an O1–B1–O2–B2–O4 bridge (Figure

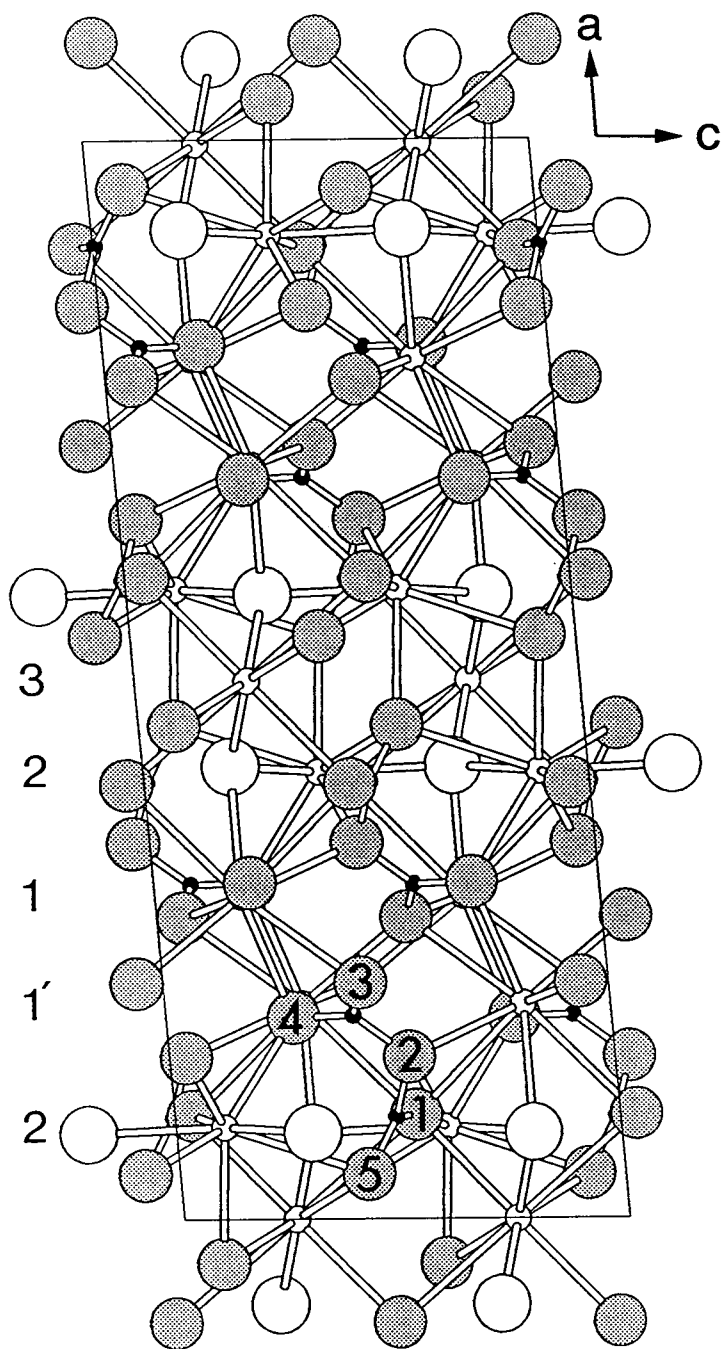


Figure 4.1. A schematic unit cell drawing of $\text{Ba}_5(\text{B}_2\text{O}_5)_2\text{F}_2$ along the b -axis. The small open circles represent Ba atoms, the large shaded circles represent O atoms, the small black circles represent B atoms, and the large open circles represent F atoms. (Atomic legend continued for subsequent figures.) The Ba layers and the O atoms are numerically labelled.

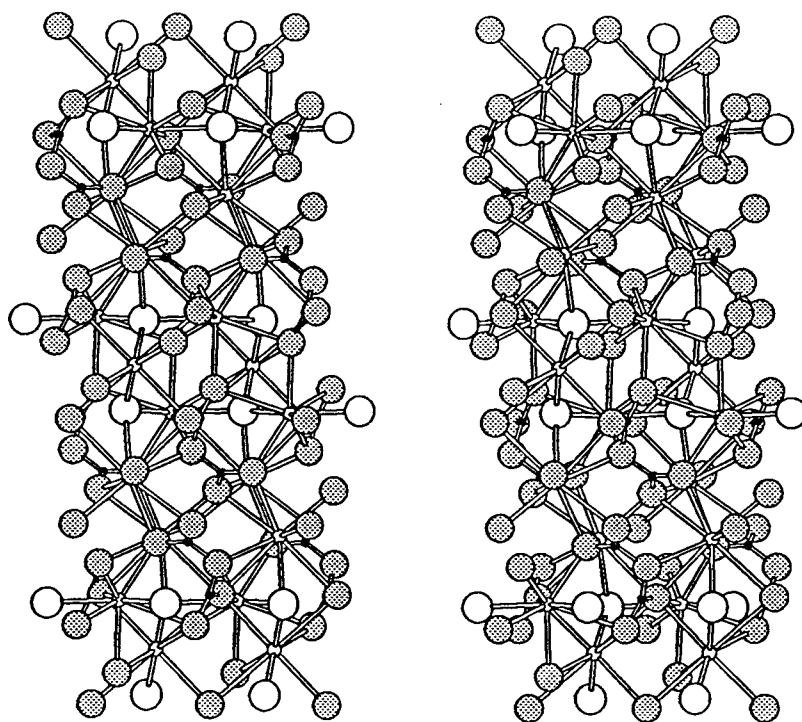
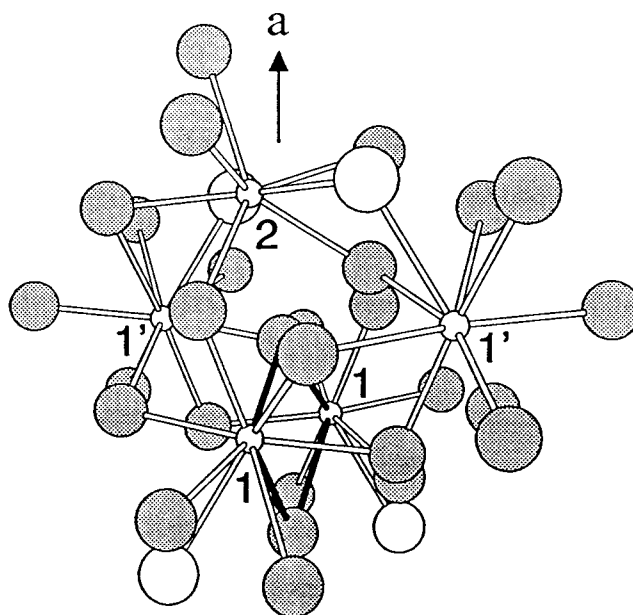
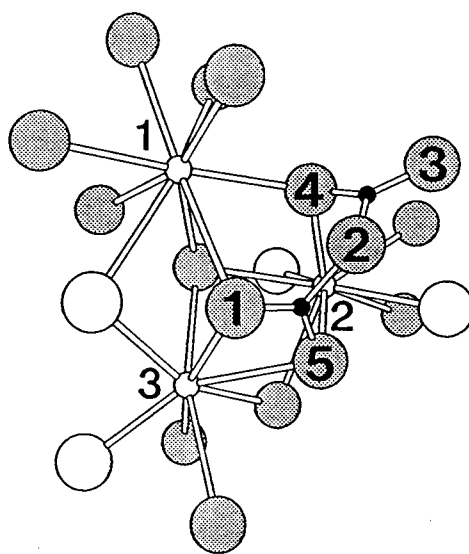


Figure 4.2. A b -axis projected stereo view of the unit cell along the b -axis.



(a)



(b)

Figure 4.3. Illustrations of the interconnectivity between selected polyhedra: (a) The shared edges between the coplanar Ba1 centers are highlighted as shaded bonds; the other layer is labeled *Ba1'*. (b) The pyroborate connectivity to the Ba polyhedra; the Ba atoms and the pyroborate O atoms are numerically labeled.

4.3b). The Ba2-centered distorted undecahedra also coordinate opposite ends of this pyroborate link by using the same $O(4)_i$ atom on one end and the complementary O_i atom of the other BO_2 end-member, thus forming another bridge ($O5-B1-O2-B2-O4$) to a single Ba center. The $Ba(2)O_6F_2$ undecahedra are connected to each other *via* $O \cdots F$ edges; additionally, they couple to $Ba(3)O_6F_2$ bicapped trigonal prisms through common $O \cdots O$ edges and shared triangular O faces. The prisms are joined to one another by common $O \cdots O$ edges, and they share edges and corners with the O_i atoms of pyroborates.

Selected interatomic distances and angles are listed in Table 4.3. Even though the average Ba–O lengths of 2.86(2) and 2.84(2) Å for the respective Ba1 and Ba2 polyhedra compare to the length 2.85 Å predicted from radii (24), both sites exhibit a wide variation of values as indicated by the large standard deviation ± 0.2 Å for each polyhedron (cf. Table 4.3). The Ba–F distances of 2.915(6) Å for Ba1, 2.673(5) and 2.633(5) Å for Ba2, and 2.552(5) Å (x 2) for Ba3 illustrate the extensibility of these interactions from the calculated distance of 2.73 Å. As a result, the F atom is coordinated by four Ba atoms that form a distorted tetrahedron with an average Ba–F–Ba angle of 108.6(5)°. The symmetric $Ba(3)O_6F_2$ exhibits the shortest Ba–F interactions and considerable deviation from characteristic Ba–O interactions with a long average Ba3–O length of 2.91(2) Å.

The pyroborate group within $Ba_5(B_2O_5)_2F_2$ contains a spread of lengths between 1.32(1) and 1.46(1) Å, but the average of 1.38(2) Å equals the expected B–O distance of a tricoordinate B atom. The distribution of the individual interactions follows a common trend for pyroborates: the B1 and B2 atoms have a short and a normal distance to the O_i atoms, while the interactions to the O_b atom are both long. This observation compares to the B–O lengths in the pyroborates $BaCuB_2O_5$ (3) and $Sr_2ScLi(B_2O_5)_2$ (4) where the B– O_b length equals 1.42(1) Å.

For the title compound, the O_i-B-O_i angles for each B type is 5° wider than the regular trigonal angle of 120°, whereas the O_i-B-O_b angles containing the bridging O2 atom are narrower than 120°. This imitates the expanded angles of

Table 4.3. Selected Bond Distances and Angles

Ba1-F	2.915 (6)	F-Ba1-O1	60.7 (1)
Ba1-O1	3.110 (6)	O1-Ba1-O1	86.5 (2)
Ba1-O1	3.157 (6)	O1-Ba1-O2	47.6 (2)
Ba1-O2	2.791 (5)	O2-Ba1-O3	75.5 (2)
Ba1-O3	3.018 (6)	O3-Ba1-O3	98.6 (2)
Ba1-O3	2.668 (6)	O3-Ba1-O3	78.8 (2)
Ba1-O3	2.794 (6)	O3-Ba1-O4	79.0 (2)
Ba1-O4	2.682 (6)	O4-Ba1-O4	112.6 (2)
Ba1-O4	2.696 (6)	O2-Ba1-O6	83.9 (3)
Ba2-F	2.673 (5)	F-Ba2-F	138.2 (2)
Ba2-F	2.633 (5)	F-Ba2-O1	68.8 (2)
Ba2-O1	2.808 (6)	O1-Ba2-O2	134.7 (2)
Ba2-O2	2.744 (6)	O2-Ba2-O4	90.6 (2)
Ba2-O4	2.643 (6)	O4-Ba2-O5	71.7 (2)
Ba2-O5	3.039 (6)	O2-Ba2-O5	48.5 (2)
Ba2-O5	3.064 (6)	O5-Ba2-O5	68.8 (2)
Ba2-O5	2.744 (6)	F-Ba2-O5	68.0 (2)
Ba3-F	2.552 (5) x 2	F-Ba3-F	82.0 (3)
Ba3-O1	3.075 (6) x 2	O1-Ba3-O1	84.9 (2)
Ba3-O1	2.838 (6) x 2	O1-Ba3-O1	93.1 (2)
Ba3-O5	2.805 (6) x 2	O5-Ba3-O5	71.5 (3)
B1-O1	1.33 (1)	O1-B1-O2	118.6 (8)
B1-O2	1.46 (1)	O1-B1-O5	124.2 (8)
B1-O5	1.36 (1)	O2-B1-O5	116.9 (7)
B2-O2	1.43 (1)	O2-B2-O3	119.5 (7)
B2-O3	1.32 (1)	O2-B2-O4	114.6 (7)
B2-O4	1.37 (1)	O3-B2-O4	125.8 (7)

the pyroborate BO_2 end-members witnessed in the compounds $\text{Sr}_2\text{Sc}_2\text{B}_4\text{O}_{11}$ and $\text{Ba}_2\text{Sc}_2\text{B}_4\text{O}_{11}$ (1). These angular distortions appear to be dictated by the coordinative stricture of the bound metals; in both of these examples, the $\text{O}_i\text{-B-O}_i$ end-members bridge two individual metal centers, so this angle is largely determined by their separation within the structure. The expanded $\text{O}_i\text{-B-O}_i$ angles within $\text{Ba}_5(\text{B}_2\text{O}_5)_2\text{F}_2$, on the other hand, are multiply governed by edge-sharing Ba1- and Ba3-centered polyhedra and by bridging the three Ba centers together.

The parameters that describe the geometric attributes of the pyroborate group, namely the B-O-B angle and the *interplanar angle*, are depicted in Figure 4.4. The interplanar angle is defined as the angle between the vectors normal to the end $\text{B}(\text{O}_i)_2$ planes. In the title structure, the $\text{B-O}_b\text{-B}$ angle of $121.2(6)^\circ$ is typical among pyroborate compounds (5,6) which can exhibit angular extremes that range from 111.8 to 180° (7,1). The notable feature of $\text{Ba}_5(\text{B}_2\text{O}_5)_2\text{F}_2$, however, is the interplanar angle of $86.6(1)^\circ$ between the double triangles; it represents the current maximum twist angle witnessed in any known pyroborate (theoretical limit = 90°). The group in $\text{Sr}_2\text{Sc}_2\text{B}_4\text{O}_{11}$ illustrates the complementary configuration, possessing coplanar double triangles (0°). These interplanar limits and the variety of intermediate angles among other compounds are consistent with the absence of a significant energy barrier that might afford a favorable geometry. This result has also been noted from the results of extended Hückel calculations where the energy differences among various geometries was found to be trivial (1).

Thermal Properties. The data obtained from the DTA measurement reveal simple single events for the heating and cooling curves (Figure 4.5). Upon heating, the sample melted at a temperature of 1040 K and exhibited no further evidence of decomposition or phase transformation. The baseline shift flanking the melting curve indicates a change in thermal conductivity of the solid *versus* the liquid. As the temperature is decreased, the melt supercools by approximately 150 K after passing through its freezing point.

Recall that the growth of the $\text{Ba}_5(\text{B}_2\text{O}_5)_2\text{F}_2$ crystals was achieved without the aid of a flux. This fact, along with the DTA findings, suggests that the title

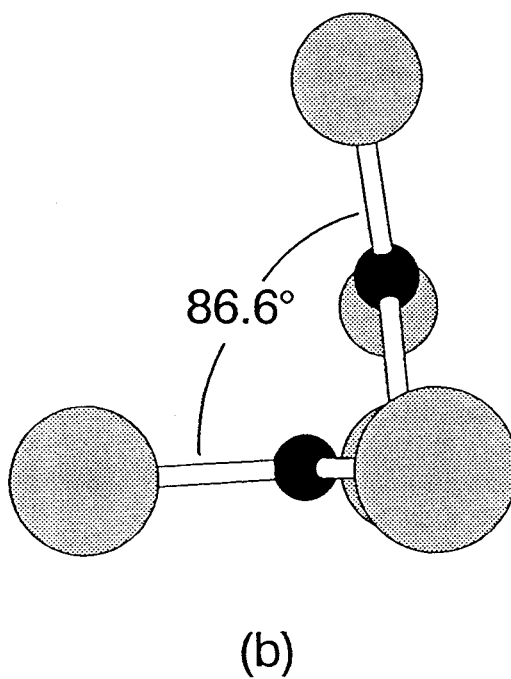
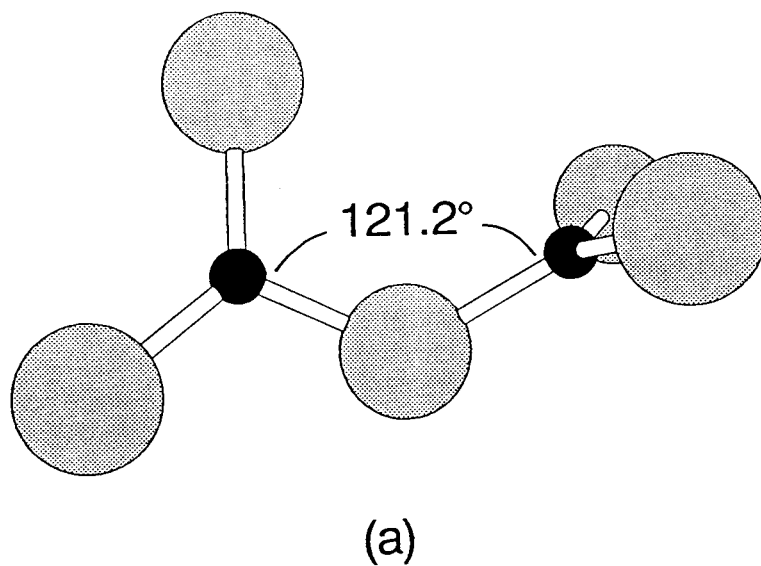


Figure 4.4. The pyroborate geometry of $\text{Ba}_5(\text{B}_2\text{O}_5)_2\text{F}_2$: (a) the B-O-B angle and (b) the interplanar angle.

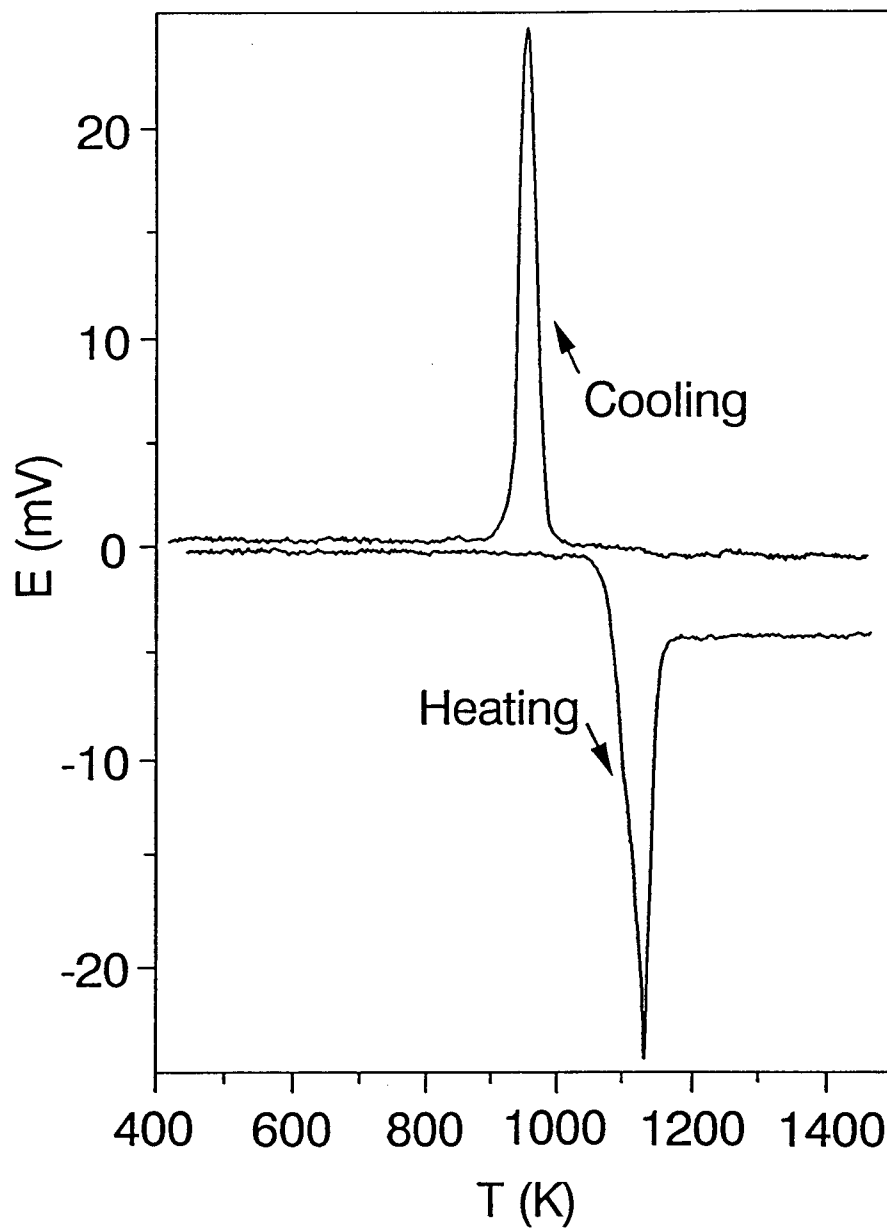


Figure 4.5. DTA data for $\text{Ba}_5(\text{B}_2\text{O}_5)_2\text{F}_2$.

compound melts congruently. In addition, upon cycling the sample through the melting point several times, the same thermal response was recorded. If on the other hand, the compound was incongruent, then decompositional phase changes would be evident, rendering the system irreversible when cycled. These results are consistent with the structural arrangement — all of the atoms are situated in favorable environments so as to form a thermodynamically stable compound from the melt composition. Evidence to support the kinetic spontaneity of formation is again drawn from the nature of the synthesis procedure. The compound can be made in a matter of minutes by melting the starting materials and quenching the liquid to room temperature by directly removing the melt from the oven; powder X-ray diffraction confirms the immediate generation of $\text{Ba}_5(\text{B}_2\text{O}_5)_2\text{F}_2$ from this accelerated synthetic procedure. Therefore, the rapid nucleation and formation of crystals signify no practical kinetic barrier to crystallization — a surprising result considering that the compositional components are common glass-formers.

Acknowledgments

This research was supported by the US National Science Foundation, Solid-State Chemistry Program (DMR-8814432). Acknowledgment is made to the Donors of The Petroleum Research Fund, administered by the American Chemical Society, for partial support of this research. DAK thanks the Alfred P. Sloan Research Foundation for a fellowship.

References

1. P.D. Thompson, J. Huang, R.W. Smith, D.A. Keszler, *J. Solid State Chem.* **95**, (1991) 126.
2. H. Bartl, W. Schuckmann, *Neues Jahrb. Min. Monatsh.*, **8**, (1966) 253.
3. R.W. Smith, Ph.D. dissertation, Oregon State University, USA (1989).
4. P.D. Thompson, D.A. Keszler, *Solid State Ionics*, **32/33**, (1989) 521.
5. O.V. Yakubovich, M.A. Simonov, E.L. Belokoneva, Y.I.C. Egorov-Tismenko, N.V. Belov, *Dokl. Acad. Nauk SSSR*, **230**, (1976) 837.
6. O.V. Yakubovich, N.A. Yamnova, B.M. Shchedrin, M.A. Simonov, N.V. Belov, *Dokl. Acad. Nauk SSSR*, **228**, (1976) 842.
7. O.V. Yakubovich, M.A. Simonov, N.V. Belov, *Dokl. Acad. Nauk SSSR*, **238**, (1978) 98.
8. Y. Takéuchi, *Acta Crystallogr.*, **5**, (1952) 572.
9. S. Block, G. Burley, A. Perloff, R.D. Mason, *J. Res. Natl. Bur. Stand.*, **62**, (1959) 95.
10. S. Berger, *Acta Chem. Scand.*, **4**, (1950) 1054.
11. H. König, R. Hoppe, and M. Jansen, *Z. Anorg. Allg. Chem.*, **449**, (1979) 91.
12. M. Gasperin, *Acta. Crystallogr., Sect. B*, **30**, (1974) 1181.
13. L. Richter, F. Müller, *Z. Anorg. Allg. Chem.*, **467**, (1980) 123.
14. K. Teske, H.A. Lehmann, *Z. Chem.*, **6**, (1966) 230.
15. L.R. Batsanova, L.A. Novosel'tseva, A.I. Madaras, *Inorg. Mat. (English Translation)*, (1974) 530.
16. The other phase discovered in this system is $\text{Ba}_7(\text{BO}_3)_3\text{F}_5$ (Ch. 7).
17. S.I. Berul', I.N. Nikonova, *Russ. J. Inorg. Chem.*, **11(4)**, (1966) 490.
18. D.M. Chackraburttty, *Acta Crystallogr.*, **10**, (1957) 199.

19. K. Yvon, W. Jeitschko, E. Parthé, *J. Appl. Crystallogr.*, **10**, (1977) 73.
20. Molecular Structure Corporation, 3200A Research Forest Drive, The Woodlands, TX 77381, USA.
21. E. Howells, D. Phillips, D. Rodgers, *Acta Crystallogr.*, **3**, (1950) 210.
22. G.M. Sheldrick, *SHELXS86 In Crystallographic Computing 3*, edited by G. M. Sheldrick, C. Krüger, R. Goddard, Oxford Univ. Press, 175 (1985).
23. N. Walker, D. Stuart, *Acta Crystallogr., Sect. A*, **39**, (1983) 158.
24. R.D. Shannon, *Acta Crystallogr., Sect. A*, **32**, (1976) 751.

CHAPTER 5

**Structure and Eu^{2+} Luminescence of New
Alkaline-Earth Borate Bromides $\text{AE}_2\text{BO}_3\text{Br}$ (AE = Sr, Ba)**

Theodore Alekel III and Douglas A. Keszler*

Department of Chemistry and

Center for Advanced Materials Research

Oregon State University

Gilbert Hall (153)

Corvallis, OR 97331-4003

In preparation for submission to *Chemistry of Materials*

Abstract

The new borate bromides AE_2BO_3Br ($AE = Sr, Ba$) crystallize in the trigonal space group $P\bar{3}m1$ with unit cell parameters $a = 5.299(1) \text{ \AA}$, $c = 10.357(1)$, and $V = 251.9(1) \text{ \AA}^3$ for the Sr compound and $a = 5.513(1) \text{ \AA}$, $c = 10.971(2)$, and $V = 288.6(1) \text{ \AA}^3$ for the Ba analogue. The highly symmetrical structure consists of independent layers of orthoborate and bromide anions that are connected by two crystallographically unique types of AE atoms. The $AE(1)O_9Br$ site is best described as a distorted monocapped trigonal – hexagonal base, while the $AE(2)O_3Br_4$ is a distorted monocapped octahedron. Thermal analyses indicate that the Sr derivative undergoes a peritectic decomposition at 1000 K, and the Ba compound melts congruently at 1148 K. Both compounds were doped with Eu^{2+} ions, and general photoexcitation and luminescence measurements were made at 300 and 77 K.

Introduction

Photostimulable luminescence (PSL) and persistent spectral hole-burning (PSHB) are two phenomena that require both the presence of an impurity metal ion that exists in two oxidation states (1-8) and a host material that is capable of transporting and localizing charges within its framework. Even though several structure types have been investigated for these processes, most studies have focused on simple alkaline earth binary halides. For example, the PSL compound BaClF:Eu^{2+} , with its $\text{Eu}^{2+} \leftrightarrow \text{Eu}^{3+}$ associated charges, has been widely used as an X-ray storage phosphor for the detection, quantification, and digitization of exposure doses (9). The PSHB compound SrClF:Sm^{2+} ($\text{Sm}^{2+} \leftrightarrow \text{Sm}^{3+}$) is a high-density optical data storage medium that retains encoded information over long time periods (10).

Under the widespread mechanistic models, both systems exploit the process of reversibly modifying the oxidation state of the active ion (11–13), although the precise mechanisms have been the topic of much discussion. Contrary to the initial conception of the PSL process in storage phosphors (11), evidence suggests that the guest cations do not undergo oxidation upon exposure to X-ray radiation, but rather the divalent Eu centers stabilize nearby holes (14). Nevertheless, common to both mechanisms is the facilitation of charge migration and stabilization within the host matrix. Compounds with high stoichiometric concentrations of halides appear to promote the storage of photoionized electrons through point defects distributed throughout the lattice.

For nearly all of the PSL materials that are synthetically induced into lower valent states of the active ion, hydrogenation has been used to reduce Eu in the sample. Since these materials are built from the framework of halides, undoubtedly hydride anions migrate into the host structure. In a recently proposed mechanism that accounts for hydride impurities (14), neighboring U-centers (15) are responsible for trapping the generated hole upon X-ray irradiation, rather than an oxidized Eu ion. Unfortunately, the authors did not report the control experiment: detecting the photoactivity of these U-centers *without* the Eu dopant to confirm

their energetic role. If one wanted to more comprehensively account for variables in a proposed mechanism, then one should also consider the ever-present oxide impurities that strongly trap mobile holes (16).

Ultimately, to completely discredit the existence of the oxidized ion hole trap appears hasty in light of recent studies that demonstrate the photooxidation process through the photoelectric effect in RE²⁺-doped fluorite upon exposure to UV radiation (17). Also, Ce:YAG has been shown to photooxidize to Ce⁴⁺ by the UV promotion of an electron to a 5d level within the conduction band of the material (18). The "anomalous yellow luminescence" in BaF₂:Eu²⁺ is accredited to excitons that are locally stabilized by the Coulombic field of photooxidized Eu³⁺ species, a common phenomenon that occurs in alkaline-earth binary halides that are doped with divalent lanthanide chromophores (19). Finally, there exist several examples of halide-containing structures where both valent forms of Eu are known to coexist in the host (20,21), including the title compounds. If a mechanism is to faithfully describe the actual processes, Eu³⁺ centers must be considered as potential hole traps, whether they were generated upon X-ray exposure, as in CaSO₄:Eu (22), or preexistent in the host.

The compounds Sr₂BO₃Br and Ba₂BO₃Br were conceptually designed as potential new X-ray storage phosphors having lower energy absorption and emission characteristics. The success of other polyanionic halides (2,4) for use in imaging and data storage applications induced us to search for other materials that could potentially exhibit the required electronic properties. The hygroscopic inclination of binary halides can be lessened by the inclusion of borates, silicates, sulfates, etc. The combination of desirable physical properties, along with the capacity to accommodate divalent lanthanide dopant ions, led us to investigate the alkaline-earth borate halide phase systems. The patented application of the Eu-doped hilgardite structures AE₂B₅O₉X (AE = Ca, Sr, Ba; X = Cl, Br, I) for X-ray imaging media (1) encouraged us to continue with the studies of A₂BO₃Br:Eu. In addition to the structure determination and the thermal properties of the two title compounds, excitation and luminescence spectra, are presented here.

Experimental

Synthesis. A microcrystalline powder of $\text{Sr}_2\text{BO}_3\text{Br}$ was formed by using standard high-temperature solid-state techniques and high purity reactants. $\text{Sr}_3(\text{BO}_3)_2$ was generated by reacting a stoichiometric mixture of $\text{Sr}(\text{NO}_3)_2$ (ÆSAR, ACS Grade) and anhydrous B_2O_3 (ÆSAR, 99.98%) at 900 K for 1 h, followed by heating at 1273 K for 24 h. $\text{Sr}_3(\text{BO}_3)_2$ and SrBr_2 (ALFA, 99%) were then reacted in an Al_2O_3 crucible in air at 1110 K for 30 h, resulting in a single new phase as determined by powder X-ray diffraction. Attempts were made to synthesize the Ca analogue in the same way, but no reactivity was observed between $\text{Ca}_3(\text{BO}_3)_2$ and CaBr_2 .

Crystals were grown from a melt with the mol% composition 35.5 SrO: 56.5 SrBr_2 : 8.0 B_2O_3 that was cooled at 8 K/hr from 1273 to 950 K in a Pt crucible. At these temperatures, many bromides will react with Pt, and this was observed in the crystal growth with the formation of red Pt-doped crystals at the periphery of the solidified melt; the coloration did not extend into the bulk of the sample. $\text{Sr}_2\text{BO}_3\text{Br}$ hexagonal plates having dimensions of approximately 0.15 x 0.15 x 0.02 mm were extracted from the center the sample for X-ray study.

Crystals of the compound $\text{Ba}_2\text{BO}_3\text{Br}$ were grown by melting a stoichiometric mixture of BaCO_3 (ALFA, 99.9%), BaBr_2 (ÆSAR, 99%), and B_2O_3 ; the mixture was heated to 1098 K and cooled at 10 K/h to 773 K, and then rapidly cooled to room temperature. A single crystal of approximate dimensions 0.15 x 0.15 x 0.05 mm was isolated and mounted for X-ray structure determination.

Samples doped with 2 mol% Eu were synthesized by using the above preparative methods. The samples were heated in a reducing atmosphere of 7 % H_2 in N_2 to convert the EuBr_3 dopant source to Eu^{2+} within the host.

Thermal Analysis. To study the crystallization behavior of the samples, differential thermal analysis (DTA) was performed. Measurements were made on a Harrop 726 Differential Thermal Analyzer that has been interfaced to a personal computer through a Metrabyte resistance-to-voltage converter and a Real Time

Devices RD100 ADC computer card. The system was calibrated with a pure gold reference, and the samples (≈ 5 mg) were held in Pt containers. The heating and cooling rates were ± 15 K/min.

Optical Apparatus. Spectral data were obtained with an optical system especially designed for solid materials. A schematic diagram of the typical optical set-up is provided in Figure 5.1. The broadband output of a 300 W Xe arc lamp was dispersed into a 0.4 m double-prism monochromator for excitation scanning and focused onto the sample. Luminescence was collected with an Oriel 0.125 m grating monochromator and detected with an R636 photomultiplier. The average photocurrent is converted into mV by either a Keithley picoammeter or a Thorn/EMI C632 transimpedance amplifier then sampled with a 12-bit ADC. Control of the wavelength drives of both monochromators and signal processing were achieved by way of PC-based software that was written in-house. Data were corrected for the throughput of the optical path and the wavelength-dependent efficiency of the detector. For the spectral measurements in this study, all of the data were obtained from microcrystalline powders. Low temperature measurements were made by placing the samples into an optical dewar and submerging them in liquid N₂.

Crystallographic Study. Crystals were affixed to glass fibers and analyzed on a Rigaku AFC6R single crystal X-ray diffractometer. The intensity data were collected at 300 K via the ω - 2θ scan technique at the rate of $16^\circ(\omega)/\text{min}$ with peak widths no larger than $1.50 + \tan \theta$. The unit cell for Sr₂BO₃Br was derived from a least-squares refinement of 20 automatically-centered reflections within the range $30^\circ \leq 2\theta \leq 36^\circ$. The integrity of the crystal was monitored by measuring the intensities of three standard reflections after each block of 200 data throughout the collection, yielding an average relative standard deviation of -0.8%. 363 unique reflections [$F_o^2 > 3\sigma(F^2)$] were measured to $\sin \theta_{\text{max}}/\lambda = 0.7017 \text{ \AA}^{-1}$ with Miller index limits $0 \leq h \leq 7, -7 \leq k \leq 7, -14 \leq l \leq 14$. The unit cell for the isostructural compound Ba₂BO₃Br was derived from 20 reflections within the range of $30 \leq 2\theta \leq 36^\circ$. The three standard reflections that were used to affirm the stability of the

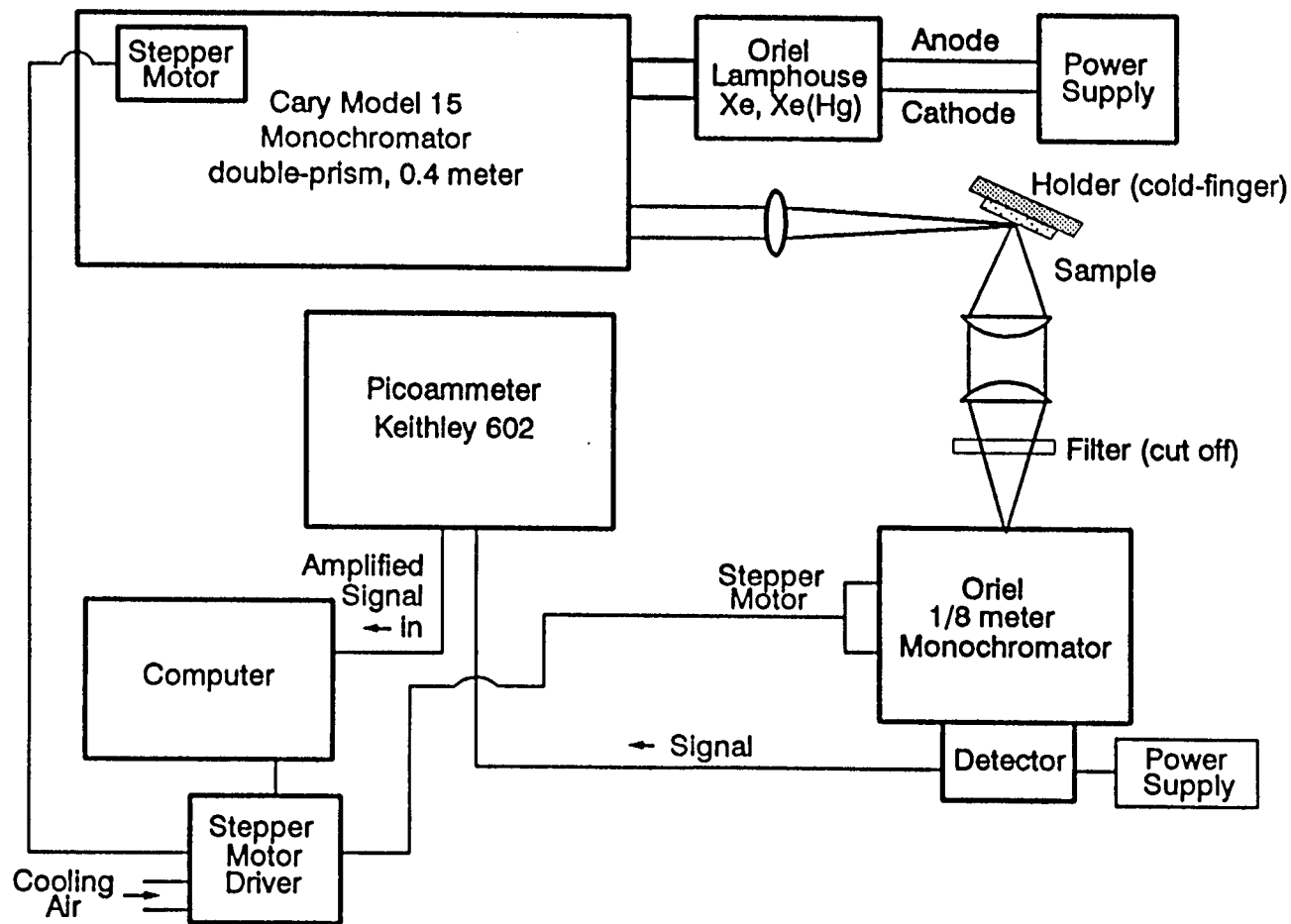


Figure 5.1. Block diagram of the optical instrumentation used for excitation and luminescence spectra.

crystal demonstrated no deterioration in peak intensities. 3505 observed peaks of 6433 total were measured within the range of $2 \leq 2\theta \leq 100^\circ$ with indices of $0 \leq h \leq 10$, $-10 \leq k \leq 10$, $-21 \leq l \leq 21$. The general crystallographic information for the title compounds is summarized in Table 5.1, and the positional parameters are listed in Table 5.2.

The determination of the atomic positions for $\text{Sr}_2\text{BO}_3\text{Br}$ and $\text{Ba}_2\text{BO}_3\text{Br}$ and the refinement of their structures were performed on a Digital microVAX II computer by using the TEXSAN crystallographic software package (23). Of the three possible space groups with Laue symmetry $\overline{3}m1$ and no reflection conditions, $P\overline{3}m1$ was determined to be the correct choice on the basis of intensity statistics, the progressive identification of symmetry elements in the cell (*vide infra*), and the successful refinement the structure.

The initial attempt of locating the Sr atoms in the unit cell via the direct methods algorithms SHELXS-86 (24) and MITHRIL (23) did not generate meaningful positions. The high symmetry of this cell (all of the atoms reside on special positions) and the inability of X-ray diffraction to resolve isoelectronic atoms (Sr^{2+} , Br^-) contributed to the difficulty in pinpointing the heavy atoms. Success was ultimately achieved by executing SHELXS-86 after removing all symmetry operations (the space group P1 was selected in the software). Four Sr atoms and two Br atoms emerged, and their interatomic distances faithfully matched the Patterson vectors. A center of symmetry was immediately evident upon relating equivalent atoms, thus fixing the origin of the lattice. After converting the positions to the simplest trigonal space group P3, the data were analyzed by successive difference electron density maps to locate the O and B atoms. Finally, inspection of these atoms in the cell revealed a (110) mirror plane, which exclusively suggested the centrosymmetric space group $P\overline{3}m1$.

Following refinement with isotropic displacement coefficients, the data were corrected for absorption with the program DIFABS (25) and averaged ($R_{\text{int}} = 0.133$). The high agreement index appears to result from a systematic error associated with the plate morphology of the crystal and large absorption coefficient.

Table 5.1. Crystallographic Data for A_2BO_3Br (A = Sr,Ba)

Formula	Sr_2BO_3Br	Ba_2BO_3Br
Formula Weight, amu	313.95	413.37
Crystal System	Trigonal	
Space Group	$\bar{P}3m1$ (#164)	
a, Å	5.299(1)	5.513(1)
c, Å	10.357(1)	10.971(2)
V, Å ³	251.9(1)	288.6(1)
Z	2	2
D_{calc} , g cm ⁻³	4.139	4.757
F(000)	280	352
Diffractometer	Rigaku AFC6R	
Radiation	Mo $K\alpha$ = 0.71069 Å graphite monochromator	
Data Collection	$\pm h, k, \pm l$	$\pm h, k, \pm l$
No. Unique Observations ($F_o^2 > 3\sigma(F_o^2)$)	363	792
Transmission Factors	0.584 – 1.755	0.696 – 1.594
Linear Absorption, cm ⁻¹	282.84	203.24
R	0.039	0.052
R_w	0.058	0.082

Table 5.2. Positional parameters and B_{eq} for A_2BO_3Br ($A = Sr, Ba$)

<u>Sr₂BO₃Br</u>	<u>x</u>	<u>y</u>	<u>z</u>	<u>B_{eq}</u>
Sr1	2/3	1/3	0.0723(1)	0.30(3)
Sr2	1/3	2/3	0.2974(1)	0.29(3)
Br	2/3	1/3	0.3876(2)	0.84(3)
O	0.150(1)	0.150(1)	-0.1333(4)	1.40(1)
B	0	0	-0.133(1)	0.7(4)
<u>Ba₂BO₃Br</u>	<u>x</u>	<u>y</u>	<u>z</u>	<u>B_{eq}</u>
Ba1	1/3	2/3	0.0744(1)	0.75(1)
Ba2	2/3	1/3	0.3044(1)	1.27(2)
Br	1/3	2/3	0.3861(2)	2.03(4)
O	0.1457(5)	0.1457(5)	0.1335(6)	1.06(6)
B	0	0	0.135(1)	0.9(2)

The final cycle of least-squares refinement with 363 reflections resulted in the final residuals $R = 0.039$ and $R_w = 0.052$. The largest peak height in the final difference electron density map is $1.65 \text{ e } \text{\AA}^{-1}$ (1.14% of the Sr1 atom), and the minimum peak intensity is $-1.60 \text{ e } \text{\AA}^{-1}$. $w = [1/\sigma^2(F_o)]$ was used for the weighted refinement with $p = 0.03$, and F_{calc} was calculated from the predetermined neutral and anomalous scattering factors (26).

The structure of the Ba derivative was established from comparison to the Sr analogue. Refinement and data manipulation followed the same course. The final least-squares fit of the 19 parameters to 792 F_o values produced agreement factors of $R = 0.058$ and $R_w = 0.082$. The largest peak intensity in the final difference electron density map is 4.38% of Ba1 ($11.16 \text{ e } \text{\AA}^{-1}$), and the smallest peak is $-6.72 \text{ e } \text{\AA}^{-1}$.

Results

Structure Description. As viewed in the packing diagram (Figure 5.2), the A_2BO_3Br structure crystallizes in a layered-type arrangement. Double layers of Br anions are interleaved between double layers of BO_3 groups. One type of alkaline-earth atom (constituting the layers labelled in Figure 5.2 as *a* and *b*) connects a double layer of orthoborate groups (A, B). The second cation type (*c* and *d*) coordinates to a single borate layer but also bonds to atoms in Br layer (C) and to a lesser extent with the adjacent Br layer (D). The stacking of the planes for both the cations and the anions results in separate ABCD (abcd) layer sequences.

Figure 5.3 is a schematic depiction of the unit cell, and the individual metal-centered polyhedra found bridging the anionic layers can be observed here. The AE1 atom assumes an unusual 10-coordinate geometry (27), formed by nine O atoms and a capping Br atom, that is best described as a trigonal-hexagonal base tridecahedron. The hexagonal base is not regular, but rather, it assumes trigonal symmetry by squeezing pairs of O atoms together through bridging edges to three regular orthoborate triangles. O atoms from neighboring BO_3 groups form a common edge between the AE1 and AE2 cations.

The AE2 site is a distorted monocapped octahedron with one smaller trigonal face composed of O atoms and the other larger face, Br atoms. A seventh Br anion caps the octahedron in the center of the Br face. In addition to sharing $O \cdots O \cdots Br$ faces (C_3 symmetry) with AE1 atoms, coplanar AE2 layers (a,b) are linked by Br corners, and AE2 adjacent layers (c,d) share edges of Br atoms.

Selected bond distances for Sr_2BO_3Br and Ba_2BO_3Br are listed in Table 5.3, and selected bond angles for these compounds are given in Table 5.4. The distances between AE1 and its trigonal and hexagonal base O atoms exhibit little deviation from the average AE1—O distances [avg. Sr—O = 2.724(3); avg. Ba—O = 2.859(3)], amounting to 0.5% for Sr(1) O_9 Br and 2.1% for Ba(1) O_9 Br. However, the average Sr(1)—O distance exceeds the value of 2.63 Å calculated from crystal radii (28), but the average Ba—O distance compares favorably to the calculated distance

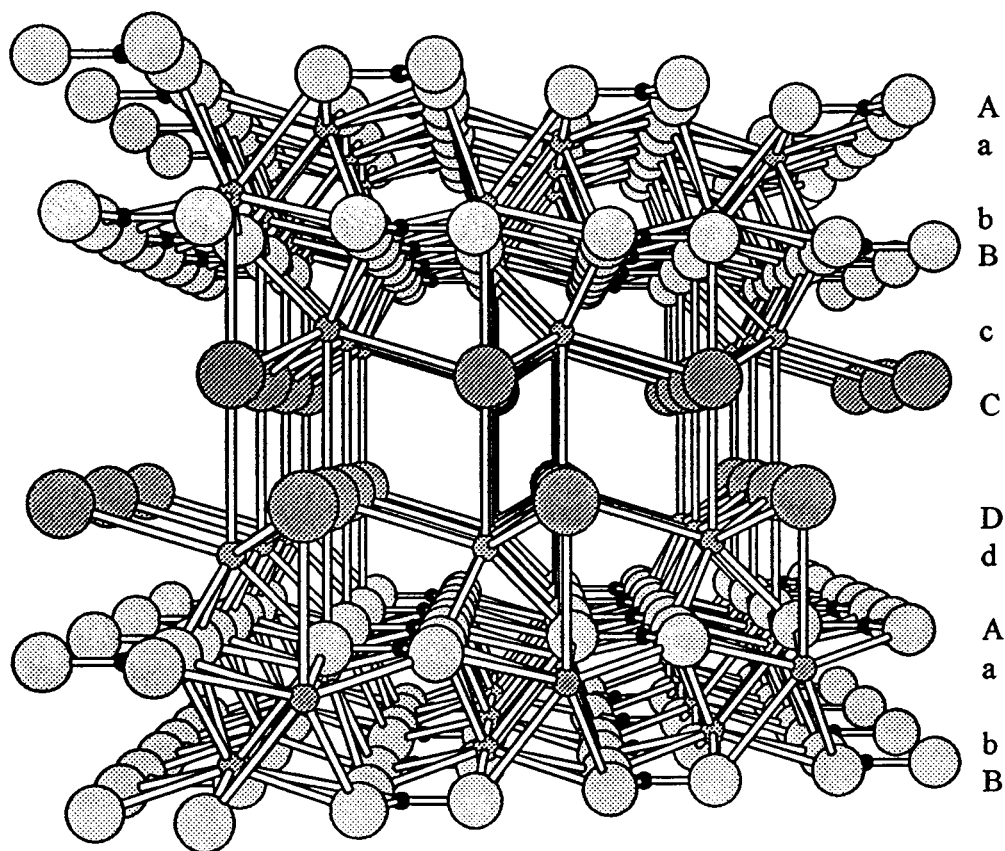


Figure 5.2. A packing diagram for the compounds AE_2BO_3Br ($AE = Sr, Ba$), viewed as a (110) projection with the c axis vertical in the page. The small empty circles represent Sr atoms, the large pale circles represent O atoms, the large shaded circles represent Br atoms, and the small black circles represent B atoms.

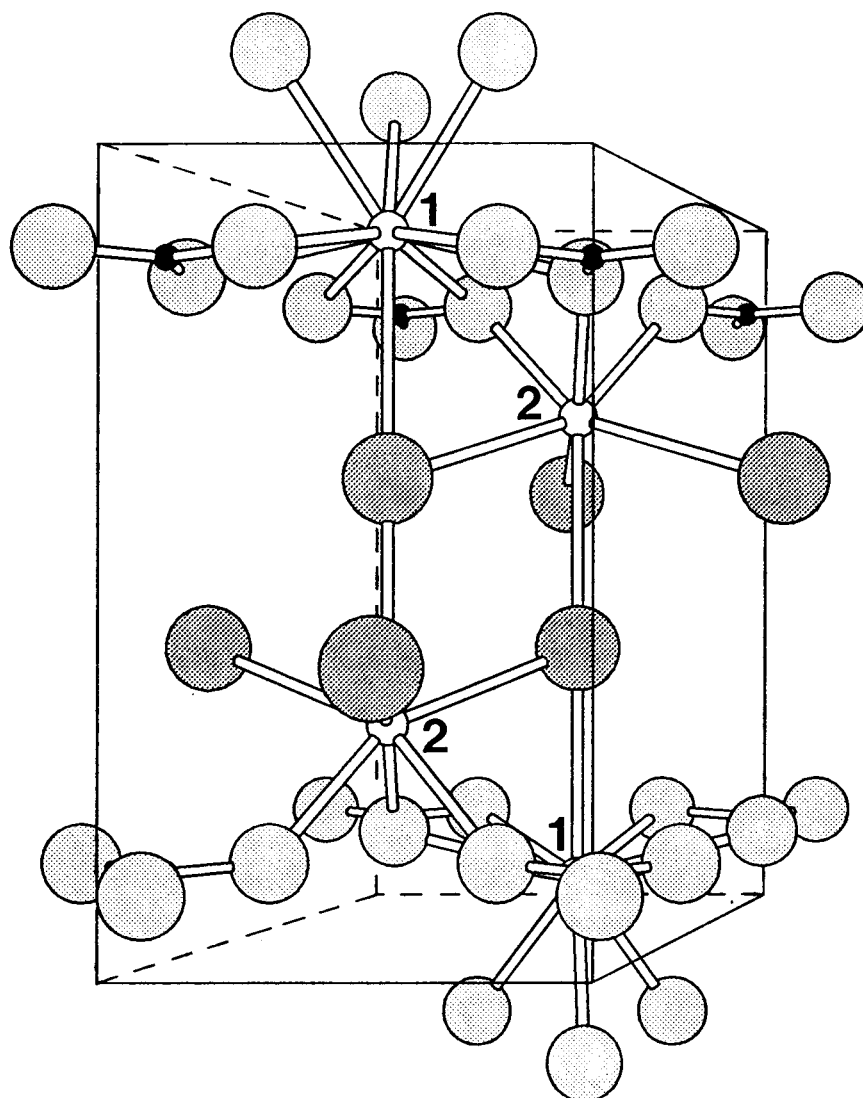


Figure 5.3. A schematic of the unit cell of AE_2BO_3Br ($AE = Sr, Ba$). The Sr atoms are numerically labeled. The shadings are duplicated from Figure 5.2.

Table 5.3. Bond Lengths of AE_2BO_3Br (AE = Sr, Ba)

		<u>AE = Sr</u>	<u>AE = Ba</u>
AE1-O	x 3	2.715(5)	2.839(2)
AE1-O	x 6	2.729(1)	2.900(6)
AE1-Br		3.266(3)	3.421(2)
AE2-O	x 3	2.393(5)	2.593(6)
AE2-Br	x 3	3.199(1)	3.307(1)
AE2-Br		3.262(2)	3.396(2)
B-O	x 3	1.375(5)	1.392(5)

Table 5.4. Selected Bond Angles for AE_2BO_3Br (AE = Sr, Ba)

	<u>AE = Sr</u>	<u>AE = Ba</u>
Br-AE1-O	76.6(1)	76.8(1)
Br-AE1-O	141.7(1)	141.8(1)
O-AE1-O	51.8(2)	50.2(2)
O-AE1-O	64.6(2)	64.7(2)
O-AE1-O	65.0(2)	66.3(2)
O-AE1-O	69.0(2)	68.8(2)
O-AE1-O	114.8(1)	114.9(1)
O-AE1-O	133.3(1)	132.6(1)
O-AE1-O	152.4(2)	152.3(3)
Br-AE2-Br	73.03(3)	74.26(3)
Br-AE2-O	82.57(7)	82.17(8)
Br-AE2-O	135.3(1)	136.3(1)
Br-AE2-O	151.7(1)	149.4(1)
O-AE2-O	75.01(2)	73.5(2)
O-B-O	120	120

of 2.85 Å. The O—AE1—O atomic angle contained in the shared edge with the orthoborate group is constrained to 51.8(2)° in the Sr compound and 50.2(2)° in the Ba derivative, while adjacent O—AE1—O angles open to 69.0(2)° and 68.8(2)°, respectively. In both compounds the monocapping Br atom is positioned slightly beyond the calculated distance of 3.17 Å in Sr₂BO₃Br and 3.35 Å for Ba₂BO₃Br with respective interactions of 3.266(3) and 3.421(2) Å. The AE(2)O₃Br₄ site in both compounds have AE2—O distances much shorter than normal: 2.393(5) Å for Sr2—O and 2.593(6) Å for Ba2—O. On the opposite Br trigonal face, however, the AE1—Br bonds maintain typical distances in both structures. The orthoborate groups in the Sr and Ba analogues have trigonal symmetry with bond lengths of 1.375(5) Å and 1.392(5) Å, respectively.

Thermal Properties. Thermal analysis data for Sr₂BO₃Br and Ba₂BO₃Br are represented in Figures 5.4 and 5.5, respectively. In the Sr derivative the DTA heating curve exhibits two features as it transforms into a liquid state, while only one peak is observed upon freezing. Analysis of an X-ray pattern of the resulting solid reveals the presence of the compound Sr₅(BO₃)₃Br (29). These results are consistent with the peritectic reaction Sr₂BO₃Br → Sr₅(BO₃)₃Br + SrBr₂ at 1020 K followed by melting at 1125 K. To grow crystal of Sr₂BO₃Br, additional SrBr₂ is added to the melt to depress the freezing point below the decomposition temperature of 1020 K.

In contrast to the Sr analogue, the DTA data for Ba₂BO₃Br exhibit only one feature through the solid-liquid phase transition, and consequently, a congruent melting process is indicated to occur at 1148 K. Laboratory syntheses also are consistent with this result, for the compound is crystallized by directly melting the reagents and cooling (slowly or even quickly) to room temperature. The presence of only single phase Ba₂BO₃Br demonstrates it to be a congruent compound.

Optical Properties. Sr₂BO₃Br and Ba₂BO₃Br exhibit luminescence in the blue-green region of the visible spectrum when photoexcited by UV or X-ray radiation. The Eu²⁺ photoexcitation and emission spectra for both derivatives are depicted in Figures 5.6 and 5.7, respectively. The room temperature luminescence

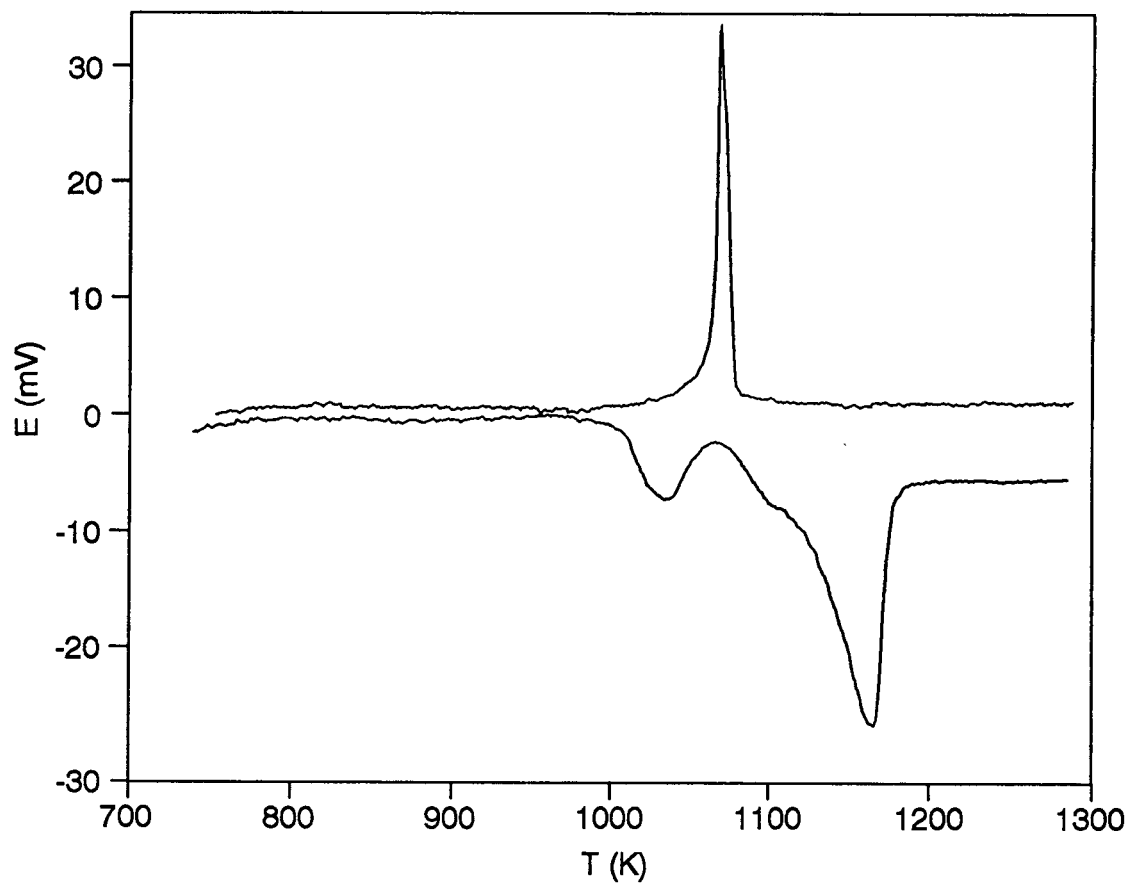


Figure 5.4. A DTA profile for $\text{Sr}_2\text{BO}_3\text{Br}$. The heating curve is below the cooling curve.

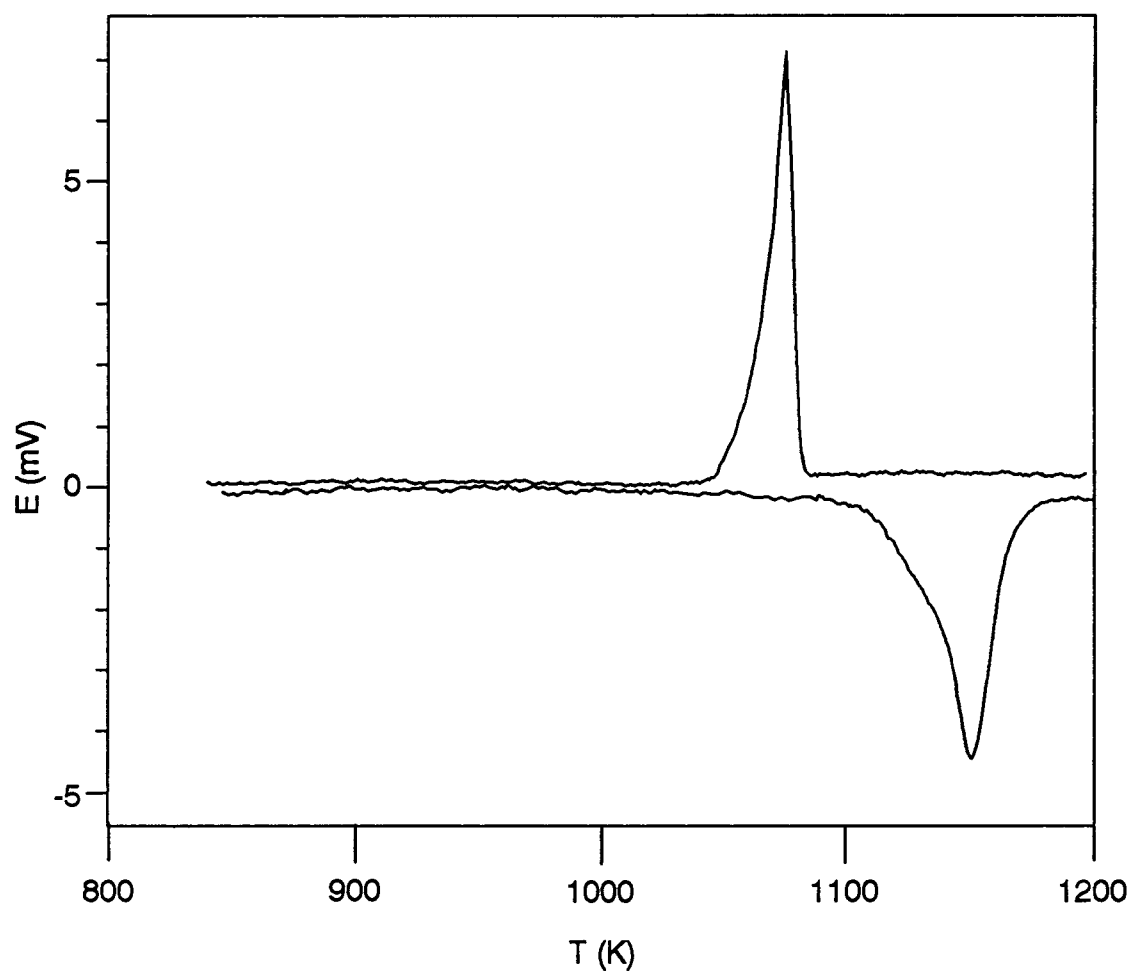


Figure 5.5. A DTA profile for $\text{Ba}_2\text{BO}_3\text{Br}$. The heating curve is below the cooling curve.

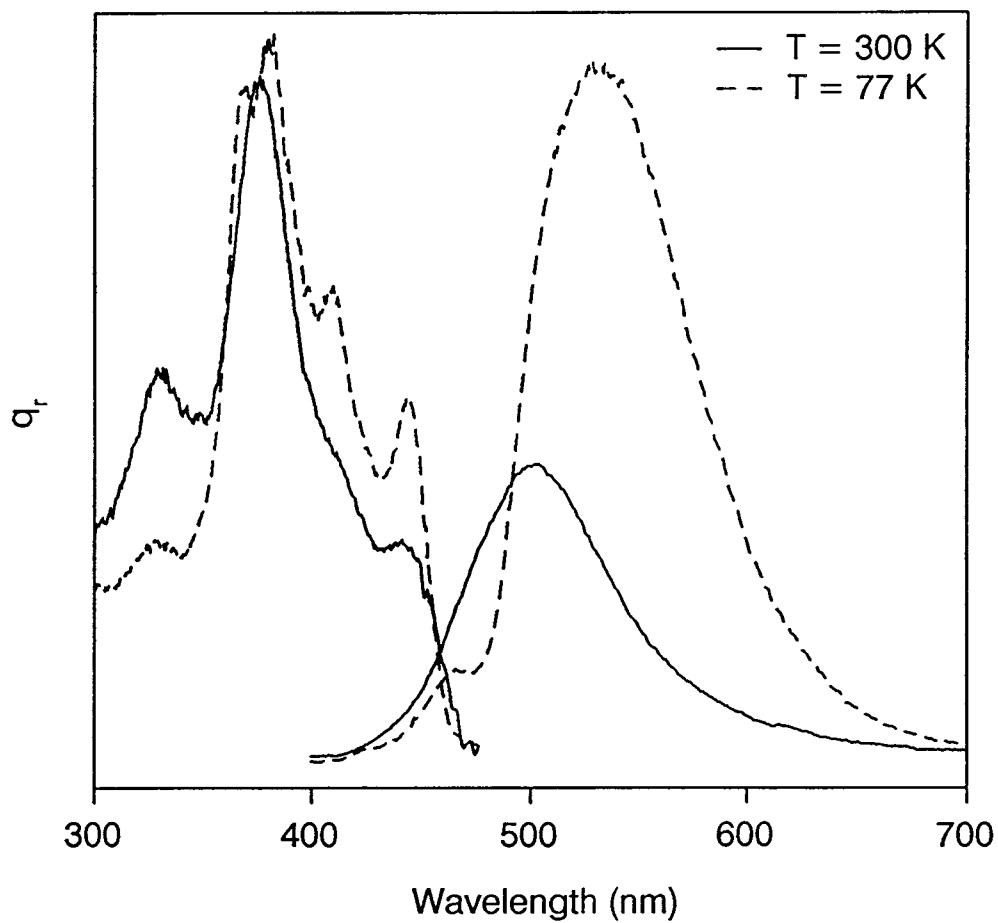


Figure 5.6. Photoexcitation and luminescence data for $\text{Sr}_2\text{BO}_3\text{Br}$.
T = 300 and 77 K. Intensities are relative.

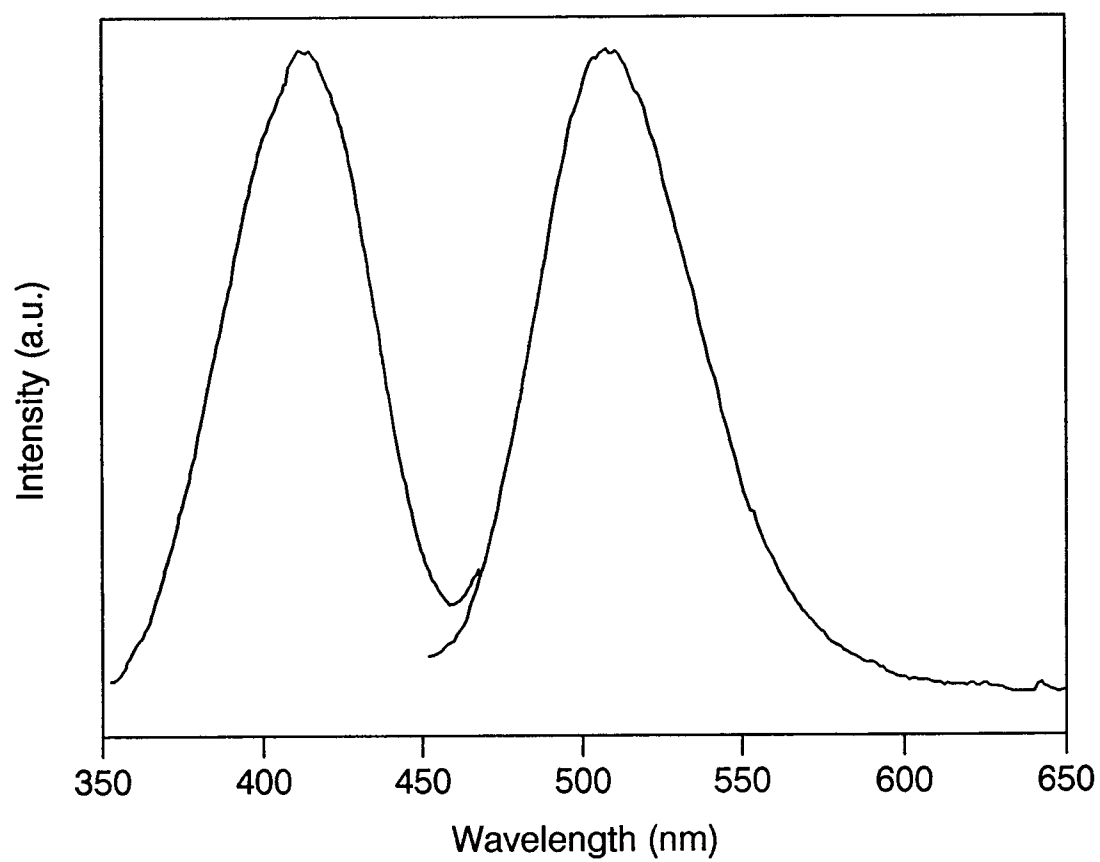


Figure 5.7. Photoexcitation and luminescence data for Ba₂BO₃Br at 300 K.

curves are single bands with maximum intensities at 500 nm for $\text{Sr}_2\text{BO}_3\text{Br}$ and 507 nm for $\text{Ba}_2\text{BO}_3\text{Br}$. By evaluating the energy difference in peak intensities of the excitation and emission curves, one can estimate the Stokes shift of these materials, since the $4f^6(7F_0)5d$ spin-orbit coupling feature is not clearly evident in the spectra. For the temperature dependence study of $\text{Sr}_2\text{BO}_3\text{Br}$, a shift in the positions and intensities of the emission bands occurs, and the full width at half maximum (FWHM) bandwidths increased when the sample was brought to 77 K. The peak maxima, bandwidths, and estimated Stokes shifts are summarized in Table 5.5.

Table 5.5. The Maxima of the $4f^6(^7F_0)5d$ Excitation / Emission Bands and the FWHM bandwidths (Γ) for A_2BO_3Br ($A = Sr, Ba$). All spectral values are expressed in nm.

	<u>T (K)</u>	<u>Ex</u>	<u>Em</u>	<u>Γ</u>
Sr ₂ BO ₃ Br	300	385	510	87
	77	390	530	79
Ba ₂ BO ₃ Br	300	412	507	64

Discussion

The transition responsible for the luminescence in these hosts occurs from the upper $4f^65d$ configuration to the $4f^7$ ground level. A schematic representation of the energy levels of Eu^{2+} is presented in Figure 5.8. The emission spectra are typically broad bands because of the vibronic coupling with the host environment through the $5d$ orbitals of the excited state. Strongly allowed $5d \rightarrow 4f$ dipole transitions usually engulf the weak intraconfigurational $4f \rightarrow 4f$ narrow band spectra, although emission associated with these line transitions is witnessed in some fluorides where the 6P_J states reside below the higher energy $5d$ levels (30). The position and shape of the $5d \rightarrow 4f$ emission curve will vary with the crystal field strength and coupling of the ion with a particular host; luminous colors of Eu^{2+} phosphors range from the UV (31) all the way into the red (32). The typical trend observed with Eu^{2+} is that as the crystal field strength of the host increases, the luminescence decreases in energy (33).

Raising the temperature in the $\text{Sr}_2\text{BO}_3\text{Br}:\text{Eu}$ sample from 77 K to 300 K shifted the emission band to a higher energy maximum by 740 cm^{-1} . This effect is common in other Eu^{2+} materials (34,35). The strength of phonon-electron interactions increase with temperature, causing the position of maximum luminescence to shift to higher energies and the emission bandwidth to broaden (36). As summarized in Table 5.5, the spectral data for the Sr analogue are consistent with this rationalization. Also, by increasing the temperature, the intensity of luminescence diminishes because of thermal quenching: the room temperature emission band is approximately 40% of the 77 K intensity whereas the excitation band intensity is not affected.

It is helpful at this point to consider the energy level diagram for a $4f^7 \text{Eu}^{2+}$ ion (Figure 5.8) to understand the origin of the structure in the excitation profile. In general, the dominant broad band is a result of exciting into the vibronically coupled $5d$ band. Nevertheless, the excited state configuration is subject to splitting that results from spin-orbit coupling, observed in the broad excitation bands of

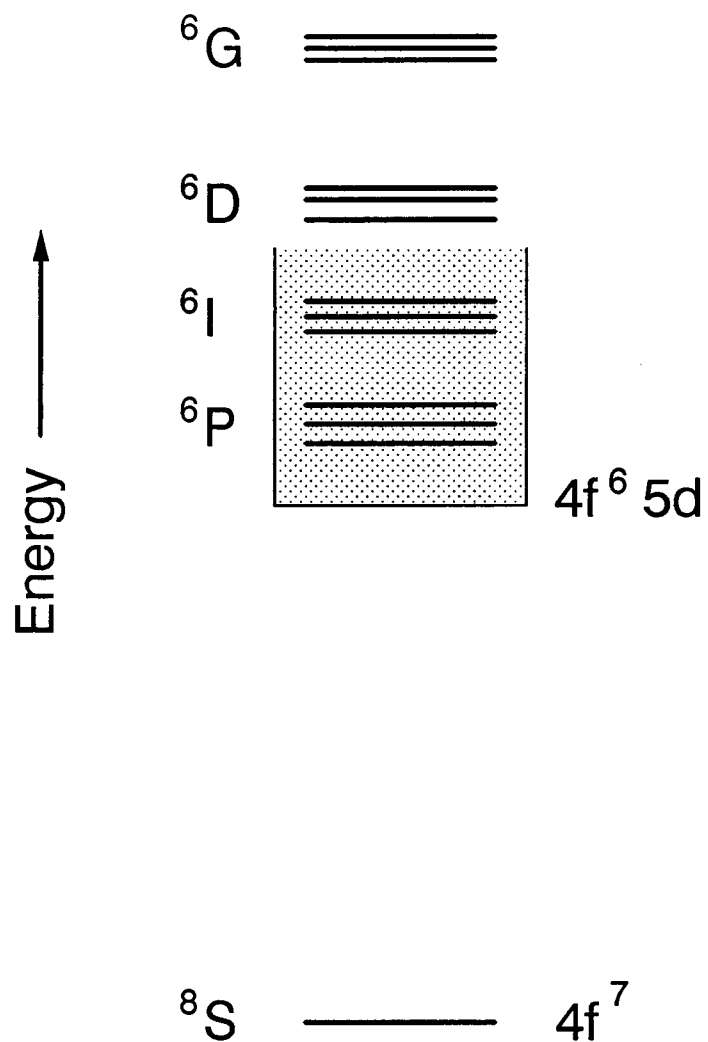


Figure 5.8. A sketch of the energy levels for Eu^{2+} ($4f^7$ configuration). The position of the 5d band is most dependent.

many Eu^{2+} hosts as superimposed structure at low-temperatures (37). At 77 K, these features become more prominent in the excitation curve of $\text{Sr}_2\text{BO}_3\text{Br}$ in Figure 5.6, but a conclusive assignment of the specific ${}^7\text{F}_j$ origins would be best achieved with data obtained at liquid He temperatures.

Some of these features may be associated with more than one Eu^{2+} centers contributing to the overall spectra. The weak high energy peaks located at 320 nm in the excitation band and 470 nm in the low temperature emission band may originate from a second Eu environment. The inability to model the data by a simple band shape analysis (38) supports the view that the curves are not simply a result of Eu environment (39). Even though there are two cation sites available for occupation by Eu (and perhaps the peaks mentioned above may indicate a discernable second site), the 300 K spectra for both materials display no lucid peak splittings indicative of site selectivity. Even at liquid helium temperatures, Eu^{2+} -doped alkaline-earth oxide halides $\text{A}_4\text{OX}_6:\text{Eu}$ ($\text{A} = \text{Ca}, \text{Sr}, \text{Ba}$), with two sites accessible for Eu population, exhibit no additional features to indicate two Eu environments (40). It is also possible that for these derivatives and the compounds studied here, Eu^{2+} may prefer only one site within the hosts. A dopant concentration study and emission lifetime measurements at very low temperatures may reduce thermal broadening to the point where the features for two Eu environments could become more salient.

One might expect the dissimilarity of the two sites in $\text{AE}_2\text{BO}_3\text{Br}$ to be notably discernable in the spectral profile — the ten-coordinate site is primarily surrounded by O atoms, whereas the 7-coordinate AE2 site is quite anisotropic; four Br atoms occupy one hemisphere, and three AE2–O bonds establish the other. However, two effects may be separately at work that would cause greater overlap of the individual band contributions: environments that are spectrochemically weak (AE2) and sites with greater coordinations (AE1) tend to emit at higher energies (41,33). Table 5.6 lists the luminescence peak wavelengths for a series of PSL compounds to demonstrate this spectrochemical trend. As the Eu^{2+} ion experiences more interaction with O atoms, the luminescence band maxima shift to lower

Table 5.6 The wavelengths (nm) at peak luminescence intensity for selected Eu²⁺-doped barium bromide materials (T = 300 K).

<u>Compound</u>	<u>λ_{\max}</u>	<u>Ref.</u>
BaFBr	400	42
Ba ₂ B ₅ O ₉ Br	425	3
Ba ₅ SiO ₄ Br ₆	440	45
Ba ₂ BO ₃ Br	507	this work

energies. Thus, the luminescence peaks from Eu^{2+} ions located at each AE site may not be as disparate as one might expect from merely structural considerations.

One practical feature for potential PSL materials is the trapped electron persistence over time and temperature changes. Its energy should only be released with the proper stimulus. If the trapped energy is highly sensitive to thermal variances or stray light, then the utility of the material becomes compromised.

The success of the material BaFBr:Eu^{2+} is thought to be a result of its high energy emission band. If the level of the 5d band is situated at an energy similar the trap, it is conceivable that trapped electrons may radiatively "bleed" its energy to a neighboring Eu center. Thus in this scheme, the material would be more sensitive to thermal agitation than expected from a predicted trap depth. If this is true, then the Sr phosphor may not possess sufficiently robust traps.

The $\text{Sr}_2\text{BO}_3\text{Br}$ compound exhibits properties that are not found in simple phosphor materials — evidence suggests that this material is capable of storing high energy photons that can later be extracted from the compound as Eu^{2+} luminescence. After the excitation energy (in the form of UV or X-ray radiation) is quickly removed from the sample, the emission continues for a fraction of a second, visible to the unaided eye. With $5d \rightarrow 4f$ transition lifetimes less than $1 \mu\text{s}$ (42) and even parity forbidden $4f \rightarrow 4f$ emission lifetimes near 1 ms (43), the delayed radiance cannot be explained by a simple luminescence scheme. Apparently, this compound undergoes an energy-storage mechanism, perhaps similar to the alkaline-earth binary halides that are used for X-ray phosphors (44).

It is believed that the excited energy electrons are held in potential wells within the host lattice itself, and upon photo- or thermal activation of these traps, the electron reassociates with Eu to emit back to the ground state. To characterize this stimulated emission, a thermoluminescence analysis would be a first step in learning more about the trap depths in this material, followed by a true X-ray exposure and PSL experiments to characterize the energy storage performance. Certainly, a more comprehensive study is warranted to closely examine these more complex processes.

Acknowledgments

The authors would like to thank Michael S. Nashner for providing the $\text{Ba}_2\text{BO}_3\text{Br:Eu}$ sample for optical studies. This research was supported by the US National Science Foundation, Solid-State Chemistry Program (DMR-8814432). Acknowledgment is made to the Donors of The Petroleum Research Fund, administered by the American Chemical Society, for partial support of the work. D.A.K. thanks the Alfred P. Sloan Research Foundation for a fellowship.

References

1. G. Blasse, A. Meijerink, D. Terrell, L. Neyens (1988) **Eur. Pat. Appl. EP 353,805** (Cl. C09K11/86), 07 Feb 1990, EP Appl. 88/201,693, 05 Aug 1990; 20 pp.
2. A. Meijerink, G. Blasse *J. Appl. Phys.*, **62(6)**, (1991) 626.
3. A. Meijerink, G. Blasse *J. Luminescence*, **43**, (1989) 283.
4. A. Meijerink, G. Blasse, L. Struye *Mater. Chem. Phys.*, **21**, (1989) 261.
5. J. Lin, M. Su *J. Luminescence*, **43**, (1988) 155.
6. H. von Seggern, A. Meijerink, T. Voigt, A. Winnacker *J. Appl. Phys.*, **66(9)**, (1989) 4418.
7. Fuji Corp., U.S. Pat. 4,239,968; U.S. Pat. 4,236,078.
8. M. Sonoda, M. Takano, J. Miyahara, H. Kato *Radiology*, **148**, (1983) 833.
9. J. Zhang, S. Huang, J. Yu *Optics Lett.*, **17(16)**, (1992) 1146.
10. R.J. Reeves, R.M. MacFarlane *Physical Rev. B*, **47(1)**, (1993) 158.
11. A. Winnacker, R.M. Shelby, R.M. MacFarlane *Optics Lett.*, **10(7)**, (1985) 350.
12. K. Takahashi, K. Kohda, J. Miyahara, Y. Kanemitsu, K. Amitani, S. Shionoya *J. Luminescence*, **31 & 32**, (1984) 266.
13. H. von Seggern, T. Voigt, W. Knüpfer, G. Lange *J. Appl. Phys.*, **64(3)**, (1988) 1405.
14. M.K. Crawford, L.H. Brixner *J. Luminescence*, **48 & 49**, (1991) 37.
15. A.M. Stoneham, *Theory of Defects in Solids*, Oxford University Press: UK, (1975).
16. F.K. Koschnick, J-M Spaeth, R.S. Eachus *J. Phys.: Condensed Matter*, **4**, (1992) 3015.
17. S.K. Sekatskii, V.S. Letokhov *Optics Comm.*, **95**, (1993) 260.

18. D.S. Hamilton, S.K. Gayen, G.J. Pogatshnik, R.D. Ghen *Phys. Rev.*, **B39**, (1989) 8807.
19. C. Dujardin, B. Moine, C. Pedrini *J. Luminescence*, **54**, (1993) 259. A topical summary is in the introduction.
20. J.P. Jouart, M. Bouffard, G. Klein, G. Mary *J. Luminescence*, **50**, (1991) 273.
21. X-P. Sun, M-Z. Su *J. Luminescence*, **40&41**, (1988) 171.
22. S.M. Dohopte, P.L. Muthal, V.K. Kondawar, S.V. Maharil *J. Luminescence*, **50**, (1991) 187.
23. Molecular Structure Corporation, 3200A Research Forest Drive, The Woodlands, TX 77381, USA.
24. G.M. Sheldrick *Crystallographic Computing 3*, Oxford: Oxford University Press, (1985) 175-189.
25. N. Walker, D. Stuart *Acta Crystallogr., Sect. A*, **39**, (1983) 158.
26. *International Tables for X-ray Crystallography, Vol. IV*, Birmingham: Kynoch Press (1974). (Present distributor: Kluwer Academic Publishers, Dordrecht.)
27. J.R. Cox, D.A. Keszler "The Layered Borates $Ba_3M(BO_3)_3$ (M = Dy, Ho, Y, Er, Tm, Yb, Lu, and Sc) *Chem. Mat.*, in preparation.
28. R. Shannon, C. Prewitt *Acta Crystallogr., Sect. B*, **25**, (1968) 925.
29. T. Alekel III, D.A. Keszler *Inorganic Chem.*, **C48**, (1992) 1382.
30. M.V. Hoffman *J. Electrochem. Soc.*, **118**, (1971) 933.
31. K.I. Schaffers, T.A. Reynolds, D.A. Keszler, "Tetrahedral Triangular 3-D Framework and Luminescence in the Borate $BaBe_2(BO_3)_2$ " *Inorganic Chem.*, in preparation.
32. G.J. Dirksen, G. Blasse *J. Solid State Chem.*, **92**, (1991) 591.
33. C. Fouassier, B. Latourrette, J. Portier, P. Hagenmuller *Mat. Res. Bull.*, **11**, (1976) 933.
34. A.M. Ghazzawi, G.E. Venikouas, R.C. Powell *J. Solid State Chem.* **57**, (1985)

- 332.
35. Z-P. Huang, S-X Liu, F-H. Liao *Eur. J. Solid State Inorg. Chem.* **28**, (1991) 147.
 36. B. Di Bartolo *Optical Interaction in Solids*, John Wiley & Sons: New York, (1968).
 37. J. Sytsma, G. Blasse *J. Luminescence*, **51**, (1992) 283.
 38. B. Henderson, G.F. Imbush *Optical Spectroscopy of Inorganic Solids*, ed. H. Fröhlich, Clarendon Press: Oxford (1989) Ch. 5.
 39. G. Huber, S. Payne, L.L. Chase, W.F. Krupke *J. Luminescence*, **39**, (1988) 259.
 40. W.J. Schipper, Z.A.E.P. Vroon, G. Blasse *Chem. Mater.*, **4**, (1992) 688.
 41. G. Blasse *Prog. Solid State Chem.*, **18**, (1988) 79.
 42. J.P. Spoonhower, M.S. Burberry *J. Luminescence*, **43**, (1989) 221.
 43. R.A. Hewes, M.V. Hoffmann *J. Luminescence*, **3**, (1971) 261.
 44. K. Takahashi, J. Miyahara, Y. Shibahara *J. Electrochem. Soc.*, **132(6)**, (1985) 1492.
 45. A. Meijerink, G. Blasse *J. Luminescence*, **47**, (1990) 1.

CHAPTER 6

Crystal Chemistry of *STACK*
 $A_6MM'(BO_3)_6$

Kathleen I. Schaffers, Paul D. Thompson, Theodore Alekel III
James R. Cox, and Douglas A. Keszler*

Department of Chemistry and
Center for Advanced Materials Research
Oregon State University
Gilbert Hall 153
Corvallis, OR 97331-4003

To be submitted to *Chemistry of Materials*

Abstract

The crystal chemistry of the STACK family of orthoborates having the formula $A_6MM'(BO_3)_6$ where $A = \text{Sr, Ba, Pb, or Ln}$ ($\text{Ln} = \text{lanthanide}$), and $M, M' = +2, +3, \text{ or } +4$ metal cation is described. Over 150 individual members of the family have been synthesized; they crystallize in the trigonal space group $R\bar{3}$ with unit cell volumes ranging from 1143.8(1) to 1365.6(3) \AA^3 . In this report, the metal site preferences, disorder, and solid solubility of these phases are discussed. Interrelationships between this structure and the layered structure type of $\text{Ba}_3\text{Sc}(\text{BO}_3)_3$ are also detailed.

Introduction

Among the myriad of known solid-state inorganic structure types, there exist common examples such as rock salt, garnet, spinel, zinc blende, elpasolite, and perovskite where a common arrangement is retained with a great variety of atomic constituents. For example, the compounds NaCl, MgO, MgS, CaO, CaS, TiO, and ScN all adopt the rock salt structure, and the oxides $\text{Ca}_3\text{Al}_2\text{Si}_3\text{O}_{12}$, $\text{Y}_3\text{Al}_5\text{O}_{12}$, $\text{Gd}_3\text{Ga}_5\text{O}_{12}$, and $\text{Ca}_3\text{Te}_2\text{Zn}_3\text{O}_{12}$ all crystallize in the garnet structure. We derive a sense of order from classifying materials in this way, but the efficacy of doing so certainly derives from the capacity to control physical properties by freely substituting selected atoms at specific sites while maintaining structural integrity. In fact, many of our modern technological advances can be traced to this ability.

In a recent contribution we reported the existence of an entirely new family of compounds whose members now comprise one of the larger structural classes of material reported to date (1). This family, which we designate STACK, is derived from the structure of the compound $\text{Sr}_3\text{Sc}(\text{BO}_3)_3$ (2,3) by substitution of a variety of atoms at the Sr and Sc sites. The general formula is $\text{A}_6\text{MM}'(\text{BO}_3)_6$ where A = Sr, Ba, Pb, or selected lanthanides; M = Ca, Sr, Y, Sc, In, Bi, or selected lanthanides; and M' = Mg, Al, Cr, Mn, Fe, Co, Rh, Zn, Sc, In, Zr, Hf, Sn, or selected lanthanides.

In developing the physical properties of these new materials, it will be necessary to grasp the structural consequences and patterns encountered with the various chemical substitutions. In this report, we discuss the crystal chemistry of this family and establish interrelationships with the layered structure type of the compound $\text{Ba}_3\text{Sc}(\text{BO}_3)_3$, which we described in the preceding report of this series.

Experimental Section

Synthesis. Powders of the Sr compounds were synthesized by using standard high-temperature solid-state methods. Stoichiometric quantities of the starting reagents (nitrates, carbonates, or oxides, typically $\geq 99.9\%$) were mixed with a 5 mol% excess of B_2O_3 , ground under hexane, and heated at 923 K for 1 h to decompose the reagents and initiate the reactions. The samples were reground and heated for 6 h at 1028 K, for 12 h at 1123 K, and for 24 h in the range 1173 - 1673 K, depending on the sintering characteristics of the sample. Analysis of powder X-ray diffraction patterns obtained with a Philips automated diffractometer confirmed the formation of the desired product. Further synthesis studies on the derivatives $Sr_3Sc(BO_3)_3$ and $Sr_6YAl(BO_3)_6$ revealed that they could be synthesized by using a flash-synthesis method. The reagents were ground under hexane and heated in a Pt crucible directly at 923 K for 20 min and 1023 K for 15 min to initiate the reaction. The powder was then ground and heated promptly at 1273 K for 3 h. It is likely that most of the Sr derivatives can be prepared by this method.

In general, a different set of conditions is necessary for synthesis of crystalline Ba derivatives. The flash-synthesis method can only be used for a few compounds, and lower heating temperatures (1123 K - 1223 K) are generally required to avoid melting the sample. Also, smaller incremental increases in temperature, 25 - 75 K after each grinding, and longer heating times are typically needed to produce homogeneous samples. Each heating period lasted 12 - 24 h but could be as long as several days. For example, the compound $Ba_6ErFe(BO_3)_6$ was prepared by grinding together stoichiometric ratios of the starting materials with 5 mol% excess B_2O_3 and heating at 898 K for 1 h, 1008 K for 19 h, 1073 K for 24 h, 1123 K for 21 h, and 1148 K for 14 h. The compound $Ba_6GdSc(BO_3)_6$, however, is readily prepared by flash heating.

Powder data for the materials were collected on an automated Philips diffractometer; peak positions were corrected by using NIST Si Standard 640b. Unit cell parameters were refined by least-squares analysis with eleven peaks in the

range $26 \leq 2\theta \leq 58^\circ$. The hkl assignments of each reflection were determined by comparison to powder X-ray patterns of the parent material $\text{Sr}_3\text{Sc}(\text{BO}_3)_3$ (2) and other selected derivatives.

To establish experimental variation in unit cell parameters, six pairs of samples were compared to determine the variance of their cell parameters **a** and **c** and unit cell volumes **V**. The maximum differences found (**a**, **c** and **V**) were used as an estimate of maximum deviation from an average value. Reported values were found to be within $\pm 0.1\%$ for **a**, $\pm 0.2\%$ for **c**, and $\pm 0.5\%$ for **V**. Actual statistical deviations from the refinements with X-ray data are included in parentheses in Table 6.3. In each case inclusion of a larger cation should result in a larger unit cell but this may not occur if the enlargement is less than the experimental errors associated with the compound synthesis and cell parameter determination. Reported e.s.d.'s in the cell parameter tables have their origin in the POLSQ program and reflect the uncertainty with which the least squares fit has settled on a specific value. Actual variations in unit cell parameters up to 0.019 \AA are an order of magnitude larger than e.s.d.'s indicated by POLSQ. Sources of experimental error include the precision in weighing the starting reagents which can skew the stoichiometry of the product. Also, in a few cases, poor sample crystallinity affords broad and asymmetric diffraction peaks that lead to uncertainties in selecting peak positions.

Crystal Growth. Single crystals of $\text{Sr}_6\text{Y}_{1.07}\text{Al}_{0.93}(\text{BO}_3)_6$, $\text{Sr}_6\text{Ho}_{0.964}\text{Sc}_{1.036}(\text{BO}_3)_6$, $\text{Sr}_6\text{Er}_{1.40}\text{Sc}_{0.60}(\text{BO}_3)_6$, $\text{Sr}_6\text{La}_{0.84}\text{Sc}_{1.16}(\text{BO}_3)_6$, and $\text{Ba}_6\text{Gd}_{1.28}\text{Sc}_{0.72}(\text{BO}_3)_6$ were grown by slowly cooling melts. Crystals of $\text{Sr}_6\text{Y}_{1.07}\text{Al}_{0.93}(\text{BO}_3)_6$ were seized from a melt with the following mol% composition: 61.5 SrO, 5.1 Y_2O_3 , 7.9 Al_2O_3 , 20.5 B_2O_3 , and 5.1 Li_2O . The melt was cooled from 1273 K to 1073 K at 10 K/h and then to room temperature at 100 K/h. A crystal was removed from the matrix by dissolution of the flux in dilute $\text{HNO}_3(\text{aq})$. Crystals of $\text{Sr}_6\text{HoSc}(\text{BO}_3)_6$ were grown by melting a stoichiometric sample in a Pt crucible at 1773 K followed by cooling at 4 K/h to 1273 K and 40 K/h to room temperature. A crystal of $\text{Sr}_6\text{Er}_{1.40}\text{Sc}_{0.60}(\text{BO}_3)_6$ was isolated from a melt corresponding to the stoichiometric proportions of

$\text{Sr}_6\text{ErSc}(\text{BO}_3)_6$. The heating and cooling programs were the same as those applied to the Ho crystals. Crystals of $\text{Sr}_6\text{La}_{0.84}\text{Sc}_{1.16}(\text{BO}_3)_6$ were obtained from a melt of 70 mol% $\text{Sr}_6\text{LaSc}(\text{BO}_3)_6$: 30 mol% CaF_2 that was cooled from 1648 to 1348 K at 15 K/h followed by cooling to room temperature at 130 K/h. Single crystals of $\text{Ba}_6\text{Gd}_{1.28}\text{Sc}_{0.72}(\text{BO}_3)_6$ were grown by melting the stoichiometric material $\text{Ba}_6\text{GdSc}(\text{BO}_3)_6$ in a Pt crucible at 1573 K and then cooling to 1373 K at 5 K/h and at 40 K/h to room temperature.

Single-crystal Work. Relevant crystal data for each of the structures are presented in Table 6.1.

$\text{Sr}_6\text{Y}_{1.07}\text{Al}_{0.93}(\text{BO}_3)_6$. A 0.2 x 0.2 x 0.2 mm crystal was selected for analysis. The data were collected on a Rigaku AFC6 rotating anode diffractometer equipped with a graphite monochromator set for Mo $K\alpha$ radiation. 2381 reflections were measured by using ω - 2θ scans in covering the range of indices $0 \leq h \leq 17$, $-17 \leq k \leq 17$, and $-12 \leq l \leq 12$ to $2\theta_{\text{max}} = 60^\circ$. From these data, 764 unique reflections with $F_o^2 \geq 3\sigma(F_o^2)$ were available for structure determination and refinement. Three standard reflections measured after each block of 200 data exhibited excursions of less than 2.5%. A Digital μ VAX-II computer, together with programs from the TEXSAN crystallographic software package (4), were used to solve the structure. The heavy atoms Sr and Y were located by using the direct methods program SHELXS (5), and the positions of the other atoms were determined from analysis of difference electron density maps. After several cycles of the least-squares refinement, the isotropic displacement coefficient at the Al site had refined to a negative value, indicating the presence of additional electron density. The multiplicity of the site was subsequently refined to a value greater than unity. It was then modeled with two disordered atoms (Y and Al) where the population was fixed at unity and the x, y, z, and B parameters of the Y atom were constrained to those of the Al atom. Refinement of the multiplicity indicated that 7.3% of the Al sites were occupied by Y atoms to give the more exacting formula $\text{Sr}_6\text{Y}(\text{Al}_{0.927}\text{Y}_{0.073})(\text{BO}_3)_6$. The data were corrected for absorption with the program DIFABS (6) and subsequently averaged ($R_{\text{int}} = 0.108$). Anisotropic displacement

Table 6.1. Crystal data for $\text{Sr}_6\text{YAl}(\text{BO}_3)_6$, $\text{Sr}_6\text{ErSc}(\text{BO}_3)_6$, $\text{Sr}_6\text{HoSc}(\text{BO}_3)_6$, $\text{LaSr}_6\text{Sc}(\text{BO}_3)_6$, and $\text{Ba}_6\text{GdSc}(\text{BO}_3)_6$.

	<u>$\text{Sr}_6\text{YAl}(\text{BO}_3)_6$</u>	<u>$\text{Sr}_6\text{ErSc}(\text{BO}_3)_6$</u>	<u>$\text{Sr}_6\text{HoSc}(\text{BO}_3)_6$</u>	<u>$\text{LaSr}_6\text{Sc}(\text{BO}_3)_6$</u>	<u>$\text{Ba}_6\text{GdSc}(\text{BO}_3)_6$</u>
Formula Weight, amu	994.46	1090.79	1088.45	1102.51	1379.04
Crystal System	-----Rhombohedral-----				
Space Group	----- $\text{R}\bar{3}$ -----				
a, Å	12.162(3)	12.322(1)	12.285(3)	12.388(1)	12.960(1)
c, Å	9.103(4)	9.293(2)	9.268(2)	9.294(2)	9.538(2)
V, Å ³	1166.1(8)	1221.8(3)	1211.2(5)	1235.2(2)	1387.2(3)
Z	3	3	3	3	3
D _{calc} , g cm ⁻³	4.248	4.447	4.476	4.446	4.952
F(000)	1362	1473	1470	1500	1785
Diffractometer	-----Rigaku AFC6R-----				
Radiation	-----Mo K α ($\lambda=0.71069$ Å)-----				
Data Collected	-----+h, \pm k, \pm l-----				
No. Observations	568	835	693	920	1191
($F_o^2 \geq 3\sigma(F_o^2)$)					
R	0.040	0.034	0.025	0.048	0.055
R _w	0.042	0.045	0.039	0.068	0.063

coefficients were applied to the Sr, Y, B, and O sites in refinement to the final residuals $R = 0.040$ and $R_w = 0.042$. The largest peak in the final difference electron density map corresponds to 0.96% of an Y atom.

$Sr_6Ho_{0.964}Sc_{1.036}(BO_3)_6$. A single crystal of approximate dimensions 0.15 x 0.17 x 0.20 mm was selected for structure analysis on the same diffractometer. From 2456 reflections measured to $2\theta_{max} = 60^\circ$ over the range of indices $0 \leq h \leq 17$, $-17 \leq k \leq 17$, and $-13 \leq l \leq 13$, 693 unique reflections with $F_o^2 \geq 3\sigma(F_o^2)$ were obtained. Three standards measured after every 200 reflections deviated on average by less than 1.5%. Each of the atoms was positioned by comparison to the isostructural compound $Sr_3Sc(BO_3)_3$ (2). After several cycles of least-squares refinement, examination of the isotropic displacement coefficients indicated a disorder over the Ho1 and Sc1 sites. They were then modeled with two atoms at each position with the occupancy constrained to unity. The x, y, z, parameters were fixed, and the B values of atoms Sc2 and Ho2 were constrained to those of atoms Ho1 and Sc1, respectively. The data were corrected for absorption with the program DIFABS and subsequently averaged ($R_{int} = 0.045$). Least-squares refinement with anisotropic displacement coefficients on the Sr, B, and O atoms and an extinction parameter = $0.19(3) \times 10^{-6}$ afforded the final residuals $R = 0.027$ and $R_w = 0.041$. The largest peak in the final difference electron density map corresponds to 0.27% of a Ho atom. A descriptive formula representing the final result is $Sr_6(Ho_{0.892(5)}Sc_{0.108})(Sc_{0.928(4)}Ho_{0.072})(BO_3)_6$.

$Sr_6Er_{1.40}Sc_{0.60}(BO_3)_6$. A crystal of approximate dimensions 0.20 x 0.20 x 0.25 mm was mounted on the Rigaku diffractometer for structure analysis. Cell constants were obtained from least-squares refinement of the setting angles of 15 reflections in the range $36 < 2\theta < 42^\circ$. From 2135 reflections of the type $h, \pm k, \pm l$ measured to $2\theta_{max} = 65^\circ$, 979 unique reflections were obtained. The positions of the heavy atoms Sr, Er, and Sc were taken from the solution of the Ho analog. The positions of the B and O atoms were subsequently determined from analyses of difference electron density maps. The occupancies of the M and M' sites were determined in a manner similar to the Ho derivative. The data were corrected for

absorption and averaged ($R_{\text{int}} = 0.067$). The Er and Sc atoms were subsequently refined with isotropic displacement coefficients while the remaining atoms were refined with anisotropic coefficients. Final refinement on F_o with data having $F_o^2 \geq 3\sigma(F_o^2)$ and a secondary extinction coefficient = $0.25(2) \times 10^{-6}$ afforded the final residuals $R = 0.034$ and $R_w = 0.045$. The largest peak in the final difference electron density map corresponds to 1.8% of a Sr atom. The formula that indicates the occupancies of the M and M' sites is $\text{Sr}_6(\text{Er}_{0.915(5)}\text{Sc}_{0.085})(\text{Er}_{0.488(5)}\text{Sc}_{0.512})(\text{BO}_3)_6$.

$\text{Sr}_6\text{La}_{0.84}\text{Sc}_{1.16}(\text{BO}_3)_6$. A crystal of approximate size 0.2 x 0.2 x 0.3 mm was mounted for structure analysis. Cell constants were obtained from least-squares refinement with the setting angles of 17 centered reflections in the range $30.5 \leq 2\theta \leq 36^\circ$. Three standard reflections measured throughout the data collection exhibited no significant variations. From 3741 reflections measured over the range of indices $-19 \leq h \leq 19$, $0 \leq k \leq 19$, and $-15 \leq l \leq 15$ to $2\theta_{\text{max}} = 70^\circ$, 1205 unique reflections were obtained. The atoms on special positions were placed by analogy to the previous structures, and the remaining atoms were found by interpretation of difference electron density maps. Approximate site occupancies were determined by refining multiplicities with Sr atoms in the general-position sites and the special position $0, 0, \frac{1}{2}$. These occupancies were subsequently modeled with partial substitution of La on the general position and Sc on the special position. The refinement was then constrained to give a total unit occupancy for the special position and an appropriate La concentration on the general position to maintain charge neutrality. Following refinement of the model with isotropic displacement factors, the data were corrected for absorption and merged ($R_{\text{int}} = 0.073$). Final refinement with anisotropic displacement coefficients on the Sc1, B, and O atoms and an extinction correction = $0.8(1) \times 10^{-6}$ afforded the residuals $R = 0.048$ and $R_w = 0.068$. The largest peak in the final difference electron density map corresponds to 4% of a Sc atom. The final results afford the descriptive formula $(\text{Sr}_{5.16}\text{La}_{0.84})(\text{Sr}_{0.84(2)}\text{Sc}_{0.16})\text{Sc}(\text{BO}_3)_6$.

$\text{Ba}_6\text{Gd}_{1.29}\text{Sc}_{0.72}(\text{BO}_3)_6$. A single crystal of approximate dimensions 0.1 x 0.1 x 0.15 mm was selected for structure determination. A total of 1176 unique

reflections having $F_o^2 \geq 3\sigma(F_o^2)$ were obtained by using the ω - 2θ scan technique to collect 4197 reflections in the range $2 \leq 2\theta \leq 80^\circ$. Three standards measured throughout the data collection exhibited an average deviation of 0.23%. The position of the Ba atom was determined from the results of the direct methods program SHELXS, and the Gd and Sc atoms were located by analogy to the structure described above. The remaining atoms were located from examination of difference electron density maps. The magnitude of the temperature factors after least squares refinement indicated disorder at the Gd and Sc sites. Refinement of the multiplicities gave 13% Sc on the Gd site and 41% Gd on the Sc site so that the formula is $\text{Ba}_6(\text{Gd}_{0.869(3)}, \text{Sc}_{0.131})(\text{Sc}_{0.589}, \text{Gd}_{0.411(4)})(\text{BO}_3)_6$. The data were corrected for absorption with the program DIFABS and averaged ($R_{\text{int}} = 0.080$). The Ba, B, and O atoms were refined with anisotropic displacement coefficients, and the remaining atoms were refined isotropically. The converged refinement affords the final residuals $R = 0.055$ and $R_w = 0.063$. The largest peak in the difference electron density map corresponds to 3.5% of a Gd atom. Positional parameters and equivalent isotropic displacement coefficients for each of the structures are summarized in Tables 6.2a and 6.2b.

Table 6.2a. Positional parameters for $\text{Sr}_6\text{YAl}(\text{BO}_3)_6$, $\text{Sr}_6\text{ErSc}(\text{BO}_3)_6$, and $\text{Sr}_6\text{HoSc}(\text{BO}_3)_6$.

		$\text{Sr}_6\text{YAl}(\text{BO}_3)_6^a$	$\text{Sr}_6\text{ErSc}(\text{BO}_3)_6^b$	$\text{Sr}_6\text{HoSc}(\text{BO}_3)_6^c$
A	x	0.57169(4)	0.57542(5)	0.57425(5)
	y	0.04230(4)	0.04144(5)	0.04197(5)
	z	0.69465(6)	0.68987(6)	0.69082(5)
	$B_{\text{c}q}$	0.70(2)	0.60(2)	0.55(2)
M	x	0	0	0
	y	0	0	0
	z	0	0	0
	$B_{\text{c}q}$	0.50(2)	0.35(2)	0.31(2)
M'	x	0	0	0
	y	0	0	0
	z	$\frac{1}{2}$	$\frac{1}{2}$	$\frac{1}{2}$
	$B_{\text{c}q}$	0.38(5)	0.46(2)	0.20(5)
B	x	0.1906(5)	0.1982(6)	0.1974(5)
	y	0.1354(5)	0.1427(5)	0.1407(5)
	z	0.7569(8)	0.7614(7)	0.7597(6)
	$B_{\text{c}q}$	0.7(2)	0.6(2)	0.5(2)
O1	x	0.1717(3)	0.1686(4)	0.1683(4)
	y	0.6327(3)	0.6254(4)	0.6276(4)
	z	0.8175(5)	0.8149(5)	0.8154(4)
	$B_{\text{c}q}$	1.1(1)	0.9(1)	0.8(1)
O2	x	0.6234(3)	0.6150(4)	0.6170(4)
	y	0.1802(3)	0.1643(4)	0.1687(4)
	z	0.9443(4)	0.9501(5)	0.9483(4)
	$B_{\text{c}q}$	0.9(1)	1.0(1)	0.8(1)
O3	x	0.5954(3)	0.5937(4)	0.5949(4)
	y	-0.0762(3)	-0.0712(4)	-0.0731(4)
	z	0.4724(5)	0.4763(5)	0.4756(4)
	$B_{\text{c}q}$	1.0(1)	1.1(1)	0.9(1)

^a A = Sr; M = Y; M' = Al(0.93), Y(0.07)

^b A = Sr; M = Er(0.915), Sc(0.085); M' = Er(0.488), Sc(0.512)

^c A = Sr; M = Ho(0.892), Sc(0.108); M' = Sc(0.928), Ho(0.072)

Table 6.2b. Positional parameters for $\text{LaSr}_6\text{Sc}(\text{BO}_3)_6$ and $\text{Ba}_6\text{GdSc}(\text{BO}_3)_6$.

		<u>$\text{LaSr}_6\text{Sc}(\text{BO}_3)_6^{\text{d}}$</u>	<u>$\text{Ba}_6\text{GdSc}(\text{BO}_3)_6^{\text{e}}$</u>
A	x	0.57741(5)	0.57506(3)
	y	0.04338(5)	0.04058(3)
	z	0.69168(6)	0.69372(4)
	$B_{\text{c}q}$	0.87(2)	1.21(2)
M	x	0	0
	y	0	0
	z	0	0
	$B_{\text{c}q}$	0.76(3)	1.05(2)
M'	x	0	0
	y	0	0
	z	$\frac{1}{2}$	$\frac{1}{2}$
	$B_{\text{c}q}$	0.89(6)	2.80(8)
B	x	0.2014(7)	0.1936(8)
	y	0.1433(7)	0.1378(7)
	z	0.7572(8)	0.7558(9)
	$B_{\text{c}q}$	0.9(2)	1.6(2)
O1	x	0.1555(4)	0.1691(6)
	y	0.6228(5)	0.6257(6)
	z	0.8255(6)	0.8217(8)
	$B_{\text{c}q}$	1.2(1)	2.6(2)
O2	x	0.6217(5)	0.6207(5)
	y	0.1669(5)	0.1734(5)
	z	0.9465(5)	0.9509(6)
	$B_{\text{c}q}$	1.6(2)	1.9(2)
O3	x	0.5911(5)	0.5879(5)
	y	-0.0720(5)	-0.0825(5)
	z	0.4766(6)	0.4726(7)
	$B_{\text{c}q}$	1.6(2)	2.1(2)

^d A = Sr(5.16), La(0.84); M = Sr(.84), Sc(0.16); M' = Sc

^e A = Ba; M = Gd(0.92), Sc(0.08); M' = Sc(0.66), Gd(0.34)

Results and Discussion

STACK Structure. A listing of the STACK compounds that we have prepared along with their unit-cell parameters is given in Table 6.3. The unit-cell volumes range from 1143.8(1) Å³ for the compound Sr₆ScAl(BO₃)₆ to 1414.0(2) Å³ for the derivative Ba₆SrZr(BO₃)₆. The precision attained in the refinement of the parameters is an indication of the high crystallinity of most of the samples. They are, in fact, hard, dense, and stable ceramic materials, much like the members of other oxide families such as spinel and perovskite. Melting points of the more stable derivatives extend to approximately 1673 K.

The nominal formula A₆MM'(BO₃)₆ results from structural considerations of the parent compound Sr₃Sc(BO₃)₃ ≡ Sr₆ScSc'(BO₃)₆. As reported in the first paper of this series, the structure is a high symmetry trigonal type forming in a rhombohedral cell. It contains two types of Sc-centered O octahedra that alternately stack between planar triangular BO₃ groups to form chains (Figure 6.1) that extend along the trigonal axis. The 3-dimensional structure (Figure 6.2) results from linkage of these chains through the 9-coordinate Sr atoms. It is the specific linkages between the Sc- and Sr-centered sites that afford the inequivalence of the octahedra. One octahedron is larger, trigonally elongated, and shares only vertices with the 9-fold site, while the other is trigonally compressed and shares its triangular faces with the 9-fold site. In the formula A₆MM'(BO₃)₆, A then represents an atom on the 9-coordinate site, M is an atom on the larger octahedral site, and M' is an atom on the smaller octahedral site. For example, the formula Sr₆YSc(BO₃)₆ contains A = Sr, M = Y, and M' = Sc.

We describe below in more detail the microscopic characteristics of these materials. In particular, we examine the distribution of cations among the A, M, and M' sites, establish regions of stability within various subclasses, and illustrate the types of chemical substitutions that will allow incorporation of ~ 50% of the elements from the periodic table into this structure type. The crystal-chemical results are certainly not exhaustive at the present time, but we can proceed in

Table 6.3. Cell parameters for the family $A_6MM'(BO_3)_6$ (STACK).

<u>Compound</u>	<u>a (Å)</u>	<u>c (Å)</u>	<u>V (Å³)</u>
Sr ₆ ScAl(BO ₃) ₆	12.082(1)	9.047(1)	1143.8(1)
Sr ₆ ScCr(BO ₃) ₆	12.104(1)	9.095(2)	1154.0(2)
Sr ₆ LuAl(BO ₃) ₆	12.141(1)	9.071(2)	1158.1(2)
Sr ₆ YbAl(BO ₃) ₆	12.147(1)	9.077(1)	1159.9(2)
Sr ₆ InCr(BO ₃) ₆	12.136(2)	9.116(3)	1162.7(4)
Sr ₆ TmAl(BO ₃) ₆	12.160(1)	9.092(1)	1164.2(1)
Sr ₆ InMn(BO ₃) ₆	12.138(2)	9.136(2)	1165.8(3)
Sr ₆ ErAl(BO ₃) ₆	12.171(1)	9.097(2)	1166.9(3)
Sr ₆ ScGa(BO ₃) ₆	12.143(1)	9.146(1)	1167.8(2)
Sr ₆ HoAl(BO ₃) ₆	12.182(1)	9.095(2)	1169.0(2)
Sr ₆ YbGa(BO ₃) ₆	12.174(1)	9.120(2)	1170.4(2)
Sr ₆ ScSc(BO ₃) ₆	12.135(1)	9.184(1)	1171.3(3)
Sr ₆ YAl(BO ₃) ₆	12.190(2)	9.109(5)	1172.3(5)
Sr ₆ LuGa(BO ₃) ₆	12.187(2)	9.130(3)	1174.5(4)
Sr ₆ ErGa(BO ₃) ₆	12.190(1)	9.128(1)	1174.6(2)
SmSr ₅ YNi(BO ₃) ₆	12.175(2)	9.159(3)	1175.9(3)
Sr ₆ DyAl(BO ₃) ₆	12.218(1)	9.111(1)	1177.9(1)
Sr ₆ TbAl(BO ₃) ₆	12.218(1)	9.115(1)	1178.3(1)
Pb ₂ Sr ₄ ScSc(BO ₃) ₆	12.171(1)	9.186(1)	1178.4(2)
PrSr ₅ YNi(BO ₃) ₆	12.182(2)	9.170(2)	1178.4(3)
NdSr ₅ YMg(BO ₃) ₆	12.185(1)	9.180(2)	1180.4(2)
Sr ₆ GdAl(BO ₃) ₆	12.230(1)	9.114(2)	1180.6(3)
Sr ₆ YCr(BO ₃) ₆	12.213(1)	9.146(1)	1181.5(2)
Sr ₆ InSc(BO ₃) ₆	12.184(2)	9.190(2)	1181.5(3)
Sr ₆ YRh(BO ₃) ₆	12.228(2)	9.126(2)	1181.7(3)
Sr ₆ HoGa(BO ₃) ₆	12.220(1)	9.150(1)	1183.3(2)
NdSr ₅ YNi(BO ₃) ₆	12.208(2)	9.169(2)	1183.4(3)
LaSr ₅ ErNi(BO ₃) ₆	12.199(1)	9.184(1)	1183.6(2)
SmSr ₅ YZn(BO ₃) ₆	12.205(1)	9.177(2)	1183.9(3)
LaSr ₅ YNi(BO ₃) ₆	12.202(1)	9.187(1)	1184.6(1)

Table 6.3. continued.

$\text{SmSr}_5\text{YMg}(\text{BO}_3)_6$	12.213(1)	9.171(2)	1184.6(3)
$\text{Sr}_6\text{YGa}(\text{BO}_3)_6$	12.223(2)	9.159(2)	1185.0(3)
$\text{LaSr}_5\text{HoNi}(\text{BO}_3)_6$	12.209(1)	9.185(1)	1185.7(1)
$\text{NdSr}_5\text{HoCo}(\text{BO}_3)_6$	12.218(1)	9.179(1)	1186.7(1)
$\text{Sr}_6\text{EuAl}(\text{BO}_3)_6$	12.254(1)	9.126(2)	1186.7(2)
$\text{Sr}_6\text{SmAl}(\text{BO}_3)_6$	12.258(1)	9.126(1)	1187.5(2)
$\text{Sr}_6\text{HoFe}(\text{BO}_3)_6$	12.223(1)	9.188(1)	1188.8(2)
$\text{PrSr}_5\text{YZn}(\text{BO}_3)_6$	12.217(2)	9.197(3)	1188.8(4)
$\text{PrSr}_5\text{YMg}(\text{BO}_3)_6$	12.227(1)	9.188(2)	1189.5(2)
$\text{LaSr}_5\text{CaAl}(\text{BO}_3)_6$	12.258(2)	9.141(2)	1189.5(3)
$\text{Sr}_6\text{YFe}(\text{BO}_3)_6$	12.235(2)	9.192(2)	1191.7(3)
$\text{LaSr}_5\text{YCo}(\text{BO}_3)_6$	12.236(1)	9.199(1)	1192.8(2)
$\text{Sr}_6\text{LuSc}(\text{BO}_3)_6$	12.225(7)	9.217(1)	1192.9(2)
$\text{NdSr}_5\text{ErCo}(\text{BO}_3)_6$	12.251(1)	9.180(2)	1193.1(2)
$\text{Sr}_6\text{EuGa}(\text{BO}_3)_6$	12.261(1)	9.166(1)	1193.3(1)
$\text{LaSr}_5\text{YZn}(\text{BO}_3)_6$	12.235(1)	9.206(1)	1193.5(1)
$\text{Sr}_6\text{BiAl}(\text{BO}_3)_6$	12.279(1)	9.142(2)	1193.7(2)
$\text{LaSr}_5\text{HoCo}(\text{BO}_3)_6$	12.241(1)	9.204(1)	1194.3(2)
$\text{LaSr}_5\text{TbNi}(\text{BO}_3)_6$	12.243(1)	9.202(1)	1194.5(2)
$\text{LaSr}_5\text{YMg}(\text{BO}_3)_6$	12.237(2)	9.215(3)	1194.9(4)
$\text{Sr}_6\text{DyGa}(\text{BO}_3)_6$	12.274(2)	9.158(2)	1194.9(4)
$\text{LaSr}_5\text{HoMg}(\text{BO}_3)_6$	12.250(1)	9.200(2)	1195.6(3)
$\text{NdSr}_5\text{YZn}(\text{BO}_3)_6$	12.257(2)	9.199(3)	1196.8(3)
$\text{NdSr}_5\text{ScMg}(\text{BO}_3)_6$	12.257(2)	9.210(3)	1198.2(4)
$\text{LaSr}_5\text{EuNi}(\text{BO}_3)_6$	12.254(1)	9.214(1)	1198.3(1)
$\text{PrSr}_5\text{ScMg}(\text{BO}_3)_6$	12.251(1)	9.222(1)	1198.7(2)
$\text{Sr}_6\text{InIn}(\text{BO}_3)_6$	12.249(2)	9.228(3)	1199.0(5)
$\text{NdSr}_5\text{TbCo}(\text{BO}_3)_6$	12.269(1)	9.199(2)	1199.2(2)
$\text{NdSr}_5\text{ScCo}(\text{BO}_3)_6$	12.257(1)	9.220(2)	1199.6(2)
$\text{LaSr}_5\text{HoZn}(\text{BO}_3)_6$	12.265(2)	9.209(3)	1199.6(5)
$\text{NdSr}_5\text{ErZn}(\text{BO}_3)_6$	12.272(1)	9.198(1)	1199.7(2)
$\text{Sr}_6\text{YbSc}(\text{BO}_3)_6$	12.242(3)	9.246(4)	1200.0(6)
$\text{Nd}_2\text{Sr}_4\text{SrMg}(\text{BO}_3)_6$	12.268(1)	9.212(1)	1200.5(2)
$\text{Sr}_6\text{SmGa}(\text{BO}_3)_6$	12.297(1)	9.170(2)	1200.9(2)
$\text{La}_2\text{Sr}_4\text{CaZn}(\text{BO}_3)_6$	12.259(1)	9.233(1)	1201.7(1)

Table 6.3. continued.

NdSr ₅ EuZn(BO ₃) ₆	12.273(1)	9.212(1)	1201.7(2)
Sr ₆ GdFe(BO ₃) ₆	12.274(1)	9.212(3)	1201.9(3)
Sr ₆ ErSc(BO ₃) ₆	12.258(1)	9.236(1)	1202.0(2)
LaSr ₅ TbMg(BO ₃) ₆	12.273(1)	9.216(2)	1202.1(2)
LaSr ₅ TbZn(BO ₃) ₆	12.273(1)	9.221(2)	1203.0(3)
LaSr ₅ ScMg(BO ₃) ₆	12.273(1)	9.229(1)	1203.9(1)
Pr ₂ Sr ₄ SrMg(BO ₃) ₆	12.279(1)	9.223(2)	1204.4(2)
Sr ₆ TbGa(BO ₃) ₆	12.324(1)	9.167(2)	1205.8(3)
Sr ₆ PrGa(BO ₃) ₆	12.315(1)	9.190(1)	1207.0(2)
Sr ₆ TmSc(BO ₃) ₆	12.271(2)	9.256(3)	1207.0(4)
Sr ₆ GdGa(BO ₃) ₆	12.333(1)	9.165(2)	1207.2(2)
NdSr ₅ ScZn(BO ₃) ₆	12.289(1)	9.245(1)	1209.0(1)
Sr ₆ YMn(BO ₃) ₆	12.320(2)	9.198(3)	1209.0(4)
Sr ₆ BiFe(BO ₃) ₆	12.310(2)	9.215(2)	1209.4(3)
Sr ₆ NdGa(BO ₃) ₆	12.330(1)	9.189(1)	1209.9(2)
LaSr ₅ ScCo(BO ₃) ₆	12.290(1)	9.251(2)	1210.1(2)
Sr ₆ DySc(BO ₃) ₆	12.288(1)	9.257(1)	1210.6(1)
LaSr ₅ ScNi(BO ₃) ₆	12.295(1)	9.250(1)	1210.9(1)
Sr ₅ BaHoFe(BO ₃) ₆	12.316(2)	9.219(2)	1211.0(3)
Sr ₆ YSc(BO ₃) ₆	12.284(1)	9.268(2)	1211.2(4)
Sr ₆ HoSc(BO ₃) ₆	12.285(3)	9.268(2)	1211.2(5)
Sr ₆ GdMn(BO ₃) ₆	12.330(4)	9.206(4)	1212.0(7)
LaSr ₅ MgAl(BO ₃) ₆	12.314(1)	9.232(1)	1212.3(2)
Sr ₆ TbIn(BO ₃) ₆	12.329(1)	9.219(1)	1213.5(3)
PrSr ₅ ScZn(BO ₃) ₆	12.307(1)	9.252(1)	1213.6(1)
Sr ₆ LaGa(BO ₃) ₆	12.339(1)	9.209(1)	1214.3(1)
Sr ₆ TbSc(BO ₃) ₆	12.306(2)	9.263(3)	1214.9(4)
La ₂ Sr ₄ SrZn(BO ₃) ₆	12.319(2)	9.264(2)	1217.4(3)
La ₂ Sr ₄ SrMg(BO ₃) ₆	12.318(1)	9.254(2)	1216.1(2)
Sr ₆ EuSc(BO ₃) ₆	12.327(1)	9.262(1)	1219.0(2)
LaSr ₅ ScZn(BO ₃) ₆	12.327(1)	9.266(2)	1219.3(2)
Sr ₆ EuIn(BO ₃) ₆	12.361(1)	9.234(1)	1221.9(2)
Sr ₆ CaSn(BO ₃) ₆	12.381(1)	9.206(1)	1222.0(1)
Sr ₆ SmSc(BO ₃) ₆	12.350(1)	9.276(2)	1225.2(2)
La ₂ Sr ₄ CdCd(BO ₃) ₆	12.364(1)	9.273(2)	1227.6(2)

Table 6.3. continued.

$\text{LaSr}_5\text{CaSc}(\text{BO}_3)_6$	12.378(1)	9.273(2)	1230.4(3)
$\text{Sr}_6\text{NdSc}(\text{BO}_3)_6$	12.373(1)	9.286(1)	1231.0(2)
$\text{Sr}_6\text{GdSc}(\text{BO}_3)_6$	12.395(3)	9.262(4)	1232.3(6)
$\text{Sr}_6\text{PrSc}(\text{BO}_3)_6$	12.384(1)	9.293(1)	1234.2(1)
$\text{Sr}_6\text{CdSn}(\text{BO}_3)_6$	12.434(2)	9.236(2)	1236.5(3)
$\text{LaSr}_5\text{SrSc}(\text{BO}_3)_6$	12.398(1)	9.302(1)	1238.1(2)
$\text{Sr}_6\text{LuLu}(\text{BO}_3)_6$	12.433(1)	9.262(2)	1239.9(3)
$\text{Sr}_6\text{SrSn}(\text{BO}_3)_6$	12.464(1)	9.241(1)	1243.2(1)
$\text{Sr}_6\text{ErEr}(\text{BO}_3)_6$	12.478(1)	9.240(1)	1246.0(2)
$\text{LaSr}_5\text{SrCd}(\text{BO}_3)_6$	12.425(1)	9.324(1)	1246.5(1)
$\text{Sr}_6\text{CdHf}(\text{BO}_3)_6$	12.412(1)	9.346(2)	1246.8(3)
$\text{Sr}_6\text{YY}(\text{BO}_3)_6$	12.503(2)	9.248(2)	1252.1(4)
$\text{Sr}_6\text{DyDy}(\text{BO}_3)_6$	12.487(3)	9.234(3)	1246.9(4)
$\text{Sr}_6\text{HoHo}(\text{BO}_3)_6$	12.509(1)	9.254(1)	1254.0(2)
$\text{Sr}_6\text{TbTb}(\text{BO}_3)_6$	12.521(1)	9.247(1)	1255.4(2)
$\text{Sr}_6\text{GdGd}(\text{BO}_3)_6$	12.534(2)	9.251(3)	1258.7(4)
$\text{Sr}_6\text{CaZr}(\text{BO}_3)_6$	12.453(1)	9.367(1)	1258.0(2)
$\text{Sr}_6\text{CaHf}(\text{BO}_3)_6$	12.460(2)	9.358(3)	1258.3(4)
$\text{Sr}_6\text{CdZr}(\text{BO}_3)_6$	12.469(2)	9.371(2)	1261.7(4)
$\text{Sr}_6\text{SrHf}(\text{BO}_3)_6$	12.493(1)	9.373(1)	1266.9(1)
$\text{Sr}_6\text{SrZr}(\text{BO}_3)_6$	12.512(1)	9.392(1)	1273.5(1)
$\text{LaSr}_5\text{SrY}(\text{BO}_3)_6$	12.578(3)	9.317(3)	1276.5(5)
$\text{Sr}_3\text{Ba}_3\text{HoFe}(\text{BO}_3)_6$	12.663(3)	9.301(3)	1291.6(5)
$\text{Ba}_6\text{InIn}(\text{BO}_3)_6$	12.769(1)	9.737(1)	1323.4(2)
$\text{Ba}_6\text{YFe}(\text{BO}_3)_6$	12.797(1)	9.372(2)	1329.1(2)
$\text{Ba}_6\text{ErFe}(\text{BO}_3)_6$	12.796(0)	9.364(0)	1327.9(1)
$\text{Ba}_6\text{HoFe}(\text{BO}_3)_6$	12.796(2)	9.383(4)	1330.4(6)
$\text{Ba}_6\text{LuIn}(\text{BO}_3)_6$	12.809(2)	9.395(2)	1334.8(3)
$\text{Ba}_6\text{DyFe}(\text{BO}_3)_6$	12.815(1)	9.387(2)	1335.1(3)
$\text{Ba}_6\text{TbFe}(\text{BO}_3)_6$	12.818(1)	9.398(1)	1337.2(1)
$\text{Ba}_6\text{YbIn}(\text{BO}_3)_6$	12.818(1)	9.414(1)	1339.6(1)
$\text{Ba}_6\text{GdFe}(\text{BO}_3)_6$	12.830(1)	9.408(1)	1341.1(1)
$\text{Ba}_6\text{TmIn}(\text{BO}_3)_6$	12.821(1)	9.421(3)	1341.2(5)

Table 6.3. continued.

$\text{Ba}_6\text{EuFe}(\text{BO}_3)_6$	12.835(1)	9.415(1)	1343.2(2)
$\text{Ba}_6\text{SmFe}(\text{BO}_3)_6$	12.835(1)	9.416(2)	1343.4(2)
$\text{Ba}_6\text{ErIn}(\text{BO}_3)_6$	12.842(1)	9.427(1)	1346.5(2)
$\text{Ba}_6\text{DySc}(\text{BO}_3)_6$	12.832(1)	9.446(1)	1347.0(2)
$\text{Ba}_6\text{HoIn}(\text{BO}_3)_6$	12.853(1)	9.424(2)	1348.4(3)
$\text{Ba}_6\text{YIn}(\text{BO}_3)_6$	12.849(1)	9.433(2)	1348.7(2)
$\text{Ba}_6\text{DyIn}(\text{BO}_3)_6$	12.852(2)	9.451(2)	1352.1(4)
$\text{Ba}_6\text{TbIn}(\text{BO}_3)_6$	12.851(1)	9.456(2)	1352.6(3)
$\text{Ba}_6\text{TbSc}(\text{BO}_3)_6$	12.849(1)	9.462(1)	1352.8(2)
$\text{Ba}_6\text{GdIn}(\text{BO}_3)_6$	12.865(2)	9.459(3)	1355.9(4)
$\text{Ba}_6\text{SmIn}(\text{BO}_3)_6$	12.878(2)	9.462(3)	1359.1(4)
$\text{Ba}_6\text{EuIn}(\text{BO}_3)_6$	12.886(1)	9.475(1)	1362.5(1)
$\text{Ba}_6\text{GdSc}(\text{BO}_3)_6$	12.880(1)	9.485(2)	1362.7(3)
$\text{Ba}_6\text{SmSc}(\text{BO}_3)_6$	12.887(1)	9.491(1)	1365.0(2)
$\text{Ba}_6\text{EuSc}(\text{BO}_3)_6$	12.888(1)	9.493(2)	1365.6(3)
$\text{Ba}_6\text{NdIn}(\text{BO}_3)_6$	12.903(1)	9.491(2)	1368.4(3)
$\text{Ba}_6\text{PrIn}(\text{BO}_3)_6$	12.918(1)	9.504(1)	1373.5(2)
$\text{Ba}_6\text{NdSc}(\text{BO}_3)_6$	12.950(1)	9.530(1)	1384.2(1)
$\text{Ba}_6\text{PrSc}(\text{BO}_3)_6$	12.946(1)	9.540(3)	1384.8(3)
$\text{Ba}_6\text{LaIn}(\text{BO}_3)_6$	12.965(1)	9.548(1)	1389.8(2)
$\text{Ba}_6\text{LaSc}(\text{BO}_3)_6$	12.981(1)	9.557(1)	1394.7(2)
$\text{Ba}_6\text{SrZr}(\text{BO}_3)_6$	13.035(1)	9.609(2)	1414.0(2)

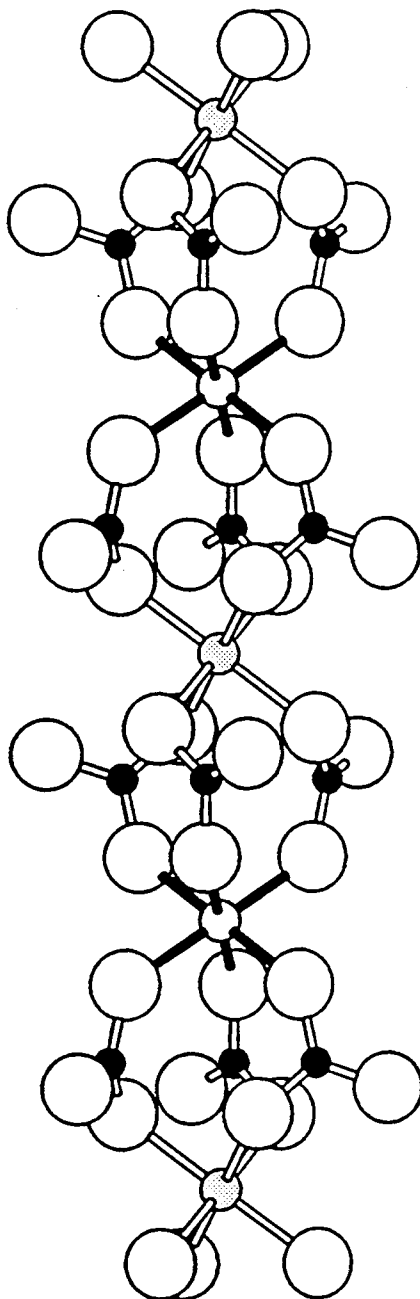


Figure 6.1. Chain of alternately stacked metal-centered octahedra linked by BO₃ groups.

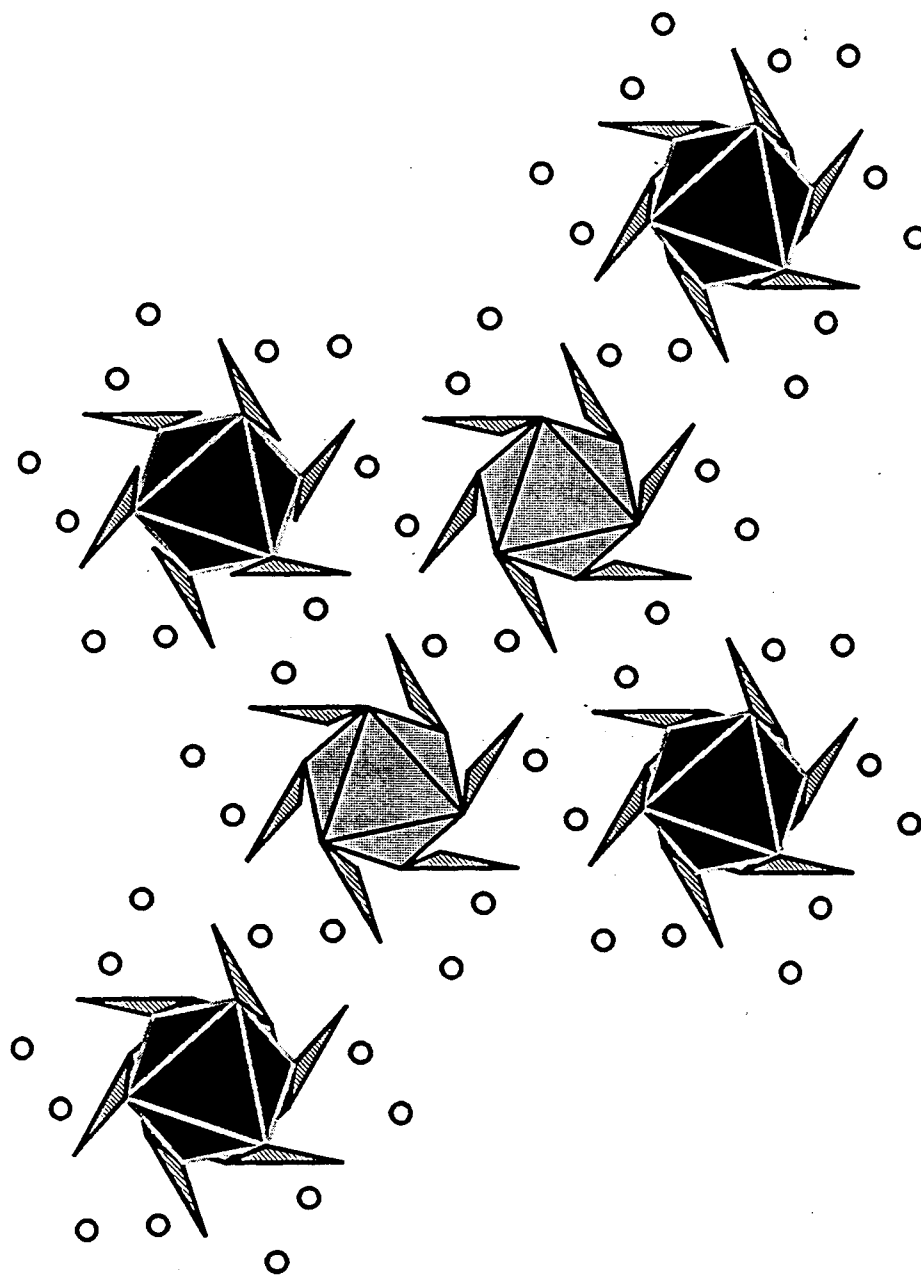


Figure 6.2. Sketch of the 3-dimensional structure of STACK viewed along the trigonal axis; the one-dimensional chains (Figure 6.1) are linked by Sr atoms.

identifying important properties and trends in the family.

One subclass of the family contains the elements $A = \text{Sr}$ and M and M' atoms of the same type ($M = M' = \text{Sc, In, Lu, Er, Y, Dy, Ho, Tb, and Gd}$). The derivative $\text{Sr}_3\text{Sc}(\text{BO}_3)_3$ ($r(\text{Sc}^{3+}) = 0.885 \text{ \AA}$) (7) contains the smallest M and M' atoms while the derivative $\text{Sr}_3\text{Gd}(\text{BO}_3)_3$ ($r(\text{Gd}^{3+}) = 1.078 \text{ \AA}$) contains the largest. By interpolation, the structure should exist for all +3 cations of intermediate size. Hypothetical compounds such as " $\text{Sr}_3\text{Al}(\text{BO}_3)_3$ " and " $\text{Sr}_3\text{Cr}(\text{BO}_3)_3$ " do not exist because the +3 ions ($r(\text{Al}^{3+}) = 0.675 \text{ \AA}$ and $r(\text{Cr}^{3+}) = 0.755 \text{ \AA}$) are too small to support the large M site. We note that no attempts have been made to employ reducing conditions for the production of Ti^{3+} ($r = 0.810 \text{ \AA}$) derivatives. In a similar manner, the derivative $\text{Sr}_3\text{Eu}(\text{BO}_3)_3$ does not exist because the Eu^{3+} ion is likely too large to fully occupy the small M' site.

A larger subclass contains $A = \text{Sr}$ and two different ions $M \neq M'$ having formal charges of +3; examples include $\text{Sr}_6\text{ScAl}(\text{BO}_3)_6$, $\text{Sr}_6\text{YFe}(\text{BO}_3)_6$, and $\text{Sr}_6\text{TbIn}(\text{BO}_3)_6$. Compounds form with M and M' cations ranging from the small Al^{3+} ion to the large lanthanide La^{3+} ($r = 1.172 \text{ \AA}$). To establish the approximate limits of the structure field within this subclass, we will first examine the distribution of cations over the A , M , and M' sites. The compounds $\text{Sr}_6\text{LnSc}(\text{BO}_3)_6$ ($\text{Ln} = \text{lanthanide or Y}$) are convenient for this purpose because the atom M may be any of those falling in the size range between Al^{3+} and La^{3+} . To probe the characteristics of Al substitution in these Sc analogs, we examined the solid solution series $\text{Sr}_6\text{Sc}_{2-x}\text{Al}_x(\text{BO}_3)_6$ over the range $0 < x \leq 2$; results from powder X-ray diffraction measurements are summarized in Figure 6.3. As seen from the steady decrease in unit-cell volume for $x = 0$ to ~ 1 , a complete solid solubility exists in this range. For $x > 1$, the volume remains constant and additional phases are observed in the powder patterns. We infer from this result that the Al atom has a preference for the smaller M' site. This supposition is consistent with the nonexistence of the phase " $\text{Sr}_3\text{Al}(\text{BO}_3)_3$ ".

The results of a solid solubility study in the series $\text{Sr}_6\text{Y}_{2-x}\text{Al}_x(\text{BO}_3)_6$ are also summarized in Figure 6.3. The behavior here differs markedly from the Sc series.

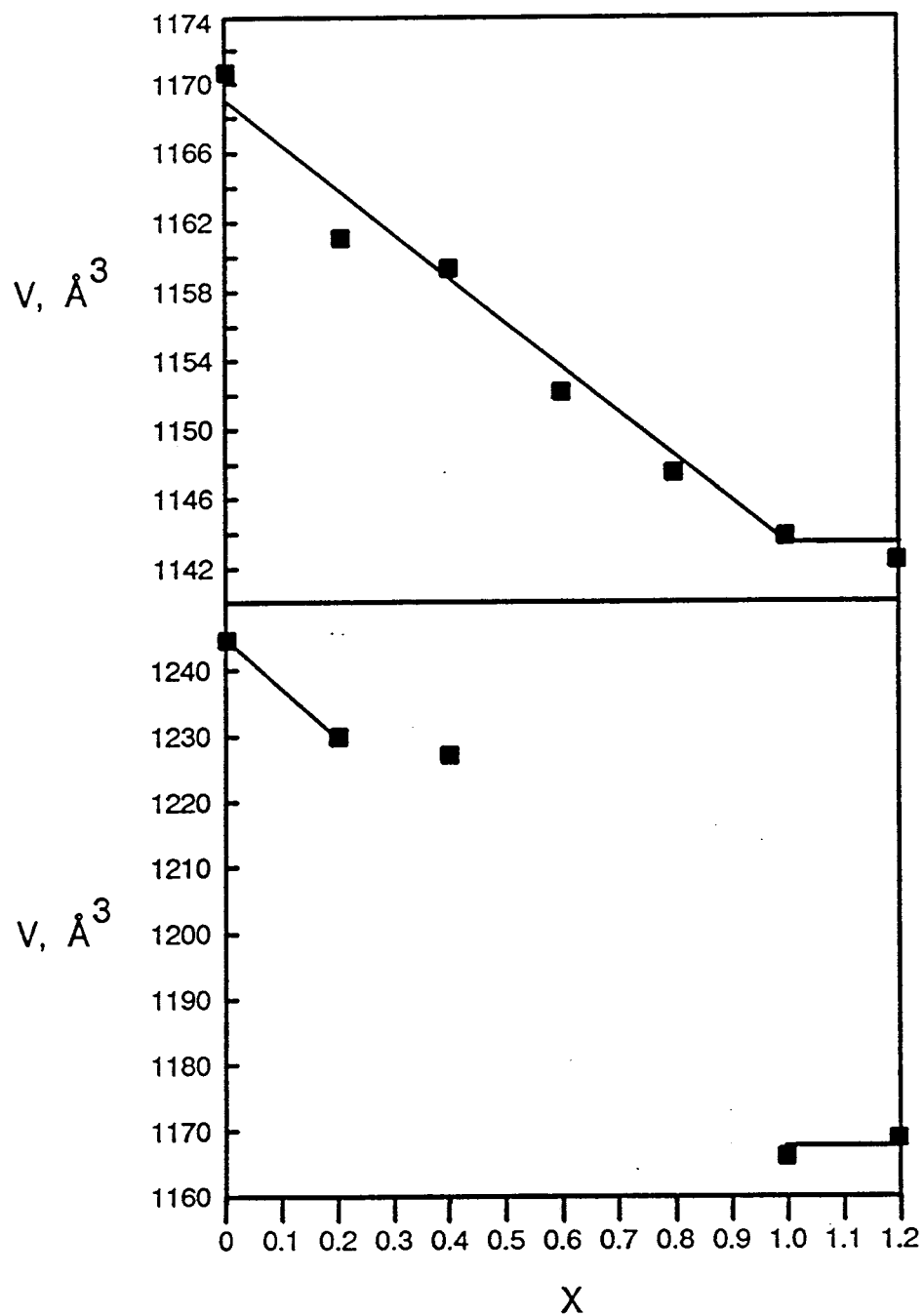


Figure 6.3. Cell volumes for the series $\text{Sr}_6\text{Sc}_{2-x}\text{Al}_x(\text{BO}_3)_6$ (top) and $\text{Sr}_6\text{Y}_{2-x}\text{Al}_x(\text{BO}_3)_6$ (bottom) for $0 \leq x \leq 1.2$.

Because of the size disparity of the Y and Al atoms, solubility exists only in the range $0 < x < \sim 0.2$. In the range $0.2 < x < 1$ simple equilibrium mixtures of the two end members, $x = \sim 0.2$ and $x = 1$, were found to exist. Again, these results are consistent with preference of Al atoms for the smaller M' site and the single-crystal structure analysis of the compound $\text{Sr}_6\text{Y}_{1.07}\text{Al}_{0.93}(\text{BO}_3)_6$. Here, the refinement clearly verifies the preference of the Al atom for the M' site (Table 6.2). We have attempted to reproduce the stoichiometry observed from the single-crystal study; the unit-cell volumes of all the nonstoichiometric samples of $\text{Sr}_6\text{Y}_{1+x}\text{Al}_{1-x}(\text{BO}_3)_6$ with $x \approx 0.1$ exhibited statistically equivalent unit-cell parameters. This discrepancy between the powder and single-crystal data may be a result of the presence of the flux in the melt growth of the single crystal.

An example of substituting a larger atom for Sc is given by the solid solution series $\text{Sr}_6\text{Ho}_x\text{Sc}_{2-x}(\text{BO}_3)_6$ ($0 < x < 2$). As seen in Figure 6.4, powder X-ray diffraction results reveal a steadily increasing cell volume with increasing content of the larger Ho atom and a complete solid solution over the entire range of x . The materials crystallize in a rhombohedral cell characterized by two parameters a and c . The c axis is coincident with the trigonal rotation element and the extension of the chains depicted in Figure 6.1; the a axis is orthogonal to c . The change in the c parameter with variation in x exhibits a peculiar behavior. The parameter increases with Ho content up to $x \approx 1$, but beyond this value the parameter *decreases* even though the *larger* Ho atom is being substituted into the structure. Of course, the volume still increases in this regime because of the more steeply increasing a parameter. Our interpretation of these results is that in the region $0 < x \leq 1$ the Ho atoms exhibits a preference for the larger octahedral M site. Beyond $x \approx 1$ the Ho atom begins to occupy the smaller octahedral M' site. The c parameter decreases because of a compression of the M' site along the trigonal axis. This compression is coupled with a more significant expansion in directions orthogonal to the c axis. This expansion is seen in the larger slope of the line representing the change in the a parameter for $x > 1$.

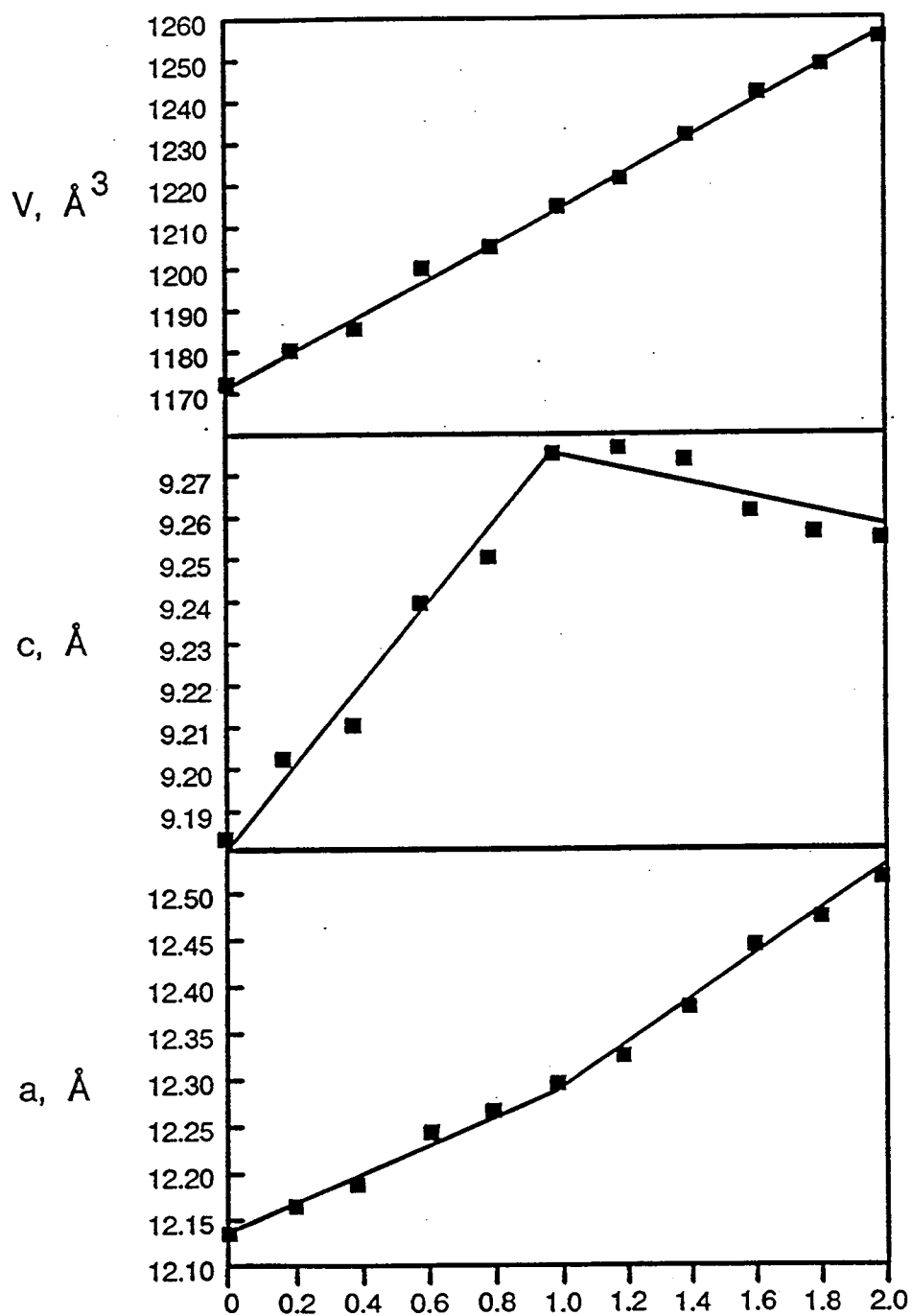


Figure 6.4. Cell parameters for the series $\text{Sr}_6^x\text{Sc}_{2-x}\text{Ho}_x(\text{BO}_3)_6$ for $0 \leq x \leq 2.0$.

This interpretation is supported by results of single-crystal structural studies of the compounds $\text{Sr}_6\text{Ho}_{0.964}\text{Sc}_{1.036}(\text{BO}_3)_6$ and $\text{Sr}_6\text{Er}_{1.4}\text{Sc}_{0.6}(\text{BO}_3)_6$. In the Ho compound, the Ho:Sc ratio is approximately 1:1, and the larger Ho atom was found to prefer occupancy of the larger M site; the occupancy of the M site is 89% Ho and 11% Sc atoms while the occupancy of the M' site is 93% Sc and 7% Ho atoms. In the Er derivative, the larger Er atoms again exhibit a preference for the larger site with occupancies of 91% Er and 9% Sc atoms on the M site and 49% Er and 51% Sc atoms on the smaller M' site. In this derivative the M' - O distance, 2.144(4) Å, is larger than the corresponding Sc2-O distance, 2.077(2) Å, in the compound $\text{Sr}_3\text{Sc}(\text{BO}_3)_3$. Also, the O2-M'-O2 angle, 83.3(2)°, represents a larger trigonal compression in comparison with the angle O2-Sc2-O2, 85.20(7)°, in the simple Sc derivative, a result that is consistent with the contraction of the *c* axis for $x > 1$ (Figure 6.4).

The results of substituting larger lanthanides into the structure are partially revealed by the solid-solution series $\text{Sr}_6\text{Sc}_{2-x}\text{La}_x(\text{BO}_3)_6$. Because of the absence of the phase "Sr₃La(BO₃)₃", incomplete solid solubility exists in this series and $x_{\text{max}} \approx 0.8$. This result, determined from powder X-ray measurements (Figure 6.5), is consistent with the stoichiometry found in a single-crystal study on the compound $\text{Sr}_6\text{La}_{0.84}\text{Sc}_{1.16}(\text{BO}_3)_6$. We also found that the La atom occupies the 9-coordinate A site. As *x* increases in this series, the Sr atoms likely slip off the A site and substitute for the Sc atoms on the M site, being replaced in the process by La atoms on the A site.

For the nominal stoichiometries $\text{Sr}_6\text{LnGa}(\text{BO}_3)_6$ containing the smaller Ga atom ($r = 0.76$ Å), STACK derivatives have also been found to exist for the complete lanthanide series. For the Al compounds $\text{Sr}_6\text{LnAl}(\text{BO}_3)_6$ ($r(\text{Al}^{3+}) = 0.675$ Å), however, the structure is formed only with those lanthanides up to the size of Sm.

Because the larger lanthanides exhibit a preference for the large A site, a means is provided for the introduction of smaller dipositive cations. Examples of these materials include the nominal formulations $\text{LaSr}_5\text{ScZn}(\text{BO}_3)_6$ (A= La and Sr,

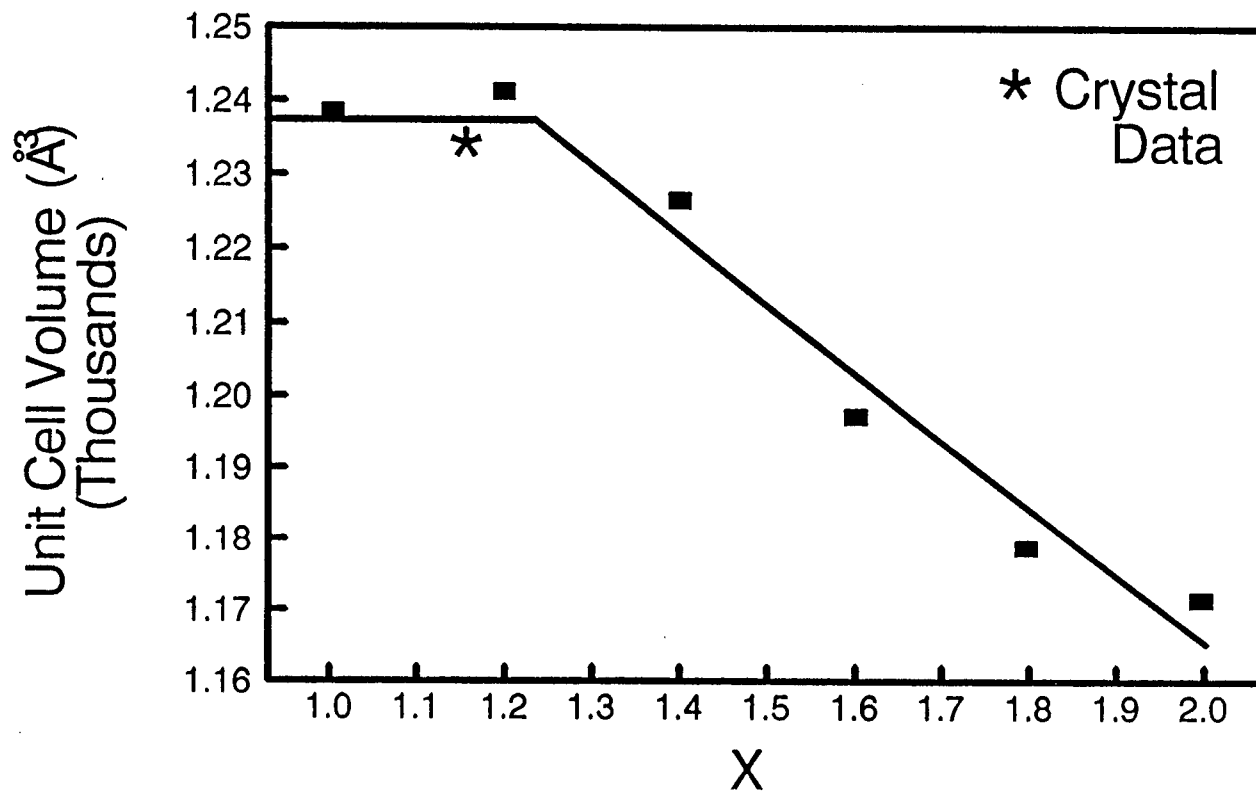


Figure 6.5. Unit cell volumes (\AA^3) for the solid solution series $\text{Sr}_6\text{Sc}_{2-x}\text{La}_x(\text{BO}_3)_6$.

M = Sc, and M' = Zn) and $\text{LaSr}_5\text{HoCo}(\text{BO}_3)_6$ (A = La and Sr, M = Ho, and M' = Co). From consideration of all the previous results, we anticipate that the small Zn^{2+} ($r = 0.88 \text{ \AA}$) and Co^{2+} ($r = 0.79 \text{ \AA}$) ions occupy the M' sites. By charge compensating in this way, it is likely that any divalent transition-metal ion that will occupy an octahedral site can be stoichiometrically incorporated into the structure. By substituting two large lanthanides onto the A site it is possible to place divalent ions on both the M and M' sites as exemplified by the derivatives $(\text{La}_2\text{Sr}_4)\text{CaZn}(\text{BO}_3)_6$ and $(\text{La}_2\text{Sr}_4)\text{CdCd}(\text{BO}_3)_6 \equiv \text{LaSr}_2\text{Cd}(\text{BO}_3)_3$. Results on these derivatives are similar to those found for the simpler compounds $\text{A}_6\text{MM}'(\text{BO}_3)_6$ where A = Sr and M and M' are +3 cations. The compound " $(\text{La}_2\text{Sr}_4)\text{MgMg}(\text{BO}_3)_6$ " does not exist. The Mg^{2+} ion ($r = 0.86 \text{ \AA}$) is slightly smaller than the Sc^{3+} ion so the absence of this compound is consistent with the result that an ion at least as large as Sc^{3+} must be present at the M site for stabilization and existence of the phase. The presence of $\text{La}_2\text{Sr}_4\text{CdCd}(\text{BO}_3)_6$ and nonexistence of " $\text{La}_2\text{Sr}_4\text{CaCa}(\text{BO}_3)_6$ " is consistent with the series $\text{Sr}_6\text{LnLn}(\text{BO}_3)_6$ where the largest lanthanide incorporated is Gd. The crystal radius of Cd^{2+} ($r = 1.09 \text{ \AA}$) is intermediate to those of the ion Gd^{3+} and Eu^{3+} , while the radius of Ca^{2+} ($r = 1.14 \text{ \AA}$) is much larger.

A small class of compounds with M = cation of formal charge +2 and M' = cation of formal charge +4 has also been prepared. In this family M = Ca, Sr, or Cd and M' = Zr, Hf, or Sn. Attempts to prepare derivatives containing Ti^{4+} and Th^{4+} did not afford the STACK structure. The sizes of ions Zr^{4+} ($r = 0.86 \text{ \AA}$), Hf^{4+} ($r = 0.85 \text{ \AA}$), and Sn^{4+} ($r = \text{ \AA}$) indicate they are likely to occupy the M' site. The distribution of X-ray intensities in the powder patterns verifies this supposition. Existence of the compound $\text{Sr}_7\text{Zr}(\text{BO}_3)_6 \equiv \text{Sr}_6\text{SrZr}(\text{BO}_3)_6$ clearly demonstrates that the Sr atom will occupy the M site. Because we have found very limited solubilities of Ca on the A site (vide infra) we anticipate that the Ca atom will reside on the larger M site in this subclass.

Before considering the characteristics of the Ba analogs, it is useful to analyze the results of the single-crystal studies in more detail. Interatomic distances

for each of the structure refinements is listed in Table 6.4. For the Sr derivatives, the average A-O and B-O distances are statistically equivalent. The M-O1 and M'-O2 distances associated with the disordered M and M' sites agree favorably with averages of crystal radii that were determined by weighting the radii according to the site occupancies. For example, the distance 2.477(5) Å for the M-O1 interaction compares to the length 2.49 Å computed for a 6-coordinate site comprised of 0.84 La and 0.16 Sc atoms bound by 4-coordinate O atoms. For each derivative, the average A-O distances increase in the order A-O2 > A-O3 > A-O1. The short A-O1 distances are consistent with the 4-coordination of atom O1 and the 5-coordination of atoms O2 and O3. The lengthened A-O2 interaction is associated with the shared triangular face of the M'-centered octahedron. There is a trend of increasing A-O2 distances with increasing sizes of the M' atoms. In the Y-Al compound the M'-O2 distance is 1.931(8) Å and the average A-O2 distance 2.72 Å. In the Er-Sc analog the M'-O2 distance is 2.144(4) Å and the average A-O2 distance is 2.78 Å. Evidence for La atoms on the A site in the La-Sc derivative is seen from the shortened A-O1 distances ($r(\text{La}^{3+})=1.36$ Å and $r(\text{Sr}^{2+})=1.45$ Å) and a general lengthening of the A-O3 distances.

Interatomic angles are listed in Table 6.5. A rather notable consistency is observed in these data, as angular values deviate by no more than 3° among the various structures. The La derivative affords a curious result in affording the most regular M site with the O1-M-O1 angle of 91.9(2)° most closely approaching orthogonality, while at the same time producing the most trigonally compressed M' site with O2-M'-O2 = 82.4(2)°. Adjacent MO₆ and M'O₆ octahedra are rotated by approximately 30°, one relative to the other, along the C₃, c axis. The largest deviation, 2.7°, from this angle is observed in the Y-Al derivative.

The structure fields of the Ba derivatives are much more restricted than those of the Sr analogs. The compound Ba₃In(BO₃)₃ is the only Ba derivative containing M = M'. We have prepared several examples with M and M' being different cations of formal charge +3. No Al or Ga derivatives, however, could be crystallized. In the series Ba₆LnIn(BO₃)₆, incorporation of each lanthanide afforded

Table 6.4. Interatomic distances (Å) for $\text{Sr}_6\text{YAl}(\text{BO}_3)_6$, $\text{Sr}_6\text{ErSc}(\text{BO}_3)_6$, $\text{Sr}_6\text{HoSc}(\text{BO}_3)_6$, $\text{LaSr}_6\text{Sc}(\text{BO}_3)_6$, and $\text{Ba}_6\text{GdSc}(\text{BO}_3)_6$.

	<u>$\text{Sr}_6\text{YAl}(\text{BO}_3)_6$</u>	<u>$\text{Sr}_6\text{ErSc}(\text{BO}_3)_6$</u>	<u>$\text{Sr}_6\text{HoSc}(\text{BO}_3)_6$</u>	<u>$\text{LaSr}_6\text{Sc}(\text{BO}_3)_6$</u>	<u>$\text{Ba}_6\text{GdSc}(\text{BO}_3)_6$</u>
A -O1	2.523(8)	2.530(4)	2.520(4)	2.473(5)	2.657(7)
-O1	2.643(8)	2.707(5)	2.683(4)	2.589(5)	2.799(7)
-O2	2.632(8)	2.768(4)	2.728(4)	2.709(6)	2.872(6)
-O2	2.810(8)	2.798(4)	2.799(4)	2.858(6)	2.975(6)
-O2	2.706(8)	2.763(5)	2.752(4)	2.723(6)	2.883(6)
-O3	2.886(9)	3.033(5)	2.983(5)	3.069(6)	3.110(6)
-O3	2.578(8)	2.495(5)	2.529(4)	2.512(5)	2.700(6)
-O3	2.561(8)	2.569(4)	2.569(5)	2.589(6)	2.746(6)
-O3	2.727(9)	2.761(5)	2.763(4)	2.769(6)	2.902(6)
A -O (avg.)	2.67(12)	2.71(16)	2.70(15)	2.70(18)	2.85(14)
M -O1	2.250(8)	2.291(4)	2.295(4)	2.477(5)	2.423(7)
M'-O2	1.931(8)	2.144(4)	2.090(4)	2.125(5)	2.162(5)
B -O1	1.37(1)	1.386(7)	1.393(7)	1.361(9)	1.40(1)
-O2	1.41(1)	1.386(7)	1.390(7)	1.390(9)	1.374(9)
-O3	1.37(1)	1.352(8)	1.353(7)	1.359(9)	1.36(1)
B -O (avg.)	1.38(2)	1.37(2)	1.38(2)	1.37(2)	1.38(2)

Table 6.5. Interatomic angles ($^{\circ}$) for $\text{Sr}_6\text{YAl}(\text{BO}_3)_6$, $\text{Sr}_6\text{ErSc}(\text{BO}_3)_6$, $\text{Sr}_6\text{HoSc}(\text{BO}_3)_6$, $\text{LaSr}_6\text{Sc}(\text{BO}_3)_6$, and $\text{Ba}_6\text{GdSc}(\text{BO}_3)_6$.

	<u>$\text{Sr}_6\text{YAl}(\text{BO}_3)_6$</u>	<u>$\text{Sr}_6\text{ErSc}(\text{BO}_3)_6$</u>	<u>$\text{Sr}_6\text{HoSc}(\text{BO}_3)_6$</u>	<u>$\text{LaSr}_6\text{Sc}(\text{BO}_3)_6$</u>	<u>$\text{Ba}_6\text{GdSc}(\text{BO}_3)_6$</u>
O1- A -O1	155.5(3)	158.6(2)	157.4(1)	158.7(2)	159.7(2)
O1- A -O2	96.6(2)	90.7(1)	91.9(1)	88.7(2)	93.5(2)
	75.3(2)	77.3(1)	77.2(1)	80.4(2)	74.6(2)
	105.7(2)	109.4(1)	108.9(1)	109.2(2)	105.3(2)
O1- A -O3	51.9(2)	50.0(1)	50.7(1)	49.4(1)	48.2(2)
	85.2(3)	87.9(1)	87.1(1)	89.7(2)	86.0(2)
	72.6(3)	72.5(1)	72.4(1)	74.9(1)	73.9(2)
	70.4(2)	70.7(1)	70.4(1)	70.4(2)	71.9(2)
O2- A -O2	63.3(3)	62.1(6)	61.2(1)	62.1(2)	66.4(2)
	58.2(3)	61.7(2)	60.3(1)	60.2(2)	59.5(2)
O2- A -O3	75.1(2)	70.6(1)	71.4(1)	78.6(2)	77.7(2)
	78.0(2)	78.0(1)	78.1(1)	78.2(2)	80.3(2)
	74.4(2)	70.7(1)	71.8(1)	73.0(2)	73.6(2)
O3- A - O3	83.26(9)	85.0(2)	85.3(1)	83.8(2)	84.43(6)
	86.9(3)	86.2(1)	86.0(1)	86.0(1)	87.1(2)
O1- M -O1	93.1(3)	92.5(2)	92.3(1)	91.9(2)	93.4(2)
O2- M'-O2	84.5(3)	83.3(2)	83.7(2)	82.4(2)	84.5(2)
O1- B -O2	119(1)	117.3(5)	117.8(5)	118.1(6)	117.9(7)
O1- B -O3	121(1)	122.2(5)	121.2(5)	122.0(5)	120.2(7)
O2- B -O3	120(1)	120.5(5)	121.0(5)	119.9(6)	121.9(7)

the STACK structure. In the series $\text{Ba}_6\text{LnFe}(\text{BO}_3)_6$ only those compounds containing $\text{Ln} = \text{Sm, Eu, Gd, Tb, Dy, Ho, Y, and Er}$ were found to form the structure, while in the series $\text{Ba}_6\text{LnSc}(\text{BO}_3)_6$ only those compounds containing $\text{Ln} = \text{La, Pr, Nd, Sm, Eu, Gd, Tb, and Dy}$ could be formed. In the Fe and Sc series a sufficient size differential between these atoms and the Ln atoms must be present for the STACK structure to form. For the Fe series the minimum differential occurs at $\text{M} = \text{Er}$ while for the Sc series it occurs at $\text{M} = \text{Dy}$. These limits are dictated by the formation of the layered-type phases $\text{Ba}_3\text{Ln}(\text{BO}_3)_3$ that were discussed in the previous report of this series. For the Fe compounds, the phases $\text{Ba}_3\text{LnFe}(\text{BO}_3)_3$ form when the radius of the Ln atoms is smaller than that of Er. For the Sc compounds, solid solutions $\text{Ba}_3(\text{Ln,Sc})(\text{BO}_3)_3$ form in the layered structure type when Ln is smaller than Dy. The structures of STACK and the layered-type Ba phases are rather complex and the energetic difference between them can be quite small. An example of this behavior is given by the solid-solution series $\text{Ba}_6\text{Dy}_{2-x}\text{Sc}_x(\text{BO}_3)_6$. This series represents equilibria between the two end members $\text{Ba}_3\text{Dy}(\text{BO}_3)_3$ and $\text{Ba}_3\text{Sc}(\text{BO}_3)_3$ which both adopt the layered-type structure. As seen in Figure 6.6, an extensive solid solution exists in this series with retention of the layered structure except, at the stoichiometry $\text{Ba}_6\text{DySc}(\text{BO}_3)_6$ where a considerable expansion of the unit cell is observed with formation of the STACK structure.

We also probed the relationship between the STACK and layered-type structures by examining the solid-solution series $\text{Ba}_{3-x}\text{Sr}_x\text{Sc}(\text{BO}_3)_3$. In this series, the compound $\text{Ba}_3\text{Sc}(\text{BO}_3)_3$ forms the layered structure and $\text{Sr}_3\text{Sc}(\text{BO}_3)_3$ is a STACK derivative. As seen in Figure 6.7, a steady decrease in unit-cell volume in the range $0 < x < 2.25$ indicates a range of solubility of Sr atoms in the Ba layered structure. The zero slope in the range $2.25 < x < 2.6$ defines a region of immiscibility, i.e., the layered-type and STACK structures are present in equilibrium mixtures. In the range $2.6 < x < 3$, only the STACK structure is observed with a steadily decreasing unit-cell volume with increasing x . This region represents the solid solubility of Ba^{2+} in the STACK derivative. These results were extended with examination of the

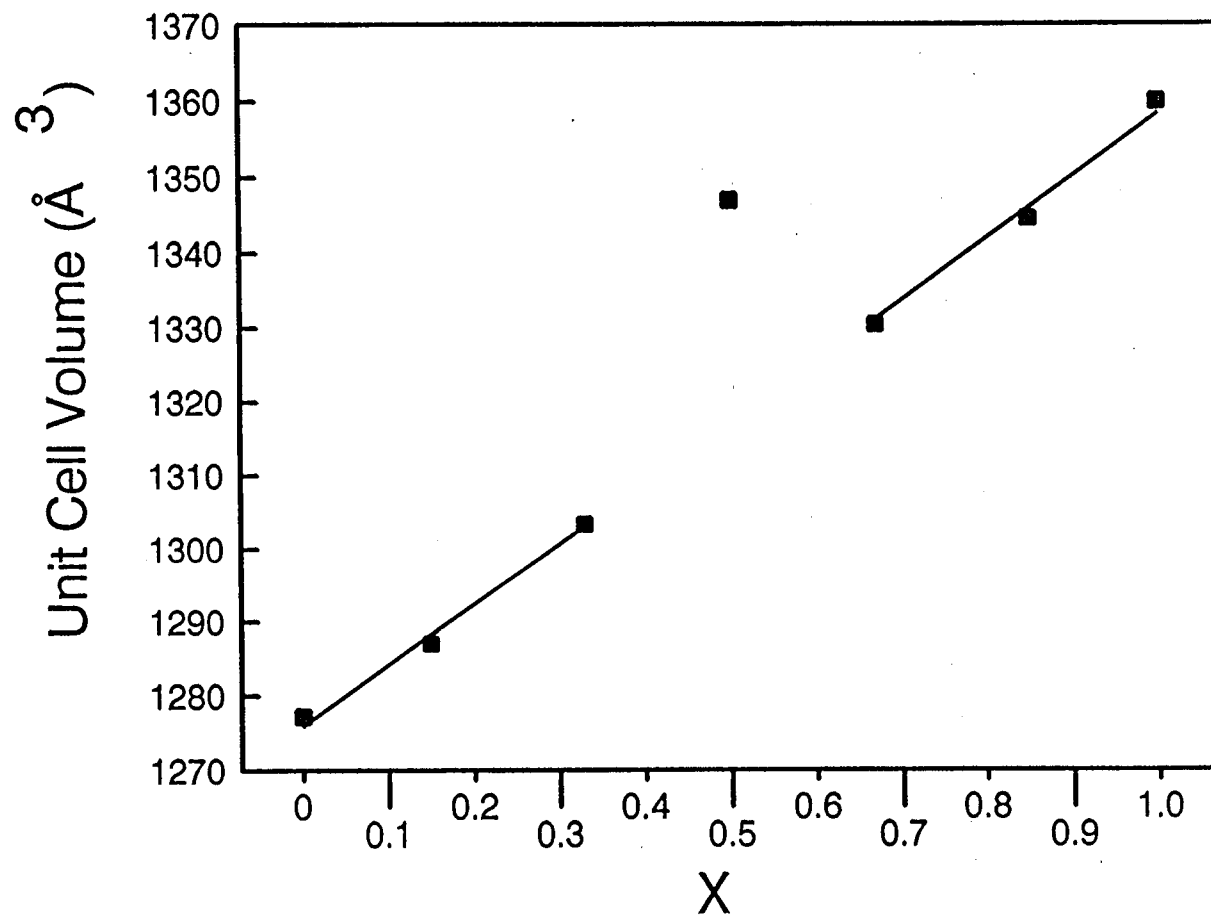


Figure 6.6. Cell parameters for the series $\text{Ba}_6\text{Dy}_{2-x}\text{Sc}_x(\text{BO}_3)_6$.

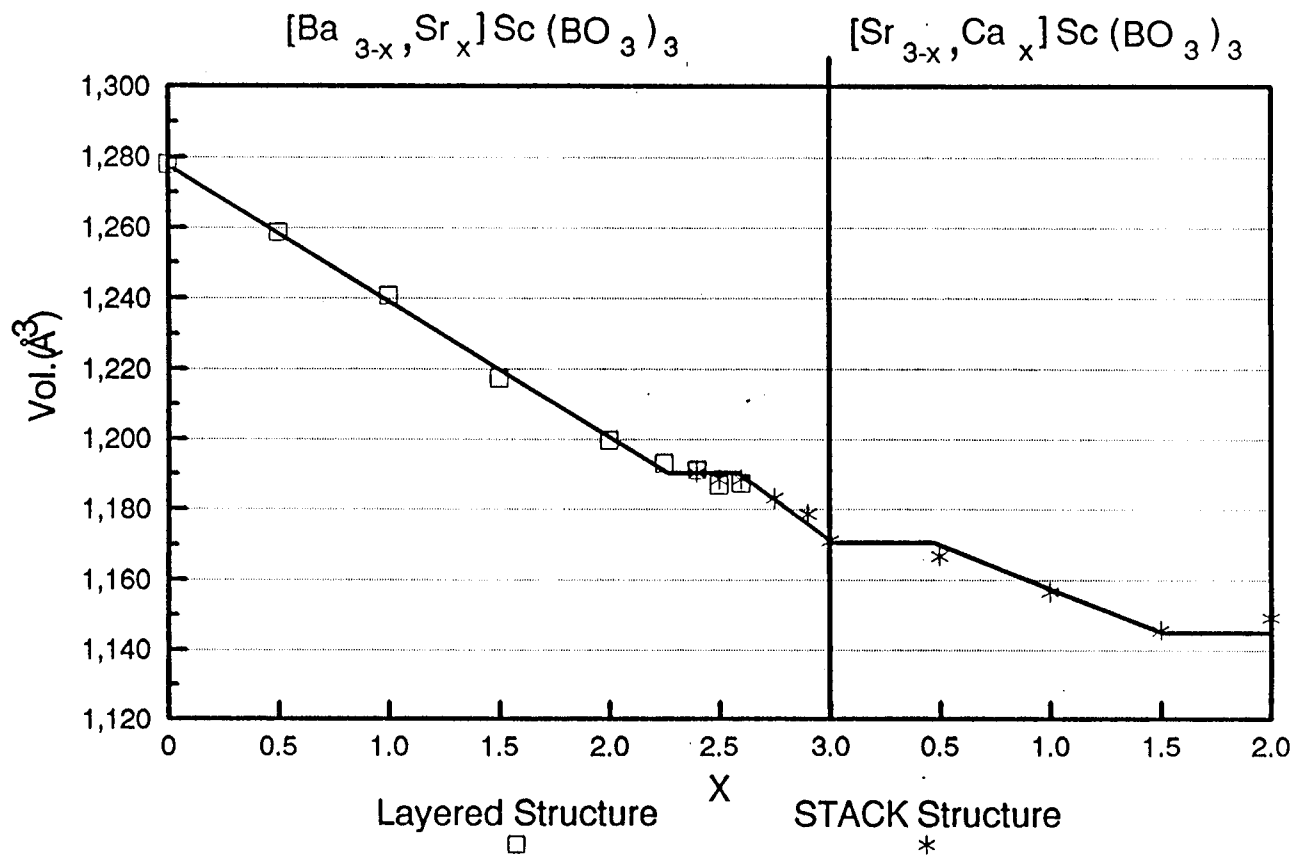


Figure 6.7. Unit cell volumes for the solid solution series $\text{Ba}_{3-x}\text{Sr}_x\text{Sc}(\text{BO}_3)_3$ and $\text{Sr}_{3-x}\text{Ca}_x\text{Sc}(\text{BO}_3)_3$.

series $\text{Sr}_{3-x}\text{Ca}_x\text{Sc}(\text{BO}_3)_3$. As seen from Figure 6.7, only small amounts of Ca may be incorporated ($x_{\text{max}} = 1.5$) into the structure in this way. The Ca atom is too small to occupy the large 9-coordinate A site where, for this derivative, the size of this site is largely determined by the integrity of the one-dimensional Sc borate chains. This result contrasts to the isostructural compounds $\text{Ca}_3(\text{BO}_3)_2$ and $\text{Sr}_3(\text{BO}_3)_2$ where the BO_3 groups are free to move in response to the size demands of the alkaline-earth atoms, maintaining in each case a 9-coordinate site in each structure.

We also synthesized compounds with $M = +2$ cation and $M' = +4$ cation. Highly crystalline samples were only realized with $M = \text{Sr}$.

Summary

The borates of composition $A_6MM'(BO_3)_6$ represent a broad new class of oxide. By utilizing appropriate charge-compensation techniques, nearly all +2, +3, or +4 ions of the elements in the periodic table can be incorporated into the structure. Analysis of the metrical details from single-crystal studies indicates little variation in nearest-neighbor interatomic angles. This feature, coupled with the centrosymmetric S_6 symmetry of the M and M' sites, indicates that physical properties will be primarily controlled by interatomic distances, the electronic nature of the A, M, and M' atoms, and stoichiometry.

Acknowledgments

Acknowledgment is made to the National Science Foundation and the Donors of the Petroleum Research Fund administered by the American Chemical Society, for support of this research. D.A.K. thanks the Alfred P. Sloan Foundation for a fellowship, and K.I.S. acknowledges Pacific Northwest Laboratories for a DOE graduate fellowship, 1991-92.

References

1. K.I. Schaffers, T. Alekel III, P.D. Thompson, J.R. Cox, D.A. Keszler, *J. Am. Chem. Soc.*, **112**, (1990) 7068.
2. P.D. Thompson, D.A. Keszler, *Chem. Mat.*, **1**, (1988) 292.
3. P.D. Thompson, D.A. Keszler, *Chem. Mat.*, (1992), submitted.
4. Molecular Structure Corporation, 3200A Research Forest Drive, The Woodlands, TX 77381.
5. G.M. Sheldrick *Crystallographic Computing 3* (G.M. Sheldrick, C. Krüger, R. Goddard, Eds.) Oxford Univ. Press: Oxford, (1985) 175-189.
6. N. Walker, D. Stuart, *Acta Crystallogr., Sect. A*, **24**, (1968) 214.
7. R.D. Shannon, *Acta Crystallogr., Sect. A*, **32**, (1976) 751.

CHAPTER 7

**Structure of $\text{Ba}_7(\text{BO}_3)_3\text{F}_5$:
A New Noncentrosymmetric Orthoborate Fluoride**

Theodore Alekel III and Douglas A. Keszler*

*Department of Chemistry and
Center for Advanced Materials Research
Oregon State University
Gilbert Hall 153
Corvallis, OR 97331-4003*

In Preparation for Submission to *Chemistry of Materials*

Abstract

From a single crystal X-ray diffraction analysis, the compound $\text{Ba}_7(\text{BO}_3)_3\text{F}_5$ has been determined to crystallize in the noncentrosymmetric trigonal space group $P31c$ with cell parameters $a = 11.208(5) \text{ \AA}$, $c = 7.250(2) \text{ \AA}$, $V = 788.7(5) \text{ \AA}^3$, and $Z = 2$. Three Ba-centered polyhedra are interconnected by F^- and BO_3^{3-} anions to form an intricate 3-dimensional framework. Groups of BO_3 triangles are trigonally arranged around the $0,0,z$ axis with B–O bonds generally oriented in the c -direction.

Introduction

Following a study of the $\text{BaO-BaF}_2\text{-B}_2\text{O}_3$ phase system, we reported the existence and structure of the pyroborate fluoride $\text{Ba}_5(\text{B}_2\text{O}_5)_2\text{F}_2$ (1). Also found from this study is the new compound $\text{Ba}_7(\text{BO}_3)_3\text{F}_5$ which we describe here. This material crystallizes in a noncentrosymmetric space group and exhibits structural features that may lead to desirable nonlinear optical properties.

Two borates, $\beta\text{-BaB}_2\text{O}_4$ (BBO) and LiB_3O_5 (LBO), are extensively used for frequency conversion of high-power laser light. The general utility of each material, however, is principally dictated by the linear, rather than nonlinear properties. We propose in the following discussion that the compound $\text{Ba}_7(\text{BO}_3)_3\text{F}_5$ may exhibit properties similar to those of LBO.

Experimental

Synthesis. The production of $\text{Ba}_7(\text{BO}_3)_3\text{F}_5$ was readily obtained by melting a stoichiometric ratio of the following starting materials in a Pt container: BaCO_3 (ÆSAR, 99.9%), BaF_2 (ALFA, optical grade), and B_2O_3 (ALFA, 99.98%). After heating to 1200 K in air, the compound was removed from the oven and quenched to room temperature. X-ray powder diffraction analysis revealed the product to be single phase, and the X-ray pattern matched that calculated from the results of the single-crystal data (*vide infra*). For single-crystal study, however, a more rigorous synthetic method was used to reduce possible CO_3^{2-} impurities and to prevent the substitution of O^{2-} anions for F^- anions. $\text{Ba}(\text{NO}_3)_2$ (ÆSAR, ACS grade) and B_2O_3 were heated at 1075 K in an O_2 atmosphere to produce an intermediate with the composition $\text{Ba}_3(\text{BO}_3)_2$. This reagent was stoichiometrically combined with BaF_2 and heated to 1200 K in a N_2 atmosphere. The melt was cooled at a rate of 8 K/h to 800 K and then rapidly cooled to room temperature. A 0.1(2) x 0.1(2) x 0.1(2) mm single crystal was removed from the bulk sample for X-ray analysis.

X-ray Work. The transparent block was mounted on a glass fiber and analyzed on a Rigaku AFC6R single crystal X-ray diffractometer. Unit cell parameters were obtained by a least-squares refinement of 20 automatically-centered reflections in the angular range $30 \leq 2\theta \leq 36^\circ$. The refractive power of the crystal was monitored every 200 reflections to ensure crystalline soundness; no decay corrections were required. Intensity data were collected ($2 \leq 2\theta \leq 60^\circ$) at 300 K by using ω - 2θ scans with widths of $1.50 + 0.30 \tan \theta$ at 16° (ω)/min. 1187 unique reflections with $F_o^2 \geq 3\sigma(F_o)^2$ were corrected for Lorentz/polarization effects and for secondary extinction with a coefficient $0.48(2) \times 10^{-6}$. The space group P31c was determined on the basis of the systematic absences **hhl**, **00l**: $l = 2n + 1$ and the successful refinement of the structure. Although nearly all of the atomic positions in the refinement coincide with the x,x,z special position of the hexagonal space group P6₃mc, the F3 atoms do not conform to this higher order of symmetry. A summary of general crystallographic information is presented in Table 7.1.

Table 7.1. Crystallographic Data for Ba₇(BO₃)₃F₅.

Formula	Ba ₇ (BO ₃) ₃ F ₅
Formula Weight, amu	1232.73
Crystal System	Trigonal
Space Group	P31c (No. 159)
a, Å	11.208(5)
c, Å	7.250(2)
V, Å ³	788.7(5)
Z	2
D _{calc} , g cm ⁻³	5.190
F(000)	1048
Diffractometer	Rigaku AFC6R
Radiation	Mo Kα = 0.71069 Å graphite monochromator
Data Collection	±h,k,±l
No. Unique Observations (F _o ² > 3σ(F _o ²))	745
Transmission Factors	0.592 – 1.328
Linear Absorption, cm ⁻¹	172.85
R	0.052
R _w	0.068

Programs from TEXSAN crystallographic package (2) were executed on a Digital microVAX II computer to solve and refine the structure. The Ba atomic positions were established with the direct methods program SHELXS-86 (3); afterward, the remaining atoms in the compound were located by succeeding analyses of difference electron density maps. F_{calc} values were corrected for neutral and anomalous scattering by using factors provided in *International Tables for X-ray Crystallography* (4). Following least-squares convergence with isotropic displacement coefficients for each atom, the data were corrected for the absorption with the empirical calculation DIFABS (5). The final refinement with 745 averaged F_o values ($I > 3\sigma$, $R_{\text{int}} = 0.09$) included the resolution of anisotropic displacement coefficients (except for the atoms F2, O1, and B). The resulting agreement factors were $R = 0.052$ and $R_w = 0.068$, where $w = 1/\sigma^2(F_o)$ and $p = 0.05$. The largest peak intensity in the final difference electron density map was $3.442 \text{ e } \text{\AA}^{-1}$, corresponding to 1.45 % of the Ba3 atom, whereas the minimum peak amounted to $-3.181 \text{ e } \text{\AA}^{-1}$. Atomic positions and equivalent isotropic displacement coefficients are listed in Table 7.2; anisotropic displacement coefficients are provided in Table 7.3.

Table 7.2. Positional parameters and B_{eq} for $\text{Ba}_7(\text{BO}_3)_3\text{F}_5$.

Atom	x	y	z	B_{eq}^a
Ba1	0.2684(1)	0.1343(1)	0	1.91(5)
Ba2	0.5318(1)	0.4686(1)	0.3344(2)	2.09(5)
Ba3	1/3	2/3	0.2449(4)	1.36(4)
B	0.186(3)	0.365(3)	0.060(3)	1.6(3)
F1	2/3	1/3	0.365(6)	4(1)
F2	0	0	0.202(3)	0(1)
F3	0.529(3)	0.353(3)	0.024(3)	11(2)
O1	0.090(2)	0.695(2)	0.141(2)	2.4(3)
O2	0.095(2)	0.399(2)	0.150(3)	2.7(6)
O3	0.300(2)	0.152(2)	0.386(3)	2.3(6)

$$^a B_{\text{eq}} = (8\pi^2/3) \sum_i \sum_j U_{ij} a_j^* a_i^* a_i a_j$$

Table 7.3. U values for Ba₇(BO₃)₃F₅

Atom	U ₁₁	U ₂₂	U ₃₃	U ₁₂	U ₁₃	U ₂₃
Ba1	0.0297(8)	0.0232(7)	0.0222(6)	0.0153(6)	0.0016(5)	0.0009(4)
Ba2	0.0260(7)	0.0230(7)	0.0266(6)	0.0094(5)	-0.0090(4)	0.0077(4)
Ba3	0.0148(6)	0.0148	0.0219(8)	0.0074	0	0
B	0.020(4)					
F1	0.03(1)	0.03	0.11(4)	0.02	0	0
F2	0.00(2)					
F3	0.18(4)	0.23(5)	0.09(3)	0.17(4)	0.06(2)	0.04(3)
O1	0.031(3)					
O2	0.05(1)	0.03(1)	0.04(1)	0.03(1)	0.017(8)	0.005(7)
O3	0.04(1)	0.012(7)	0.04(1)	0.014(7)	-0.011(8)	-0.006(6)

Results

As depicted in the unit cell diagram (Figure 7.1), $\text{Ba}_7(\text{BO}_3)_3\text{F}_5$ is a multifarious conglomeration of coordination environments that extensively interconnect with each other to form a 3-dimensional framework. The Ba-centered polyhedra are primarily joined by sharing faces and edges comprised of orthoborate and fluoride anions. Similar to the Sr1/Sr2 environment around the F atom in the orthoborate fluoride $\text{Sr}_5(\text{BO}_3)_3\text{F}$ (6), one F type in the title structure fills a channel, centered along the 0,0,z axis, that is constructed by Ba1/Ba2 atoms. The Ba3 atom and its surrounding anions occupy *en masse* the region along the 2/3, 1/3, z and 1/3, 2/3, z axes. All the Ba atoms in $\text{Ba}_7(\text{BO}_3)_3\text{F}_5$ order in pseudo-hexagonal 6_3 symmetry and propagate as zig-zag chains along the c axis. The interconnectivity of the Ba coordination environments are discussed below in more detail; bonding distances and angles are listed in Tables 7.4 and 7.5, respectively.

The Ba1 atom is positioned in a nonacoordinate site that is best described as a inordinately distorted monocapped cube. Besides sharing $\text{O} \cdots \text{O} \cdots \text{F}$ faces with both Ba2 and Ba3 polyhedra, $\text{Ba}(1)\text{O}_8\text{F}$ groupings bridge to one another through adjacent edges of common BO_3 triangles. The third edge of the BO_3 anions is bound to the 3-fold symmetrical Ba3 centers. The monocapped trigonal base – distorted hexagonal base geometry of this cation (Figure 7.2) compares to the AE1 (AE = Sr, Ba) sites in the $\text{AE}_2\text{BO}_3\text{Br}$ structure (7); the bonding restrictions of the BO_3 groups deform a regular hexagonal plane of O atoms into a trigonal arrangement, and halide anions cap the faces of these hexagonal bases in both structures. The trigonal base in the $\text{Ba}(3)\text{O}_6\text{F}_4$ polyhedra, however, is defined by F atoms rather than O atoms in the $\text{AE}(1)\text{O}_9\text{Br}$ grouping. As the structure field of borates containing the heavier alkaline-earth metals continues to increase, it is becoming evident that this type of arrangement is not so peculiar (8,9).

The curious polyhedron in this compound involves the Ba2 atom. It has an inner circle of O and F atoms at distances of 2.59 – 2.84 Å (certainly deemed as

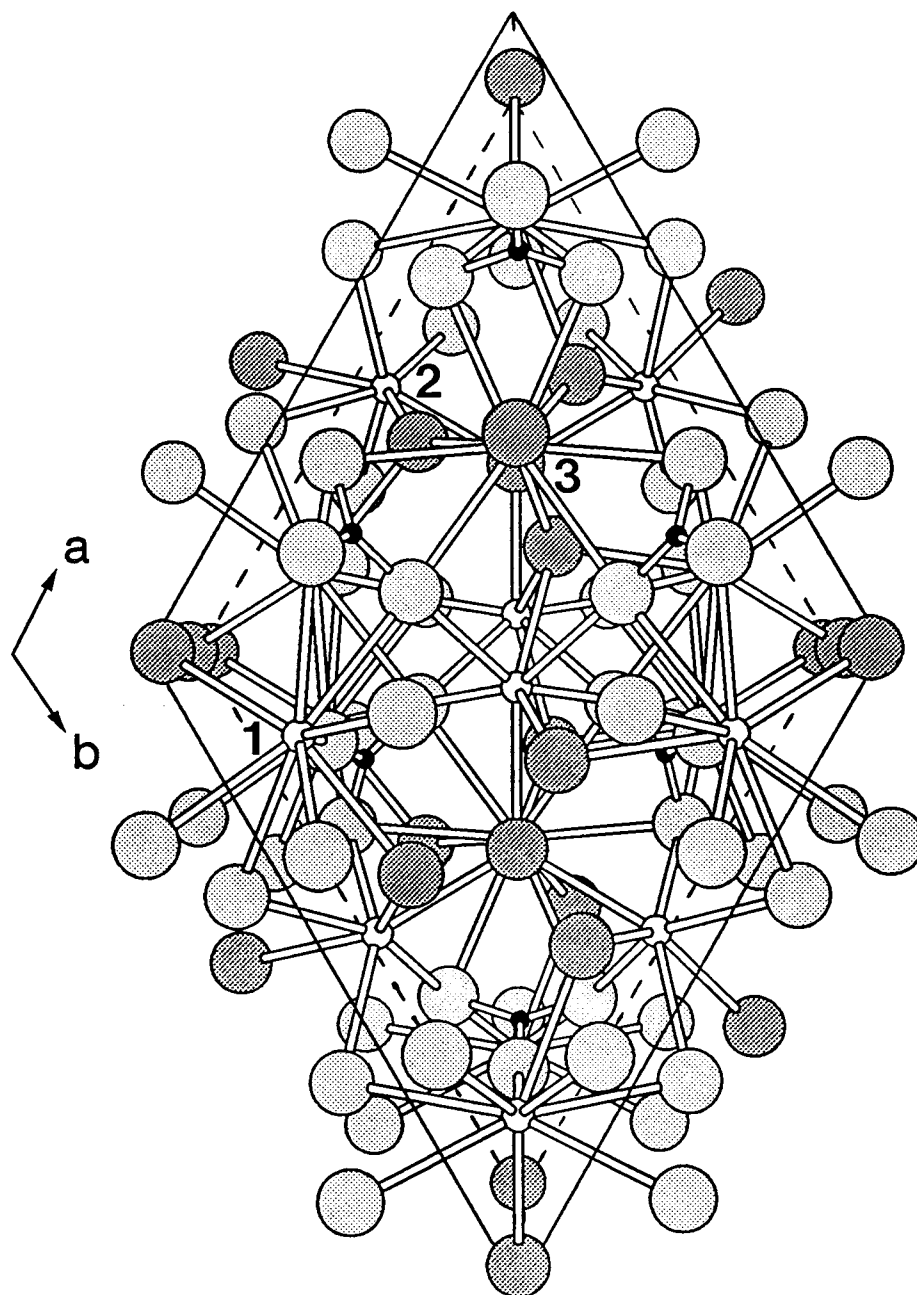


Figure 7.1. A schematic view of the unit cell for $\text{Ba}_7(\text{BO}_3)_3\text{F}_5$. The small open circles represent Ba atoms, the small black circles represent B atoms, the pale large circles represent O atoms, and the shaded large circles represent F atoms. Shading legend continued in subsequent figures. The Ba atoms are numerically labeled.

Table 7.4. Selected bond distances (Å) for Ba₇(BO₃)₃F₅.

Ba1-F2		2.99(1)
Ba1-F3		2.72(6)
Ba1-O1		3.13(2)
Ba1-O1		2.93(2)
Ba1-O2		2.99(2)
Ba1-O2		3.07(2)
Ba1-O3		2.82(2)
Ba1-O3		2.88(2)
Ba1-O3		2.91(2)
Ba2-F1		2.632(4)
Ba2-F3		2.59(3)
Ba2-F3		2.77(4)
Ba2-O1		2.65(2)
Ba2-O1		2.79(2)
Ba2-O2		2.63(2)
Ba2-O2		2.84(2)
Ba2-O2		3.21(2)
Ba2-O3		3.23(2)
Ba3-F1		2.76(4)
Ba3-F3	x 3	2.62(3)
Ba3-O1	x 3	2.99(2)
Ba3-O2	x 3	2.93(2)
B-O1		1.34(3)
B-O2		1.42(3)
B-O3		1.41(3)

Table 7.5. Selected bond angles ($^{\circ}$) for $\text{Ba}_7(\text{BO}_3)_3\text{F}_5$.

F2–Ba1–O1	86.4(4)	F1–Ba3–F3	141(1)
F2–Ba1–O2	85.6(4)	F1–Ba3–O1	75.3(3)
F2–Ba1–O3	67.0(6)	F1–Ba3–O2	76.4(4)
F2–Ba1–O3	77.9(4)	F3–Ba3–F3	67(1)
O1–Ba1–O1	83.3(5)	F3–Ba3–O1	66(1)
O1–Ba1–O2	45.2(5)	F3–Ba3–O2	82(1)
O1–Ba1–O3	48.4(5)	O1–Ba3–O1	113.8(3)
O1–Ba1–O3	65.1(5)	O1–Ba3–O2	47.4(6)
O2–Ba1–O3	66.2(6)	O1–Ba3–O2	68.6(6)
O3–Ba1–O3	108.9(5)	O2–Ba3–O2	114.6(3)
F1–Ba2–F3	70(1)	O1–B–O2	119(2)
F1–Ba2–O1	80.7(9)	O1–B–O3	120(2)
F1–Ba2–O2	80.0(9)	O2–B–O3	120(2)
F1–Ba2–O3	74.4(3)		
F3–Ba2–O1	67(1)		
F3–Ba2–O2	88(1)		
F3–Ba2–O3	75(1)		
O1–Ba2–O1	95.4(7)		
O1–Ba2–O2	72.6(6)		
O1–Ba2–O2	78.5(6)		
O1–Ba2–O3	46.2(5)		
O1–Ba2–O3	66.4(5)		
O2–Ba2–O2	96.0(7)		
O2–Ba2–O3	47.1(5)		
O2–Ba2–O3	67.0(5)		

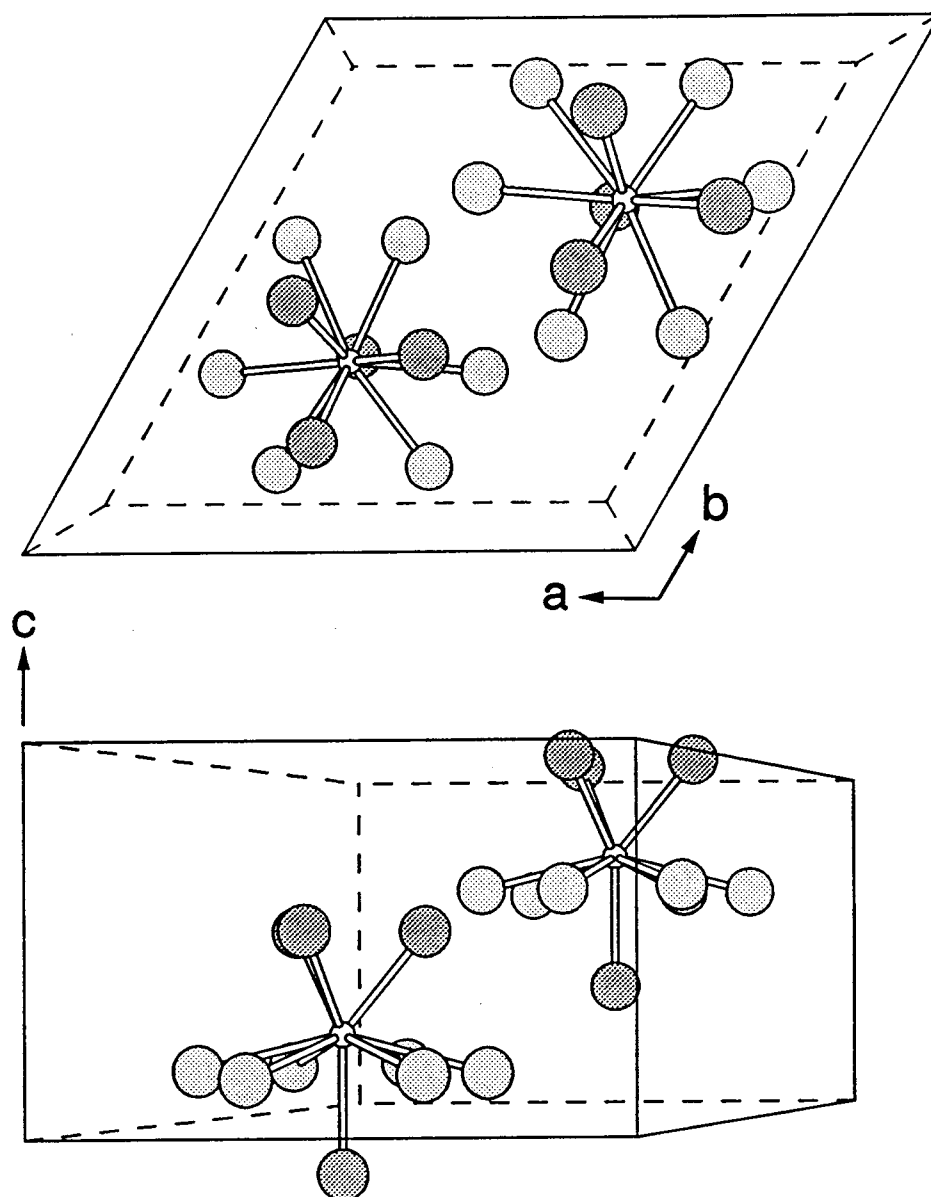


Figure 7.2. The Ba₃ coordination centers in Ba₇(BO₃)₃F₅.

bonding interactions) that form a very distorted monocapped trigonal prism. This heptacoordinate Ba(2)O₄F₃ environment appears to be small for a Ba atom, but two additional O3 atoms that reside approximately 3.2 Å away establish an ennead surrounding the Ba3 atoms. A bond valence calculation (10) for the Ba2 atom reveals only a 4 % contribution to the valency (see Table 7.6); thus, these two O3 atoms are considered to be only weakly bound.

Figure 7.3 illustrates the geometry of the three F atom types in the structure with the special position F atoms possessing C_{3v} point symmetry. The F1 atom is trigonally coordinated by Ba2 atoms, but it is not coplanar with them. Rather, they form a shallow triangular pyramid with the F⁻ anion resting below the plane of Ba2 atoms by 0.2 Å. The F1 atom is also capped by a Ba3 atom to establish an overall geometry of a trigonal base pyramid. The F2 atom assumes this polyhedral shape as well, but it is created exclusively by three Ba1 atoms. This is similar to the circumscribing cations around the F atoms in Sr₅(BO₃)₃F (6). The F atom displacement of 1.5 Å from the triangle of cations is greater in the title compound than in the Sr structure (0.92 Å). The asymmetric F3 site possesses a pyramidal Ba coordination similar to the F1 atom, but it does not have a regular planar triangular base.

The BO₃ groups follow typical orthoborate specifications (11) with statistically equivalent bond angles of 120° and an average bond distance of 1.39(5) Å.

Table 7.6. Bond Valence Calculation for Ba₇(BO₃)₃F₅

<u>Bond</u>	<u>R (Å)</u>	<u>S</u>	<u>Ba Valence Contribution (%)</u>
Ba1-F2	2.99	0.132	8.49
Ba1-F3	2.72	0.202	12.99
Ba1-O1	3.13	0.115	7.38
Ba1-O1	2.93	0.182	11.71
Ba1-O2	2.99	0.158	10.16
Ba1-O2	3.07	0.131	8.45
Ba1-O3	2.82	0.238	15.31
Ba1-O3	2.88	0.205	13.21
Ba1-O3	2.91	<u>0.191</u>	12.29
		+1.554	(77.7 % of +2 Oxidation No.)
Ba2-F1	2.63	0.234	11.16
Ba2-F3	2.59	0.252	11.99
Ba2-F3	2.77	0.186	8.86
Ba2-O1	2.65	0.368	17.53
Ba2-O1	2.79	0.256	12.22
Ba2-O2	2.63	0.388	18.48
Ba2-O2	2.84	0.226	10.79
Ba2-O3	3.21	0.096	4.58
Ba2-O3	3.23	<u>0.092</u>	4.38
		+2.098	(105 % of +2 Oxidation No.)
Ba3-F1	2.76	0.189	9.82
Ba3-F3	2.62	0.239	12.41
Ba3-F3	2.62	0.239	12.41
Ba3-F3	3.62	0.239	12.41
Ba3-O1	2.99	0.158	8.20
Ba3-O1	2.99	0.158	8.20
Ba3-O1	2.99	0.158	8.20
Ba3-O2	2.93	0.182	9.45
Ba3-O2	2.93	0.182	9.45
Ba3-O2	2.93	<u>0.182</u>	9.45
		+1.928	(96 % of +2 Oxidation No.)

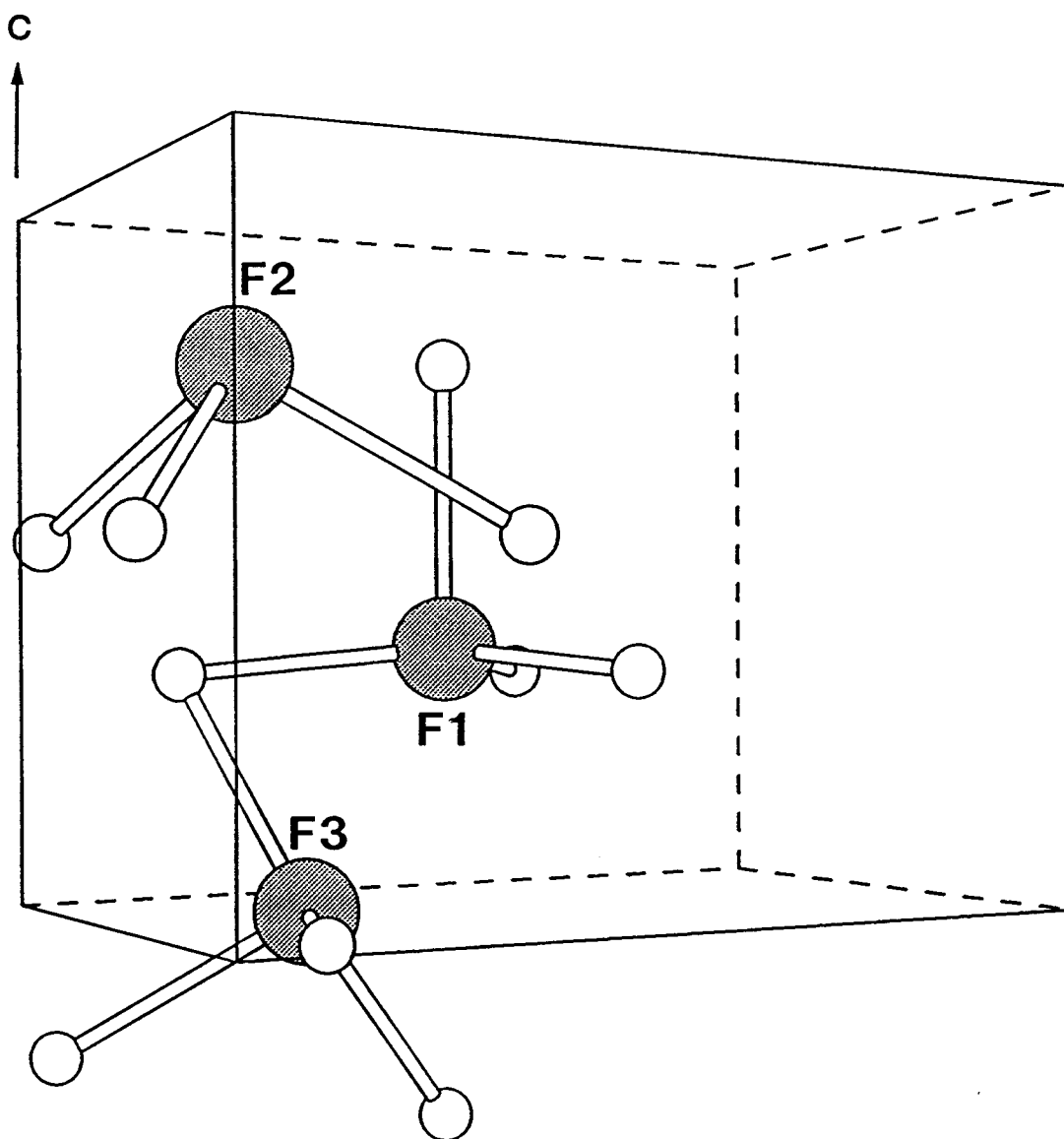


Figure 7.3. Coordination environments for the F atoms in $\text{Ba}_7(\text{BO}_3)_3\text{F}_5$. The F atoms are numerically labeled.

Discussion

Even though nearly every atom in the unit cell can be mapped into the hexagonal space group $P6_3mc$, the solution of the structure must be reduced to trigonal symmetry because of the location of the F3 atom. The Ba sites that interact with F3 atoms and the coordination of the F3 atom itself are only refined at its present location. An alternative placement of the F3 atom in the trigonal space group is at the position 0.51, 0.18, 0.02; in this position, the trigonal F3 face of the Ba₃ coordination environment is rotated by 33° . These parameters, however, produced no improvement in the refinement. The rotational median positional parameters between these two orientations at 0.58, 0.42, 0.02 satisfy the conditions for mapping into the hexagonal group $P6_3mc$, but the F3 atom does not favorably refine in this position.

Perhaps some disorder on these sites is one explanation for the exaggerated thermal displacement coefficient for the F3 atom — the anisotropic displacement coefficients indicate that the F3 atoms are roving within the **ab** plane. Other possible factors could additionally be responsible for the diffuse electron density at this site. An element of superstructure may have been overlooked in the solution of the structural arrangement. Conceivably, the F3 atom could order on the aforementioned sites over several unit-cell distances. In this case, a more exacting search in a larger unit cell for odd-order reflections may be necessary. One should also consider that if O^{2-} anions substitute for F^- anions, then vacancies are created in the structure for charge compensation that cause the displacement coefficient for those sites to appear large. As mentioned in the synthesis of this material for X-ray analysis, some attempt was made to reduce the inclusion of O^{2-} anions in the crystals, but extreme methods were not enacted in this crystal growth procedure. Hence, a small amount of O^{2-} may still reside in the material. Nevertheless, the refinement in the $P31c$ space group represents the best model at the present time. Examination of this result is ongoing.

After evaluating the structural features of the title compound with its unique

orientation of BO_3 groups, we were eager to explore its potential as a second-harmonic generator (SHG), or even a self frequency-doubling laser host. Therefore, preliminary Kurtz-Perry SHG studies (12) were performed, and the results indicated that $\text{Ba}_7(\text{BO}_3)_3\text{F}_5$ indeed may conceivably be used as a frequency converter of laser light. This result also confirms the assignment of a noncentrosymmetric space group.

The strength of the macroscopic SHG energy is directly related to the electronic properties of the microscopic units within the compound. The nonlinear effect is intensified when the micropolarizabilities of these units constructively combine to provide a significant observed response. The material $\beta\text{-BaB}_2\text{O}_4$ (BBO) derives its high nonlinear susceptibility from the summation of coplanar $\text{B}_3\text{O}_6^{3-}$ polyborate rings that generally order with the same orientations. BBO's high susceptibility comes at a cost, however — its inherent high birefringence, angular sensitivity to phasematching, and high threshold power are consequences of the highly anisotropic layered chromophore arrangement in the crystal structure. For LiB_3O_5 (LBO), a less anisotropic arrangement produces a smaller nonlinearity, but higher conversion efficiencies are attained because of the smaller birefringence and lower sensitivity to angular phasematching.

A chromophore geometry that would maintain a high susceptibility and minimize critical phasematching and threshold power properties for conversion of IR light (13) is shown in Figure 7.4. Here, the B–O bonds of three orthoborate triangles align along a principal C_3 rotation axis. Considering just the BO_3 groups throughout the title structure (Figure 7.5), it is apparent that they attain a geometry that is similar to the paragon. The pseudo-hexagonal 6_3 array of BO_3 triangles in $\text{Ba}_7(\text{BO}_3)_3\text{F}_5$ are canted from the c axis by 33° . Thus, according to the oxoanion SHG model which predicts a semiquantitative nonlinear susceptibility exclusively on the basis of the atomic structure of the compound (13), the sum of the BO_3 micropolarizabilities will be less than ideal. With the $\cos^3\theta$ functional dependence of the β_{333} coefficient for a BO_3 planar rotation that is orthogonal to the C_3 axis, as exhibited in $\text{Ba}_7(\text{BO}_3)_3\text{F}_5$, the susceptibility is calculated to be 59 % of optimum

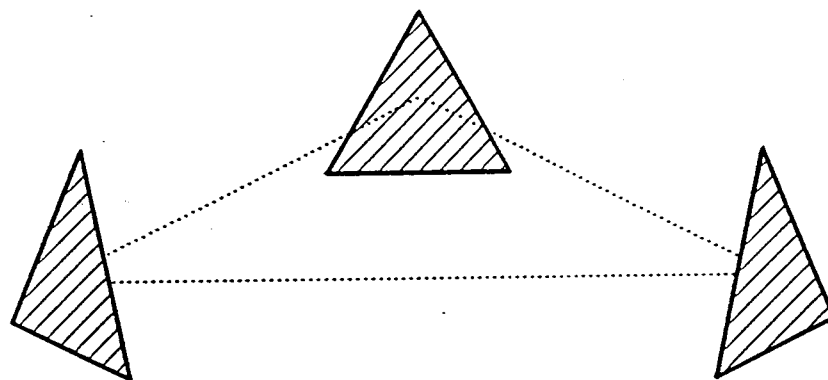


Figure 7.4. A proposed arrangement of BO_3 groups for obtaining high nonlinearity and low birefringence.

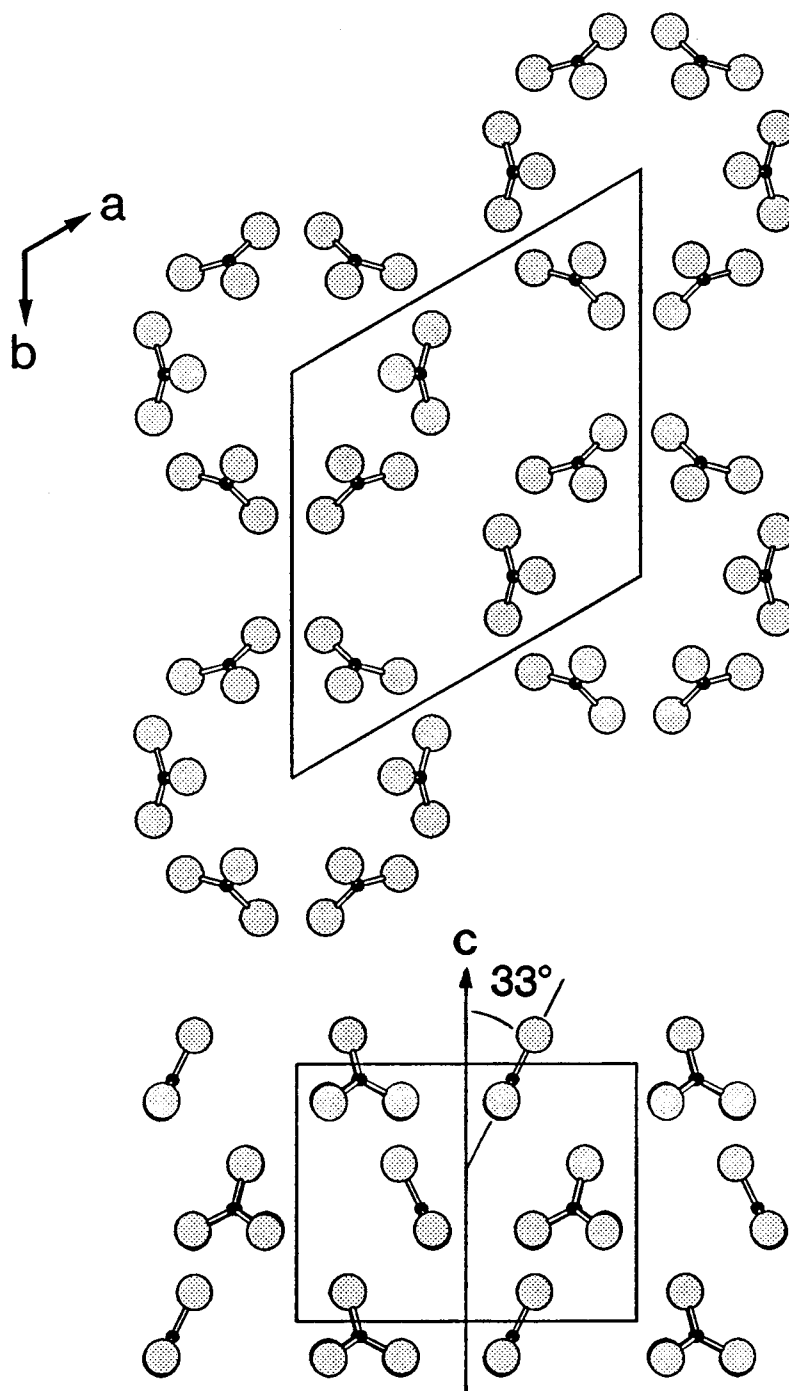


Figure 7.5. The arrangement of BO_3 groups in $\text{Ba}_7(\text{BO}_3)_3\text{F}_5$.

($\cos^3 33^\circ$). Normalizing the borate number density in the cell to the effective BO_3 number density for $\text{Y}_3\text{Al}(\text{BO}_3)_4$ (YAB) and accounting for the BO_3 orientations, one expects that the title compound will exhibit ~40 % of the susceptibility of YAB. The measured d coefficient for YAB is 1.5 pm/V (14), so we predict with oxoanion SHG modeling that $d_{33} \approx 0.6$ pm/V for $\text{Ba}_7(\text{BO}_3)_3\text{F}_5$. This value may be compared to $d_{\text{eff}} = 0.7$ pm/V for LBO. This analysis, of course, does not include possible contributions from the Ba–F matrix. The highest nonlinearities for fluorides have been observed in similar matrices containing long metal–F bonds (15).

Acknowledgments

The authors would like to thank Dr. Thomas A. Reynolds for conducting the preliminary SHG study of this compound. This research was supported by the US National Science Foundation, Solid-State Chemistry Program (DMR-8814432). Acknowledgment is made to the Donors of The Petroleum Research Fund, administered by the American Chemical Society, for partial support of the work. D.A.K. thanks the Alfred P. Sloan Research Foundation for a fellowship.

References

1. T. Alekel III, D.A. Keszler *J. Solid-State Chem.* (1993), in press.
2. Molecular Structure Corp., 3200A Research Forest Drive, The Woodlands, TX 77381.
3. G.M. Sheldrick *Crystallographic Computing 3*, Oxford: Oxford University Press, (1985) 175-189.
4. *International Tables for X-ray Crystallography, Vol. IV*, Birmingham: Kynoch Press (1974). (Present distributor: Kluwer Academic Publishers, Dordrecht.)
5. N. Walker, D. Stuart *Acta Crystallogr., Sect. A*, **39**, (1983) 158.
6. T. Alekel III, D.A. Keszler *Inorg. Chem.*, **C48**, (1992) 1382.
7. T. Alekel III, D.A. Keszler *Chem. Mat.*, to be submitted (Ch. 5).
8. J.R. Cox, D.A. Keszler, J. Huang "The Layered Borates $Ba_3M(BO_3)_3$ M = Dy, Ho, Y, Er, Tm, Yb, Lu, and Sc", *J. Solid State Chem.*, to be published.
9. A. Pabst *Amer. Mineral.*, **59**, (1974) 353.
10. I.D. Brown *Structure and Bonding in Crystals, Vol. II*, Academic Press: New York, (1981) Ch. 14.
11. H. Sun, D.A. Keszler *Acta Crystallogr., Sect. C.*, **44**, (1988) 1505.
12. S.K. Kurtz, T.T. Perry *J. Appl. Phys.*, **39**, (1968) 3798.
13. K.I. Schaffers, D.A. Keszler *Chem. Mat.*, to be published with this work.
14. Y.X. Fan, R. Schlect, M.W. Qiu, D. Luo, A.D. Jiang, Y.C. Huang *OSA Proc. on Advanced Solid-State Lasers*, Santa Fe, NM, (Eds. L.L. Chase, A.A. Pinto), **13**, (1992) 371.
15. S.P. Velsko, D. Eimerl *J. Appl. Phys.*, **62(6)**, (1987) 2461.

BIBLIOGRAPHY

- T. Alekel, D.A. Keszler *Acta Crystallogr., Sect. C* **48**, (1992), 1382.
- T. Alekel III, D.A. Keszler *Chem. Mat.*, to be submitted (Ch. 5).
- T. Alekel III, D.A. Keszler *Inorganic Chem.*, **C48**, (1992) 1382.
- T. Alekel III, D.A. Keszler *J. Solid-State Chem.* (1993), in press.
- J.W. Baer, M.G. Knights, E.P. Chiklis, H.P. Jenssen *Proc. Internat. Conf. Laser '78*, December 11-15, Orlando, STS Press: McLean, VA (1979) 770.
- H. Bartl, W. Schuckmann, *Neues Jahrb. Min. Monatsh.* **8**, (1966) 253.
- L.R. Batsanova, L.A. Novosel'tseva, A.I. Madaras, *Inorg. Mat. (English Translation)*, (1974) 530.
- S. Berger, *Acta Chem. Scand.* **4**, (1950) 1054.
- S.I. Berul', I.N. Nikonova, *Russ. J. Inorg. Chem.* **11**(4), (1966) 490.
- G. Blasse, A. Meijerink, D. Terrell, L. Neyens (1988) **Eur. Pat. Appl. EP 353,805** (Cl. C09K11/86), 07 Feb 1990, EP Appl. 88/201,693, 05 Aug 1990; 20 pp.
- G. Blasse *Prog. Solid State Chem.*, **18**, (1988) 79.
- S. Block, G. Burley, A. Perloff, R.D. Mason, *J. Res. Natl. Bur. Stand.* **62**, (1959) 95.
- A. Brovkin, L. Nikishova *Kristallographia*, **20**, (1975) 415.
- I.D. Brown *Structure and Bonding in Crystals, Vol. II*, Academic Press: New York, (1981) Ch. 14.
- D.M. Chackraburty, *Acta Crystallogr.* **10**, (1957) 199.
- D.S. Chemela *Phys. Today*, May (1985) 57.
- C. Chen, Y. Wu, L. Ru *J. Cryst. Growth* **99**, (1990), 790.
- Coherent Laser Products Division, 3210 Porter Drive, P.O. Box 10042, Palo Alto, CA 94303.

J.R. Cox, D.A. Keszler, J. Huang "The Layered Borates $Ba_3M(BO_3)_3$ M = Dy, Ho, Y, Er, Tm, Yb, Lu, and Sc", *J. Solid State Chem.*, to be published.

M.K. Crawford, L.H. Brixner *J. Luminescence*, **48 & 49**, (1991) 37.

B. Di Bartolo *Optical Interaction in Solids*, John Wiley & Sons: New York, (1968).

G.J. Dirksen, G. Blasse *J. Solid State Chem.*, **92**, (1991) 591.

S.M. Dohopte, P.L. Muthal, V.K. Kondawar, S.V. Maharil *J. Luminescence*, **50**, (1991) 187.

C. Dujardin, B. Moine, C. Pedrini *J. Luminescence*, **54**, (1993) 259. A topical summary is in the introduction.

C.A. Ebber, L.D. DeLoach, M. Webb, D. Eimerl, S.P. Velsko, D.A. Keszler *IEEE J. Quantum Elec.*, **29(2)**, (1993) 497.

D.J. Ehrlich, P.F. Moulton, R.M. Osgood *Optics Let.*, **4**, (1979) 184.

D. Eimerl, L. Davis, S. Velsko, E. Graham, A. Zalkin *J. Appl. Phys.*, **62**, (1987) 1968.

Y.X. Fan, R. Schlect, M.W. Qiu, D. Luo, A.D. Jiang, Y.C. Huang *OSA Proc. on Advanced Solid-State Lasers*, Santa Fe, NM, (Eds. L.L. Chase, A.A. Pinto), **13**, (1992) 371.

A. Filimonov, N. Leonyuk, L. Meissner, T. Timchenko, I. Rez, *Kristall und Technik*, **9(1)**, (1974) 63-66.

A. Filimonov, N. Leonyuk, L. Meissner, T. Timchenko, I. Rez *Krist. Tech.*, **9**, 63.

J.G. Fletcher, F.P. Glasser, R.A. Howie *Acta Crystallogr., Sect. C* **47**, (1991) 12.

C. Fouassier, B. Latourrette, J. Portier, P. Hagenmuller *Mat. Res. Bull.*, **11**, (1976) 933.

G.T. Forrest *Laser Focus World*, April (1990).

W.B. Fowler *The Physics of Color Centers*, (ed. W.B. Fowler), Academic Press: New York (1968) Ch. 2.

Fuji Corp., U.S. Pat. 4,239,968; U.S. Pat.4,236,078.

M. Gasperin *Acta. Crystallogr., Sect. B* **30**, (1974) 1181.

- A.M. Ghazzawi, G.E. Venikouas, R.C. Powell *J. Solid State Chem.*, **57**, (1985) 332.
- D.S. Hamilton, S.K. Gayen, G.J. Pogatshnik, R.D. Ghen *Phys. Rev.*, **B39**, (1989) 8807.
- H-D. Hattendorfff, G. Huber, H.G. Danielmeyer *J. Phys. C: Solid-State Phys.*, **11**, (1978) 2399.
- B. Henderson, G.F. Imbush *Optical Spectroscopy of Inorganic Solids*, ed. H. Fröhlich, Clarendon Press: Oxford (1989) Ch. 5.
- R.A. Hewes, M.V. Hoffmann *J. Luminescence*, **3**, (1971) 261.
- M.V. Hoffman *J. Electrochem. Soc.*, **118**, (1971) 933.
- E. Howells, D. Phillips, D. Rodgers, *Acta Crystallogr.*, **3**, (1950) 210.
- Z-P. Huang, S-X Liu, F-H. Liao *Eur. J. Solid State Inorg. Chem.*, **28**, (1991) 147.
- G. Huber, S. Payne, L.L. Chase, W.F. Krupke *J. Luminescence*, **39**, (1988) 259.
- G. Huber, F. Lutz *J. Cryst. Growth*, **52**, (1981) 646.
- International Tables for X-ray Crystallography, Vol. IV*, Birmingham: Kynoch Press (1974). (Present distributor: Kluwer Academic Publishers, Dordrecht.)
- J.P. Jouart, M. Bouffard, G. Klein, G. Mary *J. Luminescence*, **50**, (1991) 273.
- A.A. Kaminskii *Laser Crystals*, Springer-Verlag: New York (1981) 12.
- G.M. Kaye *Photonics Spectra*, **25(10)**, (1991) 62.
- D.A. Keszler, (1992), private communication.
- H. König, R. Hoppe, and M. Jansen, *Z. Anorg. Allg. Chem.*, **449**, (1979) 91.
- F.K. Koschnick, Th. Hangleiter, J-M. Spaeth, R.S. Eachus *J. Phys.: Condens. Matter*, **4**, (1992) 3001.
- F.K. Koschnick, J-M Spaeth, R.S. Eachus *J. Phys.: Condensed Matter*, **4**, (1992) 3015.
- S.K. Kurtz, T.T. Perry *J. Appl. Phys.*, **39**, (1968) 3798.
- J. Lin, M. Su *J. Luminescence*, **43**, (1988) 155.

- B-S. Lu, J. Wang, H-F. Pan, M-H. Jiang *J. Appl. Phys.*, (1989) 6052.
- Z.D. Luo, J.T. Lin, A.D. Jiang, Y.C. Huang, M.W. Qui *Proc. SPIE Int. Soc. Opt.*, (1989) 1104.
- A. Meijerink, G. Blasse *J. Luminescence*, **43(5)**, (1989) 283.
- A. Meijerink, G. Blasse *J. Phys. D: Appl. Phys.*, **24(6)**, (1991) 626.
- A. Meijerink, G. Blasse, L. Struye *Mater. Chem. Phys.*, **21**, (1989) 261.
- Molecular Structure Corporation, 3200A Research Forest Drive, The Woodlands, TX 77381, USA.
- "Newsbreaks" *Laser Focus World*, **28(9)**, (1992) 9.
- Nova Laser System, Lawrence Livermore National Laboratory, CA.
- A. Pabst *Amer. Mineral.*, **59**, (1974) 353.
- Philips Technical Review*, **31(10)**, (1970) 309.
- R.J. Reeves, R.M. MacFarlane *Physical Rev. B*, **47(1)**, (1993) 158.
- L. Richter, F. Müller *Z. Anorg. Allg. Chem.*, **467**, (1980) 123.
- F.M. Ryan *J. Luminescence*, **24&25**, (1981) 827.
- B. Saubat, C. Fouassier, P. Hagenmuller *Mat. Res. Bull.*, **16**, (1981) 193.
- K.I. Schaffers, Ph.D. dissertation, Oregon State University, (1992) Ch. 2.
- K.I. Schaffers, T. Alekel III, P.D. Thompson, J.R. Cox, D.A. Keszler *J. Am. Chem. Soc.*, **112**, (1990) 7068.
- K.I. Schaffers, D.A. Keszler *Inorganic Synthesis*, submitted.
- K.I. Schaffers, T.A. Reynolds, D.A. Keszler "Tetrahedral Triangular 3-D Framework and Luminescence in the Borate $\text{BaBe}_2(\text{BO}_3)_2$ ", *Inorganic Chem.*, in preparation.
- K.I. Schaffers, P.D. Thompson, T. Alekel III, J.R. Cox, D.A. Keszler "Crystal Chemistry of STACK", *Chem. of Mat.*, to be published.
- W.J. Schipper, Z.A.E.P. Vroon, G. Blasse *Chem. Mater.*, **4**, (1992) 688.

- I. Schütz, I. Freitag, R. Wallenstein *Optics Comm.*, **77(2,3)**, (1990) 221.
- S.K. Sekatskii, V.S. Letokhov *Optics Comm.*, **95**, (1993) 260.
- R.D. Shannon, *Acta Crystallogr., Sect. A*, **32**, (1976) 751.
- R. Shannon, C. Prewitt *Acta Crystallogr., Sect. B*, **25**, (1968) 925.
- G.M. Sheldrick *Crystallographic Computing 3*, Oxford: Oxford University Press, (1985) 175-189.
- M. Shimazu *Photonics Spectra*, **26(11)**, (1992) 66.
- L. Shirong, H. Qingzhen, Z. Yifan, J. Aidong, C. Chuangtain *Acta Crystallogr., Sect. C*, **45**, (1989) 1861.
- R.W. Smith, Ph.D. dissertation, Oregon State University, USA (1989).
- R.W. Smith, D.A. Keszler *J. Solid State Chem.*, **81**, (1989) 305.
- M. Sonoda, M. Takano, J. Miyahara, H. Kato *Radiology*, **148**, (1983) 833.
- T. Soules, M. Hoffman *Kirk-Othmer: Encyclopedia of Chemical Technology*, 3rd Ed.; Vol. 14, John Wiley & Sons: New York (1981) 527.
- "Special Report: Laser Update", *Photonics Spectra*, **25(11)**, (1991) 96.
- J.P. Spoonhower, M.S. Burberry *J. Luminescence*, **43**, (1989) 221.
- A.L.N. Stevels, A.D.M. Schrama-de Pauw *J. Electrochem. Soc.*, **123(5)** (1976) 691.
- A.M. Stoneham, *Theory of Defects in Solids*, Oxford University Press: UK, (1975).
- K. Sudarsanan, P.E. Mackie, R.A. Young *Mat. Res. Bull.*, **7**, (1972) 1331.
- K. Sudarsanan, R.A. Young *Acta Crystallogr., Sect. B.*, **30**, (1974) 1381.
- H. Sun, D.A. Keszler *Acta Crystallogr., Sect. C.*, **44**, (1988) 1505.
- X-P. Sun, M-Z. Su *J. Luminescence*, **40&41**, (1988) 171.
- J. Sytsma, G. Blasse *J. Luminescence*, **51**, (1992) 283.

- K. Takahashi, K. Kohda, J. Miyahara, Y. Kanemitsu, K. Amitani, S. Shionoya *J. Luminescence*, **31 & 32**, (1984) 266.
- K. Takahashi, J. Miyahara, Y. Shibahara *J. Electrochem. Soc.*, **132(6)**, (1985) 1492.
- K. Takahashi, Y. Shibahara, J. Miyahara, *Electrochem. Soc. 163rd Meeting*, 921RNP (1983).
- Y. Takéuchi, *Acta Crystallogr.*, **5**, (1952) 572.
- K. Teske, H.A. Lehmann, *Z. Chem.*, **6**, (1966) 230.
- P.D. Thompson, J. Huang, R.W. Smith, D.A. Keszler *J. Solid State Chem.* **95**, (1991) 126.
- P.D. Thompson, D.A. Keszler *Chem. Mat.*, **1**, (1989) 292.
- P.D. Thompson, D.A. Keszler, *Solid State Ionics*, **32/33**, (1989) 521.
- S. Velsko, Lawrence Livermore National Laboratory, (1988) private communication.
- S.P. Velsko, D. Eimerl *J. Appl. Phys.*, **62(6)**, (1987) 2461.
- H. von Sergern, A. Meijerink, T. Voigt, A. Winnacker *J. Appl. Phys.*, **66(9)**, (1989) 4418.
- H. von Seggern, T. Voigt, W. Knüpfer, G. Lange *J. Appl. Phys.*, **64(3)**, (1988) 1405.
- N. Walker, D. Stuart *Acta Crystallogr., Sect. A*, **39**, (1983) 158.
- F. Wen-Tian, C. Fouassier, P. Hagenmuller *Mat. Res. Bull.*, **22**, (1987) 899.
- T. Welker *J. Luminescence*, **48 & 49**, (1989) 49.
- A. Winnacker, R.M. Shelby, R.M. MacFarlane *Optics Lett.*, **10(7)**, (1985) 350.
- R. Wu *Applied Optics*, **32(6)**, (1993) 971.
- O.V. Yakubovich, M.A. Simonov, E.L. Belokoneva, Y.I.C. Egorov-Tismenko, N.V. Belov, *Dokl. Acad. Nauk SSSR*, **230**, (1976) 837.
- O.V. Yakubovich, M.A. Simonov, N.V. Belov, *Dokl. Acad. Nauk SSSR*, **238**, (1978) 98.

O. V. Yakubovich, N.A. Yamnova, B.M. Shchedrin, M.A. Simonov, N.V. Belov, *Dokl. Acad. Nauk SSSR*, **228**, (1976) 842.

K. Yvon, W. Jeitschko, E. Parthe *J. Appl. Cryst.*, **10**, (1977) 73.

J. Zhang, S. Huang, J. Yu *Optics Lett.*, **17(16)**, (1992) 1146.

CURRICULUM VITAE

Theodore Alekel III

Department of Chemistry
Oregon State University
Corvallis, Oregon 97331-4003

Birth Date

11 January 1965

Education

Walla Walla College

B.S. 1988

Professional Societies

Phi Lambda Upsilon

Publications

T. Alekel III and D. A. Keszler, "Structure of $\text{Sr}_5(\text{BO}_3)_3\text{Cl}$ ", *Acta Crystallographica*, **1992**, C48, 1382.

T. Alekel III and D. A. Keszler, "New Strontium Borate Halides $\text{Sr}_5(\text{BO}_3)_3\text{X}$ ($\text{X} = \text{F}$ or Br)", *Inorganic Chemistry*, **1993**, 32(1), 101.

T. Alekel III and D. A. Keszler, "The First Pyroborate Halide — $\text{Ba}_5(\text{B}_2\text{O}_5)_2\text{F}_2$ ", *Journal of Solid State Chemistry*, in press.

K. I. Schaffers, T. Alekel III, P. D. Thompson, J. R. Cox, and D. A. Keszler, "New Structural Class of Solid-State Oxide", *Journal of the American Chemical Society*, **1990**, 112, 7068.

T. Alekel, "MINSQ", *Biotechnology Software*, **1990**, 8(2), 15.

K. I. Schaffers, P. D. Thompson, T. Alekel III, J. R. Cox, and D. A. Keszler, "Crystal Chemistry of STACK", *Journal of Solid State Chemistry*, in preparation.

T. Alekel III and D. A. Keszler, "Structure of $\text{Ba}_7(\text{BO}_3)_3\text{F}_5$: A Noncentrosymmetric Orthoborate Fluoride", *Chemistry of Materials*, in preparation.

T. Alekel III and D. A. Keszler, "Structure and Eu^{2+} Luminescence of the New Borates $\text{AE}_2\text{BO}_3\text{Br}$ ($\text{AE} = \text{Sr}, \text{Ba}$)", *Chemistry of Materials*, in preparation.

Z. Zhang, M. M. Lerner, T. Alekel III, and D. A. Keszler, "Generation of A Photoluminescent Coating by the Photoelectro-chemical Oxidation of n-Si in Anhydrous Hydrogen Fluoride", *Journal of the American Chemical Society*, submitted.

Z. Zhang, M. M. Lerner, T. Alekel III, and D. A. Keszler, "Formation of a Photoluminescent Surface on n-Si by Irradiation Without an Externaily Applied Potential", *Journal of the Electrochemical Society*, submitted.

Presentations

"New Luminescent Materials" T. Alekel III, K. I. Schaffers, and D. A. Keszler. U.S.-France Workshop on Optical Materials, Manbisson, France, October 1992.

"New Strontium Borate Halides for Photostimulatable Luminescence" T. Alekel III and D. A. Keszler, 203rd ACS National Meeting, San Francisco, April 1992.

"New Haloborates for Persistent Spectral Hole-Burning" T. Alekel III and D. A. Keszler, 46th Northwest ACS Meeting, La Grande, OR, June 1991.